Titre: Title:	Experimental and Numerical Investigation of an Ultrasound-Assisted Biodiesel Transesterification with Polyalcohols
Auteur: Author:	Hela Laajimi
Date:	2022
Type:	Mémoire ou thèse / Dissertation or Thesis
Référence: Citation:	Laajimi, H. (2022). Experimental and Numerical Investigation of an Ultrasound-Assisted Biodiesel Transesterification with Polyalcohols [Ph.D. thesis, Polytechnique Montréal]. PolyPublie. https://publications.polymtl.ca/10464/

POLYTECHNIQUE MONTRÉAL
affiliée à l'Université de Montréal

Experimental and numerical investigation of an ultrasound-assisted biodiesel transesterification with polyalcohols

HELA LAAJIMI
Département de génie chimique

Thèse présentée en vue de l'obtention du diplôme de *Philosophiae Doctor*
Génie chimique
Juin 2022

POLYTECHNIQUE MONTRÉAL

affiliée à l'Université de Montréal

Cette thèse intitulée :

Experimental and numerical investigation of an ultrasound-assisted biodiesel transesterification with polyalcohols

présentée par **Hela LAAJIMI**

en vue de l'obtention du diplôme de *Philosophiæ Doctor*

a été dûment acceptée par le jury d'examen constitué de :

Charles DUBOIS, président
Daria Camilla BOFFITO, membre et directrice de recherche
Fabio CICOIRA, membre
Mélanie HAZLETT, membre externe

DEDICATION

À Lynn et Amine

ACKNOWLEDGEMENTS

First of all, I would like to express my sincere gratitude to my director, Professor Boffito, for giving me the chance to work under her supervision. I thank her for her trust, motivation, kindness, and especially for her moral support during the interruption of my thesis for parental leave. I thank her for always being understanding and encouraging me to continue without putting pressure on me. Thanks to Prof. Boffito for everything, I am so lucky and grateful to work under her supervision.

I thank Prof. Patience for collaborating with his research team and for allowing me to work in his laboratories and especially for giving me the chance to participate in his "Experimental Methods in Chemical Engineering" series.

A special thanks to Dalma for making this experience enjoyable with her positive energy, her unwavering support when I was going through a difficult time, for always correcting my poor English, for making me discover Pasticceria Alati-Caserta and, in the meantime, for motivating me to work out. She is an exceptional person, I learned a lot from her. I am so grateful to have had the opportunity to work with her and especially to have earned her precious friendship.

I thank Fede for all his precious advice, his good mood, his support and his kindness, as well as for all the coffees he offered me. I appreciated all the exchanges I had with him.

I thank Kobra for her kindness and her help with COMSOL. Without her collaboration my work would not be the same.

I thank Mina, Nooshin, Mahmoud, Cristina, Jacopo, Olga, Nicolas, Mohammad, Zahra, Arun and all the students of professors Boffito and Patience for everything and especially for the birthday cakes. I will always remember all the beautiful time we have spent together.

Thanks to my family; to Amine for believing in me and for giving me the strength and courage not to give up. Without his continued support, I would never be able to make it.

Lynn this thesis is for you! Thank you my baby for being born during these years of doctorate. Yes, it was a bit challenging, but you embellished our life so much that I forgot how tired I was and your presence gave me the strength to continue. Thanks to my brother and sister and especially my parents for all the sacrifices you have made. Education is the most precious gift you could have given me. You believed in me from a young age and you gave me independence. That's more than I could ever give you, so at least, thank you for everything! I love you all.

Finally, I would like to thank the members of the jury who accepted to evaluate this thesis.

RÉSUMÉ

L'épuisement des ressources fossiles et l'augmentation des émissions de gaz à effet de serre liées à leur exploitation ont incité les gouvernements du monde entier à envisager l'exploitation de la biomasse et des ressources renouvelables pour la production d'énergie et de produits chimiques. Les industries de la machinerie et de l'automobile ont adopté les lubrifiants biosourcés pour remplacer les lubrifiants conventionnels d'origine fossile, puisqu'ils ont démontré de meilleures propriétés lubrifiantes (meilleure adhérence aux métaux et indices de viscosité et points d'éclair plus élevés) et surtout une plus faible empreinte carbone. Les biolubrifiants peuvent être préparés par modification chimique des huiles végétales ou du biodiesel. Cependant, ces modifications nécessitent des conditions de réaction drastiques. Ce projet de recherche propose une méthode pour intensifier la production de biolubrifiants à partir de biodiesel en utilisant les ultrasons. Les ultrasons sont une technologie propre émergente qui exploite l'énergie intense générée par la cavitation acoustique pour réaliser le processus plus rapidement et dans des conditions douces. La cavitation acoustique génère des radicaux hautement réactifs, des microturbulences et des microémulsions qui étendent considérablement la surface disponible pour la réaction entre les deux phases immiscibles, augmentant ainsi les taux de réaction. Dans la première partie de la thèse, nous avons quantifié les radicaux générés par ultrasons dans le milieu réactionnel et étudié l'influence de la présence d'un catalyseur solide sur l'activité acoustique. Nous avons exploré, pour la première fois, les effets chimiques de la cavitation acoustique dans une solution organique avec un solide en suspension. Nous avons étudié l'effet des polyols (propylène glycol et triméthylène glycol) et des particules de SiO_2 sur la génération de radicaux, étant donné que ces composants interviendront dans la réaction de production du lubrifiant dans les travaux qui suivent. Des ultrasons à 20 kHz ont soniqué les polyalcools et la silice avec différentes tailles (5-15 nm, 0.2-0.3 µm, 12-26 µm) et concentrations (0.5 wt% et 3 wt%). Les radicaux générés étaient des hydroxyalkyles identifiés par spectroscopie de résonance paramagnétique électronique (RPE) avec piégeage de spin (piège de spin 5,5-diméthyl-1-pyrrolin-N-oxyde (DMPO)). En présence de solides, la cavitation acoustique a augmenté la production d'espèces radicalaires dans le milieu organique étudié. Une solution contenant de la SiO_2 de taille 12-26 µm a généré 1,5 fois plus de radicaux qu'une solution sans particules (29 µM contre 19 µM après 1 h de sonication). Cependant, une concentration élevée de particules solides a réduit les effets de l'activité acoustique et donc la quantité d'espèces radicalaires

dans le milieu. L'analyse de l'effet de la taille du catalyseur a démontré que la concentration de radicaux dans le milieu augmente avec la taille des particules. Au voisinage des particules de 12-26 µm, la quantité de radicaux produits était deux fois plus importante que celle des particules de 5-15 nm. Un plus grand nombre de radicaux a été formé dans le milieu lorsque la puissance des ultrasons et la température ont été augmentées pendant la sonication.

La deuxième partie du projet a porté sur la conversion du biodiesel en lubrifiant, assistée par ultrasons. Nous avons produit du biodiesel à partir d'une huile de canola commerciale que nous avons soniqué avec des polyalcools (propylène et triméthylène glycols) pour en faire un lubrifiant. Nous avons optimisé les conditions de réaction en présence d'un catalyseur homogène, le NaOH. Le triméthylène glycol a donné 90 % ± 1,9 % de lubrifiant avec une puissance ultrasonore de 62 W, à 80 °C, et avec un rapport molaire alcool : biodiesel de 0,25. Par la suite, nous avons testé l'activité d'un catalyseur solide CaO/SiO_2 dans ces conditions optimisées. La réaction assistée par ultrasons et catalysée par CaO/SiO_2 a produit 15 fois plus de lubrifiant que la réaction agitée classiquement (46 % de lubrifiant contre 3 % de lubrifiant obtenu avec une agitation mécanique). Le dépôt du CaO sur la SiO_2, le chargement du catalyseur dans le réacteur, ainsi que sa lixiviation et son recyclage, ont été étudiés. Les résultats de cette partie ont confirmé ceux de la première partie de la thèse concernant l'effet de la charge du catalyseur sur la performance de la réaction assistée par ultrasons. Au-delà d'une certaine concentration, le catalyseur commence à amortir les effets des ultrasons et à ralentir leur propagation, ce qui diminue les taux de transfert de masse autour des particules. Après trois cycles de réaction, les ultrasons n'ont pas affecté la morphologie et la taille du catalyseur, mais ils ont lessivé les sites actifs, ce qui a fait baisser l'activité du catalyseur de 20 % pour les utilisations consécutives.

La dernière partie du projet visait à étudier numériquement les performances du sonoréacteur et à optimiser sa configuration géométrique en termes de position et de diamètre de la sonde à ultrasons. Nous avons simulé l'écoulement réactif acoustique en couplant des modèles acoustiques, de dynamique des fluides et de réaction chimique via le logiciel d'éléments finis COMSOL Multiphysics. Le modèle numérique a calculé les champs de pression et de vitesse acoustiques, ainsi que le profil de concentration du lubrifiant à l'intérieur du sonoréacteur. Nous avons validé le modèle en le comparant aux résultats expérimentaux de la deuxième partie du projet. Ensuite, nous avons étudié les effets de différentes profondeurs d'immersion et de différents diamètres de sonde

sur le rendement en lubrifiant. La sonde ultrasonique placée à mi-hauteur du réacteur (à 3 cm de profondeur) a généré plus de lubrifiant que celle placée en haut (à 1 cm) et près du fond (à 4 cm de profondeur) (les rendements respectifs étaient de 94 %, 81 % et 86 % en lubrifiant). En maintenant la puissance ultrasonore constante, une sonde de plus large diamètre (1,9 cm de diamètre) a produit 10 à 12 % de lubrifiant en plus qu'une sonde plus fine (1,3 cm).

ABSTRACT

The depletion of fossil resources and the greenhouse gas emissions associated with their exploitation have prompted governments around the world to focus on harnessing biomass and renewable resources to produce energy and chemicals. The machinery and automotive industries adopted bio-based lubricants to replace conventional fossil-based lubricants, as they have demonstrated better lubricating properties (stronger adhesion to metals and higher viscosity indices and flash points) and a smaller carbon footprint. Biolubricants are prepared by chemical modification of vegetable oils or biodiesel. However, these modifications require drastic reaction conditions. This research project proposes a method to intensify the production of biolubricants from biodiesel using ultrasound. Ultrasound is an emerging clean technology that exploits the intense energy generated by the acoustic cavitation to achieve the process faster and under mild conditions. Acoustic cavitation generates highly reactive radicals, micro-turbulence and micro-emulsions that greatly expand the surface area accessible for reaction between the two immiscible phases, thereby increasing reaction rates. In the first part of the thesis, we quantified the ultrasonically generated radicals in the reaction medium and studied the influence of the presence of a solid catalyst on the acoustic activity. We explored, for the first time, the chemical effects of acoustic cavitation in an organic slurry solution. We investigated the effect of polyols (propylene glycol and trimethylene glycol) and the SiO_2 particles on the radicals' generation, as these alcohols and catalyst will be the components of the lubricant production reaction in the works that follow. 20 kHz ultrasound sonicated the polyalcohols and silica with different sizes (5-15 nm, 0.2-0.3 µm, 12-26 µm) and concentrations (0.5 wt% and 3 wt%). The generated radicals were hydroxyalkyls identified by electron paramagnetic resonance (EPR) spectroscopy with spin trapping (5,5-dimethyl-1-pyrrolin-N-oxide (DMPO) was the spin trap). In the presence of solids, acoustic cavitation increased the production of radical species in the investigated organic medium. A solution containing SiO_2 of size 12-26 µm generated 1.5 times more radicals than a solution without particles (29 µM versus 19 µM after 1 h sonication). However, a high concentration of solid particles reduced the effects of acoustic activity and thereby the amount of the generated radical species. The analysis of the catalyst size effect demonstrated that the concentration of radicals in the medium increases with the particles size. In the vicinity of 12-26 µm particles, the amount of

radicals produced was twice that of 5-15 nm particles. More radical adducts were formed in the medium when the ultrasound power and temperature were increased during sonication.

The second part of the project investigated the ultrasound-assisted biodiesel conversion into lubricant. We produced biodiesel from a commercial canola oil that we sonicated with polyalcohols (propylene and trimethylene glycols) to make lubricant. We optimized the reaction condition in the presence of a homogenous catalyst NaOH. Trimethylene glycol yielded 90 % ± 1.9 % of lubricant with an ultrasound power of 62 W, at 80 °C, and with an alcohol: biodiesel molar ratio of 0.25. Subsequently, we tested the activity of CaO/SiO_2 under these optimized conditions. The ultrasound-assisted reaction produced 15 times more lubricant than the conventionally stirred reaction (46 % lubricant compared to 3 % lubricant obtained with mechanical stirring). The loading of CaO onto SiO_2, the charging of the catalyst into the reactor, as well as its leaching and recycling, were investigated. The findings of this part supported the ones of the first part of the thesis regarding the catalyst loading effect on the performance of the ultrasonically assisted reaction. Above a certain concentration, the catalyst starts to dampen the effects of ultrasound and slow down their propagation, which decreases the mass transfer rates around the particles. After three reaction cycles, ultrasound did not affect the morphology and size of the catalyst. However, it leached the active sites, which decreased the catalyst activity by 20 % for consecutive uses.

The last part of the project aimed to numerically study the performance of the sonoreactor and to optimize its geometrical configuration in terms of position and diameter of the ultrasonic probe.

We simulated the acoustic reactive flow by coupling acoustic, fluid dynamics, and chemical reaction models via the finite element software COMSOL Multiphysics. The numerical model calculated the acoustic pressure and velocity fields, and the lubricant concentration profile inside the sono-reactor. We validated the model by comparing it to the experimental results of the second part of the project. Then, we investigated the effects of different probe immersion depths and diameters on lubricant yield. The ultrasonic probe placed halfway up the reactor (at 3 cm depth) generated more lubricant than when placed at the top (at 1 cm) and near the bottom (at 4 cm depth) (the respective efficiencies were 94 %, 81 % and 86 %). While keeping the ultrasound power constant, a larger diameter probe (1.9 cm diameter) produced 10-12 % more lubricant than a thinner probe (1.3 cm).

TABLE OF CONTENTS

LIST OF TABLES

LIST OF FIGURES

LIST OF SYMBOLS AND ABBREVIATIONS

a_0	Normal acceleration [m s^{-2}]
A_m	Amplitude of ultrasound [m]
C	Molar concentration [mol m^{-3}]
d_p	Probe diameter [cm]
E_a	Activation energy [J mol^{-1}]
f	Ultrasound frequency [kHz]
F	Volume force of acoustic flow [N m^{-3}]
I	Turbulent intensity
k	Turbulent kinetic energy [m^2 s^{-2}]
k_1	First-order rate constant [s^{-1}]
k_2	Second order rate constant [mol^{-1} m^3 s^{-1}]
k_{son}	Rate constant with ultrasound [s^{-1}]
P	Acoustic pressure [Pa]
P_{Blake}	Threshold pressure [Pa]
P_T	Total pressure in the streaming [Pa]
P_{US}	Acoustic power [W]
P_v	the vapor pressure of the solvent [Pa]
R_{rx}	Reaction rate [mol m^{-3} s^{-1}]
s	Speed of sound [m s^{-1}]
S_A	Probe surface area [m^2]
t	Time [s]
T_{liq}	Temperature of the liquid [K]

T_{max}	Temperature at a point of cavitation collapse [K]
u	Velocity field of acoustic streaming [m s^{-1}]
u_i	Vibration velocity (i-direction) in the sound wave [m s^{-1}]
u_j	Vibration velocity (j-direction) in the sound wave [m s^{-1}]
α	Absorption coefficient [m^{-1}]
β	Cavitation volume fraction
μ	Dynamic viscosity [Pa s]
μ_T	Turbulent viscosity [Pa s]
ρ	Density [kg m^{-3}]
ω	Angular frequency [rad s^{-1}]
BET	Brunauer-Emmett-Teller
BJH	Barrett-Joyner-Hallender
C16	Methyl palmitate
C18:1	Methyl oleate
C18:2	Methyl linoleate
C18:3	Methyl linolenate
DE	Diester-biolubricant
DMPO	5,5-dimethyl-1-pyrroline *N*-oxide
ECN	Effective carbon number
EDX	Energy-dispersive X-ray
EPR	Electron paramagnetic resonance
FAME	Fatty acid methyl esters
FFAs	Free fatty acids

FID	Flame ionization detector
FTIR	Fourier-transform infrared
GC	Gas chromatography
GHG	Greenhouse gas
Gly	Glycols
HTA	Hydroxy terephthalate anion
ISTD	Internal standards
ME	Monoester
NPG	Neopentyl glycol
PE	Pentaerythritol
PG	Propylene glycol
PSD	Particle size distribution
RRF	Relative response factor
SEM	Scanning electron microscope
TEMPO	2,2,6,6-tetramethyl-1-piperidinyloxy
TG	Trimethylene glycol
TMP	Trimethylolpropane
US	Ultrasound
XRD	X-ray diffraction
XRF	X-ray fluorescence

CHAPTER 1 INTRODUCTION

1.1 Background and problem identification

Orientation towards green materials and improved stewardship of the Earth's natural resources is no longer an option, but a must. The increase in anthropogenic greenhouse gas (GHG) emissions has a tremendous impact on climate change. The Earth is now around 1.2 °C warmer than it was in pre-industrial times (1850-1900)[1]. The Paris Agreement, signed at the United Nations Climate Change Conference (COP21) in December 2015, imposes the reduction of GHG emissions by 45 % by 2030 and aims at carbon neutrality by 2050 to limit the global temperature rise to a maximum of 1.5 °C [2]. Fossil CO_2 emissions peaked at 36.64 $GtCO_2$ in 2019, and although the COVID-19 pandemic has lowered them by 5.6 % in 2020 [3], they will not stop increasing in the upcoming years. To reduce these emissions, the fossil fuel production must abate by around 6 % per year between 2020 and 2030 [4], [5]. Most countries in the world target a bio-based economy and are moving towards the exploitation of renewable energies and biomass to replace the fossil energy. Canada is committed to transitioning to a low-carbon economy. The Quebec government is aiming for a 50 % increase in bioenergy production by 2030 [6] and it supports the production and utilization of bio-based chemicals envisioning their integration into the economy of the province. Biolubricants are a subset of these bio-based chemicals and their adoption is being promoted by regulations and mandates that require the application of biodegradable products. They replace petroleum-based lubricants thereby contributing to the reduction of GHG emissions.

Canada is a leader in the development of high oleic canola and high erucic rapeseed oils [7]. Canadian farmers produce approximately 20 million tonnes of canola per year [8]. Canola cultivation generates about a quarter of all agricultural crop income. These facts motivated our interest in exploiting canola oil to produce biodiesel and biolubricant. In addition to being cleaner, biolubricants have demonstrated better characteristics than mineral lubricants, including lower volatility, higher viscosity indices and thermo-oxidative stability. These properties lead to the growth of the global biolubricants market (4.8 % CAGR), which is expected to reach 4.5 billion USD by 2027 [9]. In 2021, North America dominated the global biolubricants market share with a quota of 47.8 % [10].

Conventional processes for producing lubricants are lengthy (more than 6-8 h long) and require drastic reaction conditions (e.g., reduced pressures and temperatures above 150 °C). To overcome

these conditions, we opted for a process intensification technology, ultrasound, to intensify the lubricant production process. Ultrasonic processing consumes, on average, 45 % less energy than a traditional process while providing the system with a 10 to 30 times greater energy density [11]. In this project, we established an ultrasound-based process to synthesize lubricants from canola oil through biodiesel transesterification. We utilized, for the first time, polyalcohols potentially derived from biomass (propylene and trimethylene glycols) to transesterify the biodiesel.

Through acoustic cavitation, ultrasound induces physical and chemical effects that enhance reaction rates. The chemical effects translate to the generation of radical species in the processing medium. Although many heterogeneous catalytic reactions occur in organic solvents, data on the quantification of ultrasound-induced chemical effects in organic media and in the presence of solids is very limited, In the first part of the thesis, we identified and quantified, for the first time, the radicals generated by ultrasound in an organic medium and in the presence of solid particles. The goal is to study the synergistic effect of heterogeneous catalysis and ultrasonic cavitation on the yield of an organic synthesis. The organic solvents of interest are propylene glycol and trimethylene glycol, while the solid under investigation is the catalyst support (SiO_2). The findings of the first part of the thesis are necessary to select the optimal operating conditions, as well as the size and the amount of solid material to be applied in the second part of this doctoral project.

In the second part of the thesis, we synthesized biodiesel from canola oil, and then transesterified it to lubricants. Most of the data on transesterifications to produce lubricants is in the presence of a homogeneous alkaline catalyst. As we aimed for an ecological and economically attractive process, we synthesized and studied the activity of a heterogeneous catalyst, namely CaO/SiO_2, on the reaction. We investigated its recyclability and its stability under ultrasound exposure.

On the other hand, an appropriate geometrical configuration of an ultrasonic reactor is crucial to ensure the efficiency of the process. To this end, in the third part of the project, we conducted a numerical study to evaluate how certain geometrical parameters (ultrasonic probe position and diameter) of the ultrasonic reactor affect the biolubricant yield.

1.2 Objectives

The main objective of the project is to produce lubricant from the biodiesel ultrasound-assisted transesterification with polyalcohols. To achieve the main goal, we divided the research project into three specific sub-objectives, that resulted in three papers published or submitted to peer-reviewed journals. The sub-objectives of this work and their corresponding milestones are:

1. Investigate the chemical effects of the acoustic cavitation generated by ultrasound in an organic slurry solution. The results of this objective are described in chapter 4, and published as a scientific article in **Ultrasonics sonochemistry (IF. 7.5)**.
   - Sonicate trimethylene and propylene glycol in presence of silica particles of different sizes (5-15 nm, 0.2-0.3 µm, 12-26 µm) and amounts (0.5 wt% and 3 wt%).
   - EPR spin-trapping to identify and quantify the acoustically generated radicals.
   - Identify the glycol with the best acoustic activity.
   - Determine the size and concentration of SiO_2 that generate the maximum radicals amount.

2. Experimental investigation of the synergy between heterogeneous catalysis and ultrasound on the production of the biolubricant. Results are submitted as a scientific article in **Biomass & Bioenergy (I.F. 5.1)**.
   - Screen the effects of different types of polyalcohol, ultrasound powers, alcohol to biodiesel molar ratio, and reaction temperature on the lubricant yield and optimize the reaction conditions in the presence of a homogeneous catalyst (NaOH).
   - Synthesize and characterize a solid catalyst CaO/SiO_2.
   - Test the reaction with CaO/SiO_2 at the optimized conditions.
   - Compare the lubricant yield obtained by ultrasound with that obtained with the conventional process.
   - Determine the optimal loading of CaO over SiO_2 and consider leaching and reusability of the catalyst.

3. Investigate numerically the ultrasound-assisted biodiesel transesterification. Results are submitted as a scientific article in **Chemical Engineering and Processing: Process Intensification (IF. 4.2).**

- Kinetic modelling of the transesterification reaction.
- Simulate the acoustic pressure, the velocity distribution, and the lubricant concentration inside the sono-reactor.
- Verify the model accuracy by comparing it to the experimental results of the second sub-objective.
- Evaluate the effects of the probe diameter and its immersion depth on sono-reactor performance.

CHAPTER 2 COHERENCE OF THE ARTICLES

Chapter 1: This chapter introduces the environmental situation in the world and the need to replace fossil resources with biodegradable renewable resources. We discuss our interest in biodiesel and biolubricant production while describing the current global lubricant market. This chapter also stresses the advantages of biolubricants over fossil-based lubricants. After highlighting the problem associated with a conventional lubricant production process, we proposed ultrasound as a process intensification technology to improve production. To achieve the project's main objective, we suggest three specific goals, describing the main steps for each of them.

Chapter 2: This section outlines the general structure of the manuscript, highlighting the consistency of the articles with the project's objectives.

Chapter 3: This chapter is divided into four major sections. The first part describes the different types of lubricants and their importance in modern machinery. It also presents different types of vegetable oils, their main industrial applications, and their main advantages and disadvantages as lubricants. The principal chemical modifications of vegetable oils to improve their lubricating properties are discussed in a general overview. Particular emphasis is placed on the transesterification reaction. The second section explains some basic concepts of ultrasonic acoustic cavitation and the key parameters affecting the sonochemical process. A third section presents some physical and chemical methods for the characterization of the acoustic activity. The last section illustrates the potential of ultrasound in the intensification of transesterification reactions.

Chapter 4: This chapter covers to the first specific objective. It describes a methodology to quantify and identify the radicals generated by ultrasound in organic slurry solution. In this part, we studied the cavitation of propylene glycol and trimethylene glycol (which will subsequently trans-esterify the biodiesel to produce the lubricant) and the effect of the presence of SiO_2 (will be used as a support of the reaction’s catalyst) on the production of highly reactive radicals. The EPR spin-trapping method identified and quantified the generated radicals. Besides studying the acoustic activity in the two organic solvents, we also measured the effects of the temperature and the ultrasonic power, to identify the optimal parameters to intensify the sono-reaction. The results are published in **Ultrasonics sonochemistry**.

Chapter 5: According to the second sub-objective, this chapter describes the ultrasonic transesterification of canola oil methyl esters with propylene and trimethylene glycol to produce lubricants. A homogeneous catalyst NaOH catalyzed the reaction. GC-MS and GC-FID analyzed qualitatively and quantitatively the products. We studied the effects of type of alcohol, different ultrasound (US) powers, alcohol to biodiesel molar ratios, and reaction temperature on the lubricant yield. After optimizing the reaction conditions in the presence of the homogeneous catalyst, we tested them with calcium oxide supported on silica (CaO/SiO_2) that we synthesized by incipient wetness impregnation. The choice of the SiO_2 size was based on the results of the first sub-objective. We characterized the CaO/SiO_2 by BET, PSD, FTIR, XRD, XRF, and SEM. We compared the ultrasound-assisted reaction with the traditional process. We surveyed the optimal loading of CaO over SiO_2, the catalyst loading with respect to the reaction medium, as well as its leaching and reusability. The results are submitted to **Biomass & Bioenergy** journal.

Chapter 6: This section complements the previous sub-objectives with a numerical simulation to optimize the functional and geometrical parameters (diameter and position of the probe) of the reactor. We coupled the acoustic pressure and reactive turbulent flow to simulate the transesterification reaction in the ultrasonic batch reactor. We simulated, via COMSOL Multiphysics, the acoustic pressure and velocity distributions. We determined the transesterification reaction rate considering the collective effects of sonication and flow agitation in the reactor. On this basis, we determined the lubricant concentration profile in the reactor. After validating the accuracy of the model with the experimental results from the previous sub-objective, we examined the effect of changing the immersion depth and probe diameter on the reaction performance. The results are submitted to **Chemical Engineering and Processing: Process Intensification** journal.

Chapter 7: This chapter reports a general discussion of the work and a summary of the findings.

Chapter 8: Here we summarize the project and emphasize its contribution to the advancement of knowledge, while identifying its limitations and providing recommendations for future work.

CHAPTER 3 LITERATURE REVIEW

3.1 Biolubricant

Lubricants are required in virtually every aspect of modern machinery. They are widely used in industrial, automotive and aerospace applications to lubricate the surfaces in mutual contact to facilitate the components movement and reduce materials friction and wear. Lubricants also increase process efficiency by ensuring uniform heat distribution, improving corrosion resistance of equipment, and reducing energy losses. Saving energy and resources, as well as decreasing emissions, became major environmental concerns as sustainability became a driving force in the industry. There are three types of lubricants: mineral (petroleum-based) lubricants, synthetic lubricants and bio-based lubricants. The latter are formulated from renewable and biodegradable raw materials. Mineral oils are traditionally the most widely used lubricants. They are mainly composed of hydrocarbons and naphthenic, paraffinic or aromatic structures. Petroleum-based lubricants can be very toxic to the environment, hazardous to wildlife and are not degradable. Synthetic oils are also common lubricants. They have improved intrinsic qualities such as viscosity and thermal stability and are resistant to extreme pressure and temperature conditions. These lubricants include silicones, dibasic acid esters, phosphate esters, polyglycols and silicate esters [12]. Ester-based synthetic oils are characterized by excellent lubricating characteristics due to the polar nature of the ester functions. These molecules' polar groups bond to positively charged metal surfaces, forming protective films that slow metal surface wear [13]. The main disadvantage of this class of oils is their relatively high cost since their synthesis requires several reaction steps and expensive raw materials and technology [14]. The third group is vegetable oils (e.g., sunflower, rapeseed, canola, soybean, palm, coconut oils), and it is this category of lubricants that we are interested in. Vegetable oils can be used directly as lubricants or can be renewable and environmentally friendly sources for commercial use to produce biolubricants [15]. They find applications in several industries as emulsifiers, lubricants, plasticizers, resins, surfactants, plastics, solvents (Table 3.1). Vegetable oils are primarily composed of triglycerides. The fatty acid chains of triglycerides in vegetable oils have 12 to 22 carbon atoms, with different levels of unsaturation. The lubricant quality depends on the triglyceride structure of the vegetable oil. The long polar fatty acid chains produce very strong lubricating films that interact vigorously with metal surfaces,

reducing wear and friction. The strong intermolecular interactions provide good corrosion resistance to temperature changes, resulting in a high viscosity index. The quality of a lubricant depends mainly on its physical properties: viscosity index, thermal stability, oxidation stability, flash point, pour point and cloud point (temperature at which a liquid starts to agglomerate at the molecular level and exhibit solid particles, giving it a cloudy appearance). The best lubricant has the highest viscosity index, flash point, thermal and oxidative stability and the lowest pour point and cloud point.

Table 3.1 Main industrial applications of various vegetable-based lubricants [16]–[18].

Vegetable oil	Main application
Jojoba oil	Grease, lubricants, cosmetics industry
Jatropha oil	automotive engine
Sunflower oil	Grease, fuel substitute
Soybean oil	Lubricant, plasticizer, soap, pesticide
Palm oil	Lubricant in steel industry, grease
Castor oil	Lubricant, for gears grease
Canola oil	Metalworking fluid, hydraulic oils
Coconut oil	Cosmetics, automotive lubricant
Rapeseed oil	Hydraulic and chainsaw oil

3.1.1 Advantages and drawbacks of plant-based lubricants

Advantages

- **Biodegradable and nontoxic:** Biodegradability is the ability of a material to be degraded by microorganisms. The most obvious advantage of vegetable-based lubricants is their biodegradability. Plant oils have a higher biodegradability rate than mineral oils (in the range of 70-99 % compared to 15-35 % for mineral oils) [19], [20]. They are less toxic than synthetic and mineral oils and less expensive to clean up in the event of a spill.
- **High flash point:** Vegetable oils are safer than petroleum oils because they have a higher flash point and are not volatile. For example, the flash point of soybean oil is 326 °C, while that of mineral oil is 200 °C [21]. This reduces the risk of fire in various applications, including foundries and metalworking.

- **High lubricity:** When compared to mineral-based lubricants, bio-based lubricants have a higher lubricity and thus a much lower coefficient of friction. Increased lubricity minimizes friction and wear, reducing the need for costly additives (e.g., to withstand extreme pressures and temperatures). While biolubricants are more expensive to purchase for most applications, the extra cost is often offset by the energy savings of higher lubricity especially in applications involving high pressures and temperatures [22].
- **High viscosity index:** The viscosity index measures the viscosity variations with temperature. Lubricants with a high viscosity index remain stable at high temperatures. Mineral oils have a lower viscosity index than vegetable oils (80 to 120 compared to the viscosity index range of vegetable oils of equivalent viscosity which is 200 to 250) [23], [24].
- **Good metal adherence:** Triglycerides from vegetable oils are more polar than petroleum-based oils and therefore have a greater affinity for metals [25].Triglyceride molecules orient their polar ends toward the metal surface in order to adsorb to it and form a closed monomolecular or multimolecular layer, resulting in a lubricating film that decreases friction and wear (Figure 3.1).

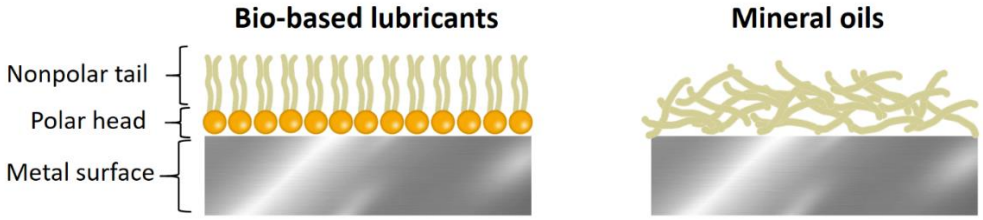

Figure 3.1: Affinity of bio-based and petroleum-based lubricants to metals [24], [26].

Disadvantages

- **Oxidative instability:** Vegetable oils have a low oxidative stability compared to mineral oils. When oil oxidizes (usually at high temperatures and in the presence of moisture), it undergoes a chemical reaction producing acid and sludge that polymerizes and can be deposited in crucial sections of the equipment and corrode it. The poor oxidation stability of plant oils is due to the double bond (C=C) in their fatty acid chains of triglycerides. The

presence of allyl protons in the triglyceride molecule makes vegetable oils very sensitive to free radical attacks [13], [27]. Chemical modifications of the oils or the addition of additives increase the oxidation stability [26].

- **High Pour Point:** The pour point is the coldest temperature at which a fluid flows. Unmodified vegetable oils have higher pour point than synthetic and mineral lubricants (e.g., rapeseed and canola oils have pour points around -9 °C and compared to -18 °C to -30 °C for petroleum-based lubricants) [28]. However, chemically modified vegetable-based lubricants have pour points as low as -40 °C [20]. Oil pour point issues can be resolved with additives or chemical modifications. The goal is to keep the lubricant as biodegradable as possible while keeping the cost low.
- **Expensive:** Biobased lubricants are generally more expensive than conventional ones, e.g., industrial biobased hydraulic fluid is 1 to 2 times more expensive than conventional fluid, biobased metalworking lubricants are 1 to 1.5 times more expensive and biobased gear lubricants are 1.5 to 2 times more expensive [29], [30].

Based on these aspects, vegetable oils are undergoing extensive research in order to improve their physicochemical properties to compete with petroleum-based lubricants. To this end, they were subjected to chemical modifications such as esterification, transesterification, epoxidation and catalytic hydrogenation [31].

3.1.2 Chemical modification of vegetable oils

A glycerol molecule and three fatty acids constitute the structure of triglycerides. The vegetable oils fatty acids are generally long, linear carbon chains with nonconjugated double bonds. Oleic, linoleic and linolenic acids are predominant in the triglycerides of some vegetable oils, such as sunflower oil, palm oil, linseed oil, and soybean oil. The main weakness of vegetable oils, as lubricants, is their thermal and oxidation instability, which is due to the fact that (i) the β-hydrogen atom of glycerol is readily detached from the molecular structure, splitting the esters into acid and olefin, and (ii) the unsaturations of the fatty acid chains are highly reactive and react easily with oxygen in the air (Figure 3.2).

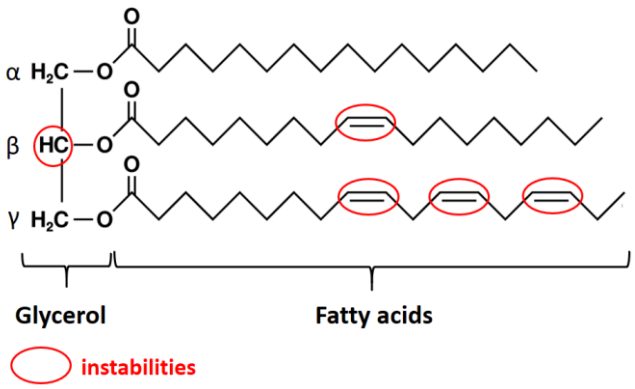

Figure 3.2: Example of a triglyceride structure. The red circle indicates the β-hydrogen and the unsaturation in the fatty acid chains [26].

Chemical modifications of vegetable oils can minimize these instabilities. They can be done by reactions on the carboxyl groups of triglycerides or on the olefinic function of the fatty acid chain (Figure 3.3). Transesterification/esterification reactions, hydrogenation, epoxidation, and the formation of estolides are the most common methods for modifying vegetable oils [32], [33]. Chemically modified vegetable oils are commonly applied directly as lubricants or additives for lubricant formulation. In the literature, additives produced from vegetable oils have shown remarkable tribological properties, even at severe pressures [18], [30].

In this project, we are interested in the transesterification method. It is a reaction in which an ester is transformed into another ester by exchanging the alkyl group. It produces fatty acid alkyl esters that can be directly utilized as biofuels or transesterified with polyalcohols to produce polyol esters as biolubricants. This reaction removes the hydrogen atom on the β-carbon from the oil structure, giving the formed esters a high degree of thermo-oxidative stability that is rarely found in vegetable oils [34], [35].

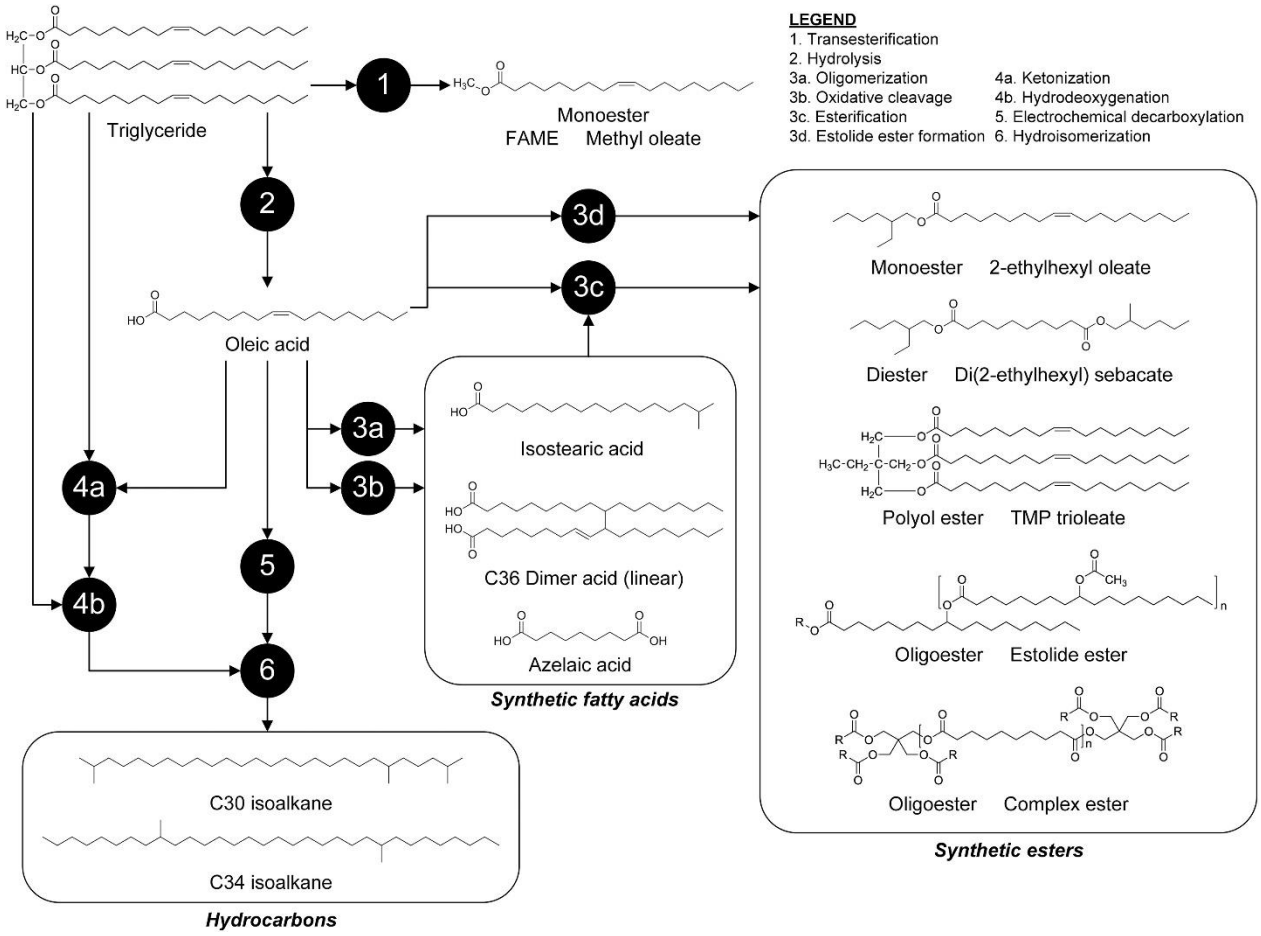

Figure 3.3: Possible biolubricants obtained by chemical modification of vegetable oil. Reprinted with permission from [36]. Copyright © 2015 Elsevier.

Esterification/Transesterification reactions

The production of biolubricants can be achieved by a two-step transesterification reaction (Figure 3.4). In the first step, the triglyceride reacts with a short chain primary alcohol such as methanol to form glycerol and a mixture of fatty acid methyl esters (FAME) [37]. The second step is the transesterification of the FAME with polyols (such as neopentyl glycol (NPG), trimethylolpropane (TMP), pentaerythritol (PE) and glycols (Gly)) to produce diesters or triesters biolubricants [38]–[40]. The length of the fatty acid chain in the triglyceride molecule (usually between 12 and 24 carbons) and the number of double bonds in that chain are the two most important factors affecting the characteristics of biolubricants. The longer the fatty acid, the higher

the viscosity and melting point of the biolubricant. However, the presence of double bonds reduces their viscosity and melting point as well as their oxidation stability [24].

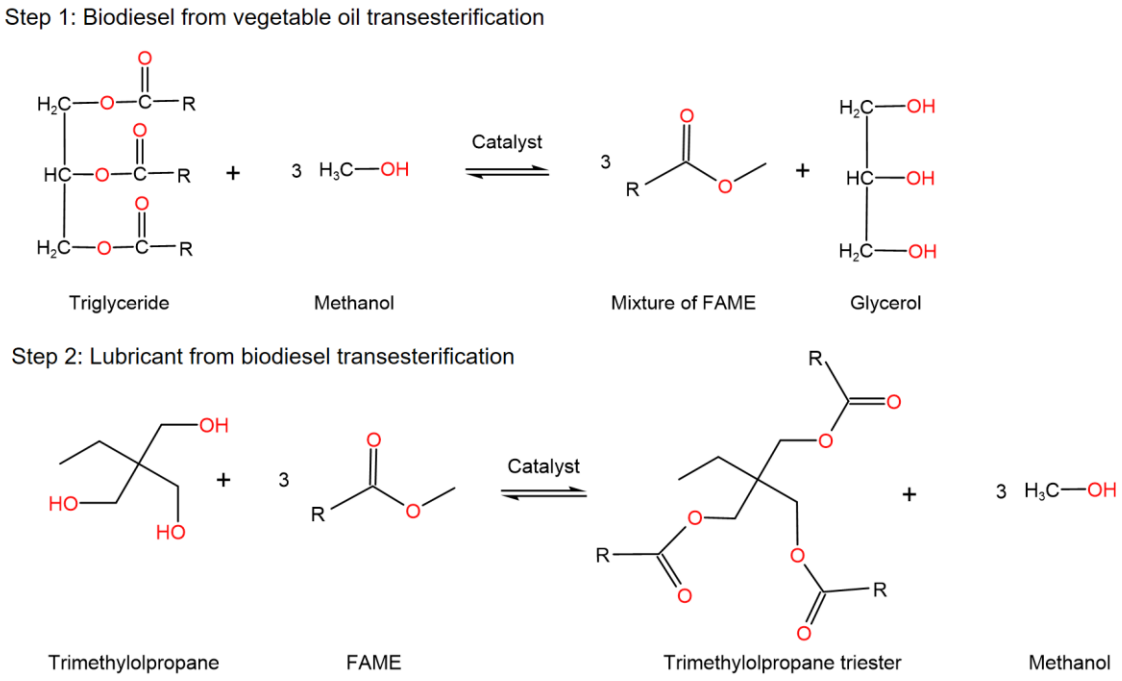

Figure 3.4: Two-step transesterification for the biolubricants production.

Different types of catalysts, homogeneous or heterogeneous with basic or acidic nature, or enzymes catalyzed the esterification or transesterification reactions. Homogeneous basic catalysts (like alkali hydroxides and alcoholates) are difficult to recycle and are prone to react with free fatty acids to form undesirable soap [38], [41], [42]. The acidic homogeneous catalysts (such as HCl, H_3PO_4, H_2SO_4) are also challenging to recycle, require high temperature operation, must be in high concentrations, and also pose severe corrosion and environmental problems [43]–[46]. Acid-catalyzed transesterification is rarely commercialized and is limited to the laboratory scale. The base-catalyzed reaction involves lower temperatures and is about 4000 times faster than the acid-catalyzed reaction [47]–[49]. Enzymes also catalyze transesterification, for example a lipase, Canda rugosa yielded 70 % of triester with a low reaction temperature (47 °C). However, this yield required a very long reaction time (72 h) [50]. Regardless of the long reaction time, the operational capacity of biocatalysts in a reaction is greatly impacted by the free fatty acids presence. Due to the problems mentioned with homogeneous catalysts and biocatalysts, heterogeneous basic

catalysts are more interesting for this type of reaction. The main advantage of using solid catalysts is their easy separation from the reaction medium (by simple filtration or centrifugation) and the possibility of reusing them [51]. The resulting process would therefore be less expensive and more environmentally friendly. Heterogeneous basic catalysts, such as supported metal oxides, alkaline earth oxides, and mixed oxides catalyzed transesterifications to produce biodiesel (Table 3.2). Various factors must be considered during transesterification, among which: alcohol:oil molar ratio, reaction temperature, catalyst type and concentration, and purity of reagents [16] .

Table 3.2: Examples of heterogeneous catalysts used in transesterification reactions to produce biodiesel.

Oil/ Reference	**MeOH:oil molar ratio**	**Catalyst type**	**Reaction conditions**	**Yield (%)**
Palm oil/ [52]	18:1	La-Ca/halloysit	150 °C, 7 wt%	97
Rapeseed oil/ [53]	24:1	Mg-Al-Na mixed oxide	117 °C, 4 wt%	75
Waste cooking oil /[54]	20:1	Cu/Zn/ γ-Al_2O_3	65 °C, 10 wt%	89
Palm oil/ [55]	15:1	CaO/wollastonite	65°C, 8 wt%	97
Rapeseed oil, [56]	18:1	CaO/MgO	64.5 °C, 6h, 2 wt%	92
Palm oil/[57]	5:3	TiO_2-CaO	65 °C, 0.5 wt%	95
Soybean oil, [58]	12:1	CaO	65 °C, 8 wt%, 3 h	95
Canola oil, [59]	9:1	K_2CO_3/nano CaO	65 °C, 3 wt%, 8 h	98
Castor oil/ [60]	6 BuOH:1 oil	MgO-Al_2O_3 ZnO/γ-Al_2O_3	80 °C , 5 wt%	97 85
Corn oil/[61]	16:1	CaO/SiO_2	60 °C, 6 wt%, 8 h	85
Rapeseed oil/ [62]	24:1	Mg-Fe mixed oxide	117 °C, 4 wt%	70
Palm kernel and coconut oils, [63]	65:1	$Ca(NO_3)_2/Al_2O_3$	60 °C, 15-20 wt%, 3h	94
Waste cooking oil /[64]	20:1	Zn/CaO	65 °C, 5 wt%	97
Soybean oil, [65]	9:1	CaO/Al_2O_3	150 °C, 3 wt%, 6 h	90
Waste cooking oil/ [66]	18:1	Fe/Ba/Al_2O_3	65 °C, 6 wt%	84
Jatropha oil/[67]	4:1	Ca-Mg-Al hydrotalcite	65 °C, 1.5 wt%	94
Sunflower oil/[68]	12:1	CaO/ZnO	60 °C, 1.3 wt%, 2h	> 90

Mechanism of transesterification catalyzed by a heterogeneous base

A base-catalyzed transesterification reaction proceeds in three steps (Figure 3.5)[69], [70]: In the first step, the base (B) reacts with the alcohol, generating an alcoholate (1) and a protonated catalyst. The alcoholate's nucleophilic attack on the ester's carbonyl group generates a tetrahedral intermediate (2) (step 2). This intermediate decomposes by expelling the alcoholate group (4) that was initially on the ester, forming the substitution product (3). The removed alcoholate deprotonates the catalyst (step 3), regenerating the active sites, which are then ready to react with another alcohol molecule, thus starting a new catalytic cycle.

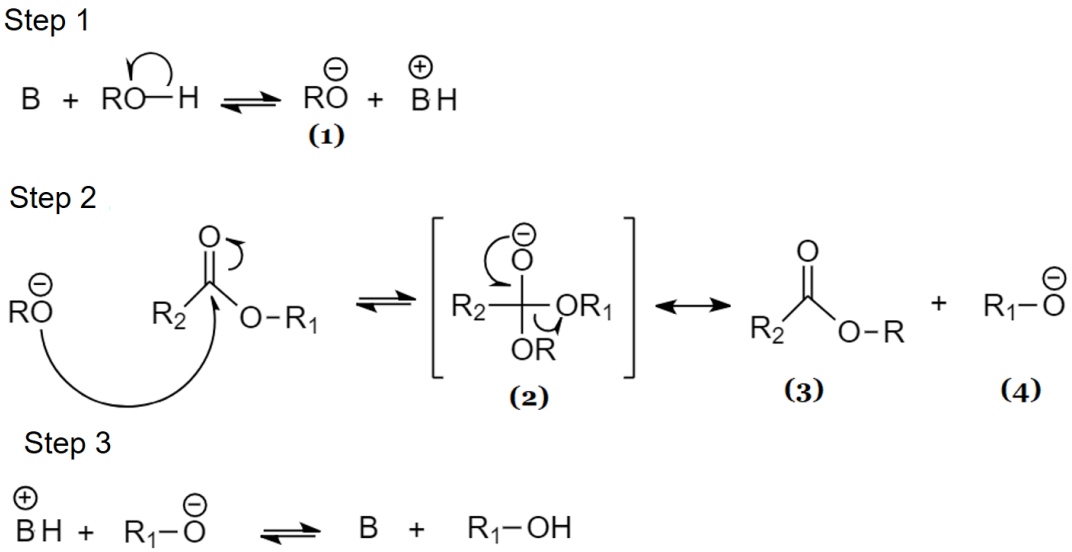

Figure 3.5: General mechanism of a base-catalyzed transesterification [69].

Referring to the mechanism described above, we propose a mechanism for the transesterification of a Fatty Acid Methyl Ester (FAME) with Trimethylene Glycol using CaO/SiO_2 as a basic heterogeneous catalyst (Figure 3.6). The abstraction of the Trimethylene Glycol proton through the active sites of the catalyst (Ca and O) to form an alcoholate anion is the first step of the reaction. The latter attacks the carbonyl group of the FAME forming an intermediate A. This intermediate decomposes to form the methanolate ion and the monoester (ME). The ME follows the same steps and reacts with another FAME molecule to form the diester (DE) lubricant. Since the

transesterification reaction is reversible, an excess of biodiesel and continuous methanol removal will aid in the reaction's completion.

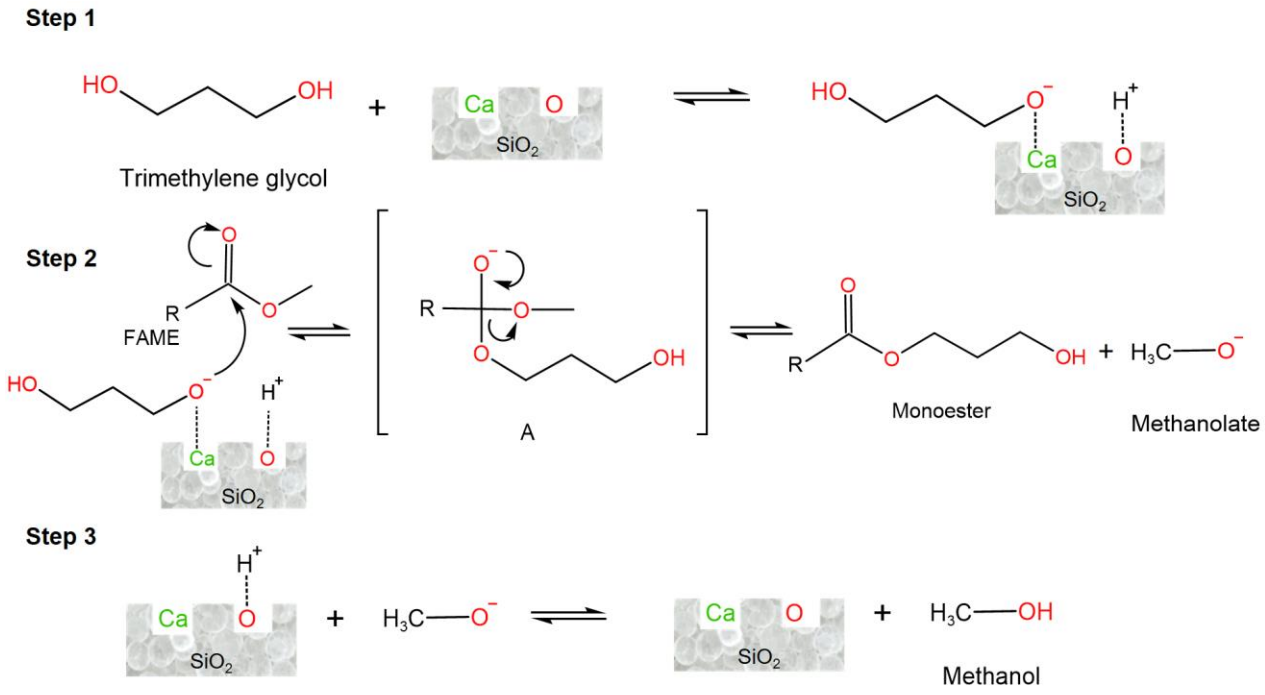

Figure 3.6: Mechanism of CaO/SiO_2-catalyzed transesterification of a FAME with Trimethylene Glycol to produce a diester-lubricant.

Conventional biolubricant synthesis processes are energy demanding, operate at reduced pressures and high temperatures (above 120 °C) (Table 3.3). Process intensification technologies improved yields of esterification and transesterification reactions and accelerated them under mild conditions. These technologies include; Reactive distillations[71]–[73], micro-reactors[74]–[76], centrifugal contractors[77]–[79], ultrasound [80]–[82], and microwave reactors [83]–[85].

Table 3.3: Reaction conditions for lubricant synthesis from traditional biodiesel transesterification [86].

Oil/ Reference	Polyalcohol	Catalyst	Reaction condition	Lubricant yield (%)
Palm biodiesel /[87]	TMP	$NaOCH_3$	140 °C, 25 mbar, 25 min, oscillatory	94.6
Jatropha biodiesel/ [88]	TMP	$NaOCH_3$	150 °C, 10 mbar, 3h	>80
Palm biodiesel/[38]	TMP	Calcium methoxide	180 °C, 50 mbar, 8h	92
Waste cooking oil biodiesel/ [89]	TMP	KOH	128 °C, 200 Pa, 1.5 h	86
Sunflower oil/[90]	Octanol	Fe-Zn double metal cyanide complexes	170 °C, 8h	98
Rapeseed biodiesel/[91]	PE ,NPG, TMP,	C Antrarctica lipase	35 °C, 50 h, 150 h, 200 h	98

3.2 Ultrasound basics

Ultrasound is a mechanical and elastic wave, which propagates through matter in liquid, solid or gaseous state. Ultrasound frequency surpasses the limit of human audibility (above 20 kHz). Low frequency ultrasound ranges from 20 to 100 kHz, intermediate frequency varies from 100 kHz to 1 MHz, and high frequency ranges from 1 to 10 MHz [92]. During the application of ultrasound, there is no direct interaction between the waves and the matter and they have no effect on the chemical bonds. The indirect phenomenon that induces chemical reactions is the acoustic cavitation.

3.2.1 Acoustic cavitation

Acoustic cavitation is the formation, growth, and implosion of bubbles in ultrasound-treated liquid. Sound waves create zones of compression (positive pressure) and expansion (negative pressure) as they propagate through the liquid. The intermolecular spaces, in the expansion zone, exceed the critical molecular distance, at very low pressure, resulting in the formation of void spaces or microbubbles in the liquid [34]. These cavities formed by mixtures of gases and vapours grow by

oscillating under the action of the acoustic pressure field and by agglomerating with other microbubbles [35]. In a few cycles, they grow to an unstable size and collapse violently, liberating an enormous amount of energy: the pressure and temperature can reach thousands of bars and Kelvin [93]–[96].These conditions lead to creation of radical species accompanied by light emission (sonoluminescence) [97](Figure 3.7). These radical species produced by acoustic cavitation can, under certain conditions, react with the surrounding medium. Cavitation generates shock waves and turbulent mixing of the liquid, promoting heat and mass transfer. It also generates very fine emulsions which considerably increase the reaction surface between the two phases. Thus, cavitation: (1) improves mass transfer by breaking the interfacial boundary layers between two immiscible liquid reactants [98], (2) generates high shear stresses that vigorously mix the liquid and reduce the particle size in the vicinity.

The physical effects of cavitation activate chemical reactions in heterogeneous systems. The cavitation bubble implosion, in a solid/liquid system, leads in significant physical and structural damage. Collapse in the vicinity of the powder surface generates sufficient energy to fragment the powder (even for finely divided particles). Therefore, ultrasound may increase the specific surface area of a catalyst in a heterogeneous reaction and provides further activation by enhancing mixing and mass transfer [99].

To summarize, acoustic cavitation may [39], [99];

- Generate free radicals, resulting in the initiation and propagation of new chemical reactions and reaction intensification.
- Increase selectivity and reaction yields.
- Reduce the reaction time.
- Allow working in mild conditions compared to conventional methods.
- Increase the catalyst efficiency used in the reaction (by increasing its specific surface area).

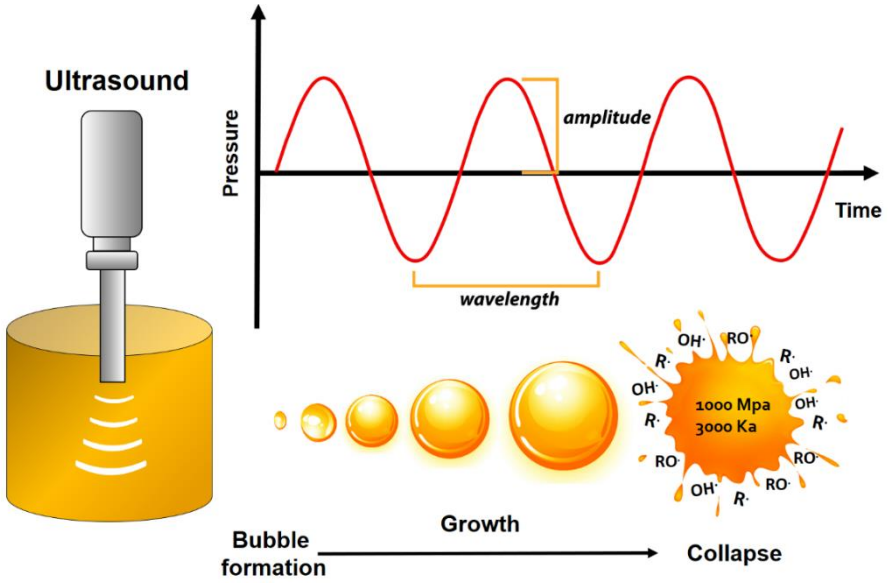

Figure 3.7: Acoustic cavitation mechanism [97].

3.2.2 Parameters affecting the sonochemical process

Temperature

When considering reaction conditions for a sonochemical process, it is important to carefully choose the operating temperature and solvent, as these are important and often interdependent factors. Any rise in temperature will increase the solvent vapor pressure and thereby facilitate the cavitation, but with a less violent collapse (decrease in maximum implosion temperature and pressure). This phenomenon is associated with a decrease in the surface tension and viscosity of the solvent. For a reaction activated by acoustic cavitation, a lower operating temperature is preferred if the solvent boiling point is low. Vice versa, for a reaction demanding high temperatures, a solvent with a high boiling point is recommended. Furthermore, higher temperatures reduce the solubility of gas in liquid, minimizing the amount of cavitation nuclei available. Consequently, raising the temperature may affect negatively the intensity of cavitation. An increase in temperature, on the other hand, may promote the kinetics of the reaction, so it exists an optimal temperature for a given system [100]. Since ultrasonic irradiation releases a large amount of heat into the system, it's critical to keep the temperature rises under control via jacketed

reactors or Rosett cells in order to keep the reaction at a specific temperature or prevent thermolabile chemicals from degrading [101].

Presence of dissolved gases and solids

Gases provide cavitation nuclei, which enhances the acoustic activity in the reactor and results in increased chemical and physical effects of cavitation. In the case of a dissolved gas loss in the system (which can occur due to overheating), bubbling of gas into the liquid may be employed to sustain the cavitation. The presence of dispersed solids has various effects on cavitation activity. Some studies reported positive effects[102], [103] (solid particles acting as cavitation nuclei) and others report negative effects, i.e., the presence of powders attenuates sound waves [104].

Physicochemical properties of the medium

The physico-chemical characteristics of the solvent, or gas in the bubble have an important impact on the bubble implosion. Bubbles form more easily when working with high vapor pressure, low viscosity, and low surface tension solvents, but the cavitation intensity is low. In fact, the higher the liquid vapor pressure, the higher the concentration of vapor in the bubbles, which dampens collapse. However, the cavitation intensity is striking when working with solvents with opposite properties (low vapour pressure and high viscosity and surface tension). The liquid's intermolecular forces need to be broken to form the cavities. Therefore, very dense solvents with high surface tensions and viscosity tend to have a higher cavitation threshold, but extreme conditions during cavitation [40], [105]. When working with high viscosity liquids, the ultrasonic amplitudes must be increased.

Ultrasound frequency

Low frequency ultrasound (20 kHz-100 kHz) generates intense acoustic cavitation that intensifies chemical reactions [35]. As the frequency of ultrasound increases to the MHz region, it becomes challenging to induce cavitation in liquids. Indeed, at very high frequencies, the expansion (and compression) cycle is extremely short, resulting in the formation of a very small bubble due to the small quantity of vapor diffusing inside the bubble [106]. This decreases the intensity of the collapse. For example, under constant conditions, irradiations at 20 and 500 kHz generated average bubble diameters of 330 and 13 µm, respectively, and the time of collapse was 10 and 0.4 µs [107].

Acoustic power

Increasing acoustic power improves acoustic yield by expanding the amount and diameter of the cavitation bubbles, as well as the maximum pressure and temperature during collapse [108]. However, this is only true up to a certain optimal power level, beyond which we may notice borderline effects or a decrease in sound processor performance [101], [109], [110]. Therefore, it is critical to tailor the power and experimental conditions to the application. It is also important to consider that very high power can quickly deteriorate the ultrasound transducer, affecting the sound waves transmission and contaminate the liquid.

An ultrasonic reactor operates in either continuous or pulsed mode. Boffito et al. [111], [112] reported that the pulsed sonication mode improved the conversion of triglycerides into esters. In fact, pulses reduce the rise in temperature in the reaction medium, thus avoiding overheating which risks evaporating the reagents and degassing the system, knowing that the dissolved gases promote acoustic cavitation.

3.3 Cavitation activity characterization in ultrasonic reactors

To optimize the operating parameters of a sono-reactor, it is essential to characterize the acoustic cavitation activity. This activity can be characterized by chemical or physical experimental methods that can be coupled with numerical simulations to optimize the acoustic field distribution in the reactor. Experimental methods such as calorimetry, thermal mapping, and hydrophonic measurements can be used to measure acoustic activity in the form of temperature and pressure changes in the reactor. Other methods, including aluminum erosion, electrochemical scattering, sonochemiluminescence, chemical dosimeters, electron paramagnetic resonance spectroscopy, and particle image velocimetry, can also quantify acoustic activity in terms of radical formation, micro-jets, or acoustic streaming in the system.

3.3.1 Physical methods

Calorimetry

The medium absorbs and scatters the ultrasonic waves as they pass through a liquid. The absorption of the sound waves convey to the medium an energy that increases its temperature.

The total amount of energy dissipated in the system can be determined by measuring the temperature change of the liquid. Calorimetry, a standard dosimetry method for measuring power rates in varied radiation fields and calibrating standard and regular dosimeters, quantifies the actual power given to the solution [113], [114]. Quantifying the temperature rise in calorimetric dosimeters gives a direct measure of the ultrasonic power dissipation. A thermocouple measures the temperature rise, and the power dissipated in the solution is calculated by (Eq. 3.1):

$$\text{Power (w)} = \left(\frac{dT}{dt}\right) C_p m \quad (3.1)$$

Where C_p, m, and (dT/dt) are respectively the specific heat capacity of the liquid ($J \cdot g^{-1} \cdot K^{-1}$)), the mass of the liquid (g) and the temperature difference per second ($K \cdot s^{-1}$).

The calorimetric technique can be utilized to calculate the system's energy efficiency by comparing the amount of energy dissipated in the system to the amount of electrical energy supplied.

Sonochemiluminescence

During the implosion of cavitation bubbles, heat generated can raise the liquid temperature to thousands of degrees during a very short time (microseconds). These intense thermal conditions induce the emission of light from the bubbles, a phenomenon called sonoluminescence. The intensity and duration of sonoluminescence are proportional to the bubble radius and depend on the frequency and amplitude of the ultrasound, the liquid nature, quantity of dissolved gases and the presence of solid particles [115]–[117]. The luminescent emission intensity from cavitation bubbles is significantly increased by adding a small quantity of luminol (3-aminophthalhydrazide) in alkaline solutions. This emission is termed sonochimiluminescence and is due to the oxidation of luminol by OH radicals (produced from water sonolysis) to yield 3-amino phthalate that gives a blue light spectrum (Figure 3.8) [118]. The SCL intensity can be measured with photocells or optical fibers connected to a photomultiplier in a dark environment [35]. Sonochemiluminescence is a common approach for mapping active cavitation zones in a reactor. Areas of active cavitation are indicated as illuminated regions, and the luminescence is proportional to the intensity of cavitation in terms of the number of implosions.

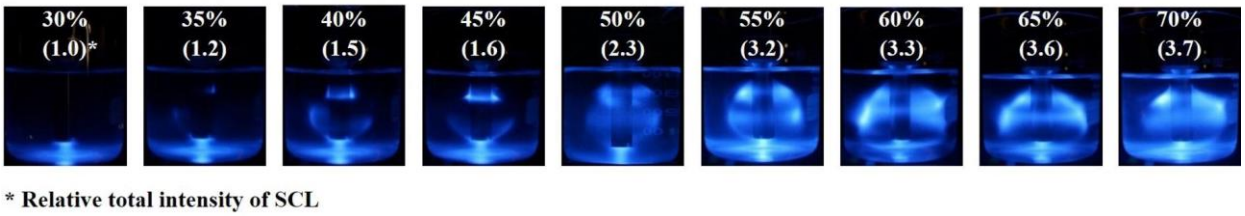

Figure 3.8: Sonochemiluminescence at different power intensities; adapted with permission from [119]. Copyright © 2020 Elsevier.

Hydrophone measurements

Hydrophones measure the intensity of the acoustic pressure generated by cavitation in a sonicated medium [118], [120]. Bubble oscillations in an acoustic field and shock waves due to bubble collapse introduce a variety of subharmonic/harmonic frequencies as background noise. Hydrophones use spectral frequency analysis to locate cavitation zones (Figure 3.9) [121]. The main limitation of this method is that they can be damaged by the intense cavitation since they are immersed in the sonicated liquid [101]. This distorts the distribution of cavitation activity in the reactor and affects the results.

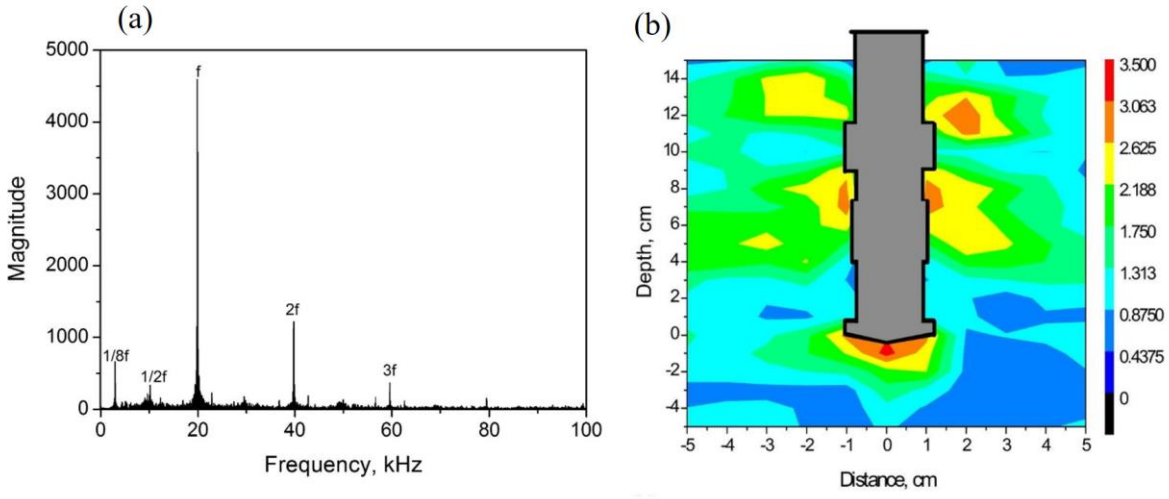

Figure 3.9: (a) Frequency spectrum measured by a hydrophone (1/8f and 1/2f are subharmonic frequencies, f is the resonant frequency, and 2f and 3f are ultraharmonic frequencies). (b) Acoustic field distribution around a probe from hydrophone measurements; reproduced with permission from [121]. Copyright © 2015 Elsevier.

Aluminum foil erosion

This process estimates qualitatively the acoustic pressure in the reactor as an erosion pattern on the aluminum foil (Figure 3.10) [120]. Erosion patterns are captured with a high-resolution digital camera, and this method is only suitable for low-frequency operation when the physical effects are considerable [118]. When operating at low frequencies, the cavitation bubble diameters are larger than when operating at high frequencies, resulting in the formation of micro-jets of higher intensity and thus significant physical impacts. The major limitation of this method is that it provides only qualitative distributions of cavitation activity. The aluminum presence in the medium may also disturb the propagation of sound waves and lead to biased results.

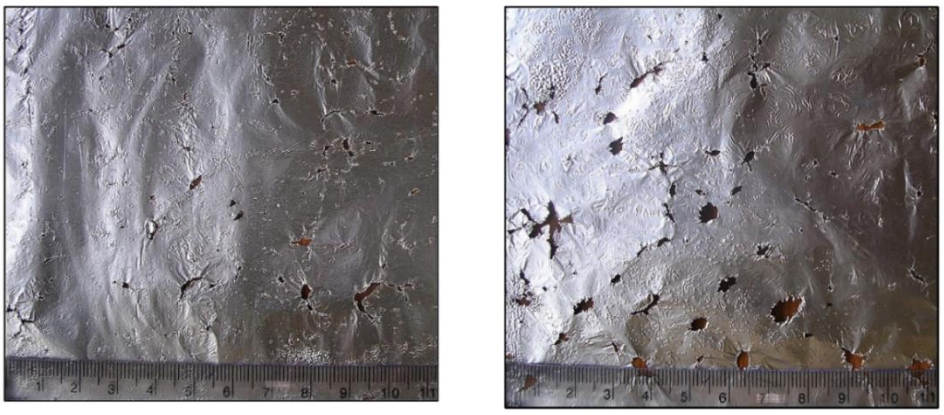

Figure 3.10:Aluminium foil erosion measured under dual and triple frequencies. Adapted with permission from [120]. Copyright © 2007 Elsevier.

3.3.2 Chemical methods

Electron Paramagnetic Resonance (EPR)

The electron paramagnetic resonance (EPR) spectroscopy characterizes and quantifies radicals using microwave absorption of these paramagnetic species in a magnetic field. Since free radicals decompose rapidly, their concentration is poorly detectable by EPR [122]. To address this, EPR is usually combined with a spin-trapping method. This method stabilizes short-lived

radicals R• by reacting them with the spin trap (often nitrones or nitroso compounds such as 5,5-dimethyl-1-pyrroline *N*-oxide (DMPO)), forming a more stable covalent paramagnetic adduct (spin adduct) that is detectable by EPR (Figure 3.11). Trapped radicals are then quantified and identified using EPR spectra of spin adducts [123], [124].

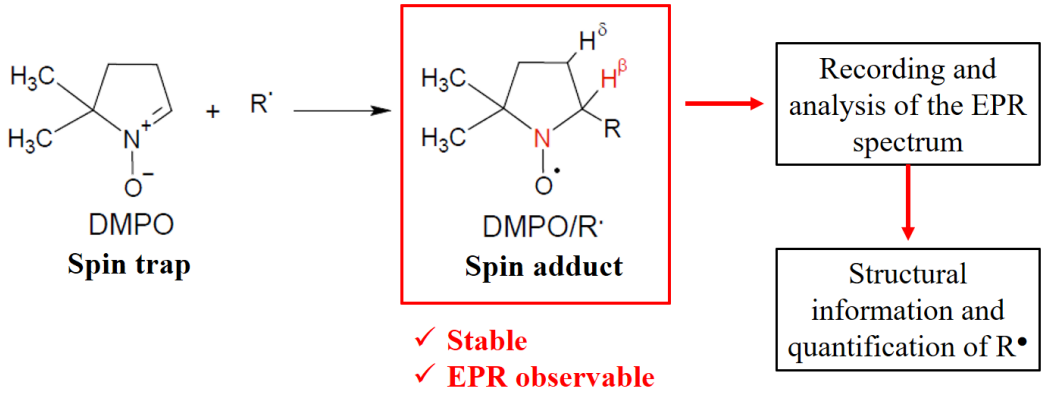

Figure 3.11: Example of spin trapping reaction with DMPO followed by EPR analysis.

Chemical dosimeters

Cavitation activity is measured by chemical dosimetry in terms of radical formation during bubble collapse. These reactive species initiate and propagate chemical reactions. Chemical dosimeters correlate the concentration of reacting molecules with the ultrasonic energy to calculate the sonochemical efficiency. The most common dosimeters are the terephthalate dosimeter [125], [126], the Fricke dosimeter [113], [127], [128] and the Weissler dosimeter.

- **Weissler dosimetry**

Weissler or KI dosimetry is a standard method for quantifying chemical cavitation effects adopted by Kumar et al. [12], [129], [130]. Cavitation measurements are performed by determining the amount of iodine released upon application of ultrasound to an aqueous potassium iodide solution. Cavitation activates the generation of hydroxyl radicals (•OH) and the reaction between these species leads to the formation of hydrogen peroxide (H_2O_2). The latter and the hydroxyl radicals act as oxidizing agents for iodide ions (I^-), and diiodine (I_2) is then released (reactions 1 to 4). Diiodine reacts with excess iodide ions and forms triiodide ions (I_3^-) (reaction 5); its absorption at

350 nm is utilized to quantify the iodine by UV spectrophotometry, and thus determine the concentration of •OH radicals generated.

$$OH^{\bullet} + I^{-} \rightarrow OH^{-} + I^{\bullet} \quad (1)$$

$$I^{\bullet} + I^{-} \rightarrow I_2^{-\bullet} \quad (2)$$

$$2\, I_2^{-\bullet} \rightarrow I_2 + 2I^{-} \quad (3)$$

$$H_2O_2 + 2I^{-} + 2\, H^{+} \rightarrow I_2 + 2H_2O \quad (4)$$

$$I_2 + I^{-} \rightarrow I_3^{-} \quad (5)$$

- **Terephthalate-based dosimeter**

This method is based on the reaction between terephthalate anions (terephthalic acid in alkaline aqueous solution) and hydroxyl radicals •OH that results in the generation of a highly fluorescent hydroxy terephthalate anion (HTA) (Figure 3.12) [115], [126]. The concentration of HTA is determined by fluorescence measurements. The fluorescence intensity is used to quantify the OH radicals generated during cavitational collapse [126].

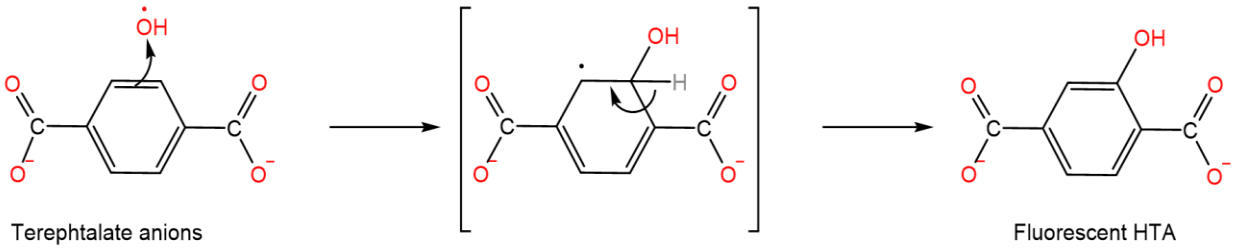

Figure 3.12: Mechanism of HTA formation.

- **Fricke dosimeter**

The Fricke dosimeter is a liquid chemical dosimeter, based on the ultrasonic irradiation-induced oxidation of ferrous ions, Fe^{2+}, to ferric ions, Fe^{3+}, in an acid medium [113]. In general, the Fricke solution contains $FeSO_4$ and sulfuric acid. The concentration of Fe^{3+} is measured by UV spectroscopy at 304 nm [127]. This dosimeter reacts with •OH radicals, hydrogen peroxide, H^{+}. From the oxidation reactions of Fe^{2+} to Fe^{3+} in Fricke's solution (equations1 to 3), the quantity

of radicals formed is estimated from the spectrophotometric measurement of the Fe^{3+} ions produced [128].

$$Fe^{2+} + OH^{\bullet} \rightarrow Fe^{3+} + OH^{-} \quad (1)$$

$$Fe^{2+} + OH^{\bullet} + H^{+} \rightarrow Fe^{3+} + H_2O \quad (2)$$

$$Fe^{2+} + H_2O_2 + H^{+} \rightarrow Fe^{3+} + H_2O + OH^{\bullet} \quad (3)$$

The main disadvantage of these dosimeters is that their application is restricted to water and quantifies hydroxyl radicals only. The Weissler and Fricke dosimeters' reliability has been questioned due to the presence of the hydroxylated compound, which may cause an overestimation of the $^{\bullet}OH$ radicals concentration produced during sonication [131].

3.4 Ultrasound-assisted transesterifications

Ultrasound enhanced several transesterification reactions particularly for biodiesel synthesis [111], [132]–[136]. Transesterification for biodiesel production involves reactions between oil and alcohol in the presence of a catalyst. Since the oil and alcohol are immiscible, the traditional reaction requires continuous mixing for long periods of time to facilitate contact between the reactants and the catalyst. Ultrasound intensified these reactions through the chemical and physical effects of acoustic cavitation. The physical effects arise as fine emulsions between immiscible reactants [137]. The bubbles collapse generates microturbulence that disrupts the phase boundary and leads to the formation of microemulsion, providing large surfaces for the reaction. This increases the interfacial exchange area between the micro-phases and improves heat and mass transfer. Georgogianni et al. demonstrated that emulsions generated by ultrasound have smaller and more stable droplets than those obtained by traditional techniques, which improves the mass transfer in the liquid-liquid reaction system [82]. In addition, the amount of catalyst required for an ultrasonically assisted process is generally less than that required for mechanical agitation [136]. Ultrasound chemical effects result in the formation of radical species (e.g., alkoxy radicals) that initiate and propagate transesterification reactions. The optimization of these effects lead to a significant increase in reaction rates. Deng et al. proved that ultrasonically assisted transesterification is an effective approach for the production of biodiesel from jatropha oil [138]. They obtained a fatty acid methyl ester yield of 96.4 % in only 30 minutes. Georgogianni et al.

reported that ultrasound-assisted transesterification of cottonseed oil under optimized reaction parameters achieved 90 % yield in 60 min, while they obtained 80 % ester using mechanical agitation for the same reaction time [139]. Boffito et al. compared the performance of conventional transesterification with that assisted by ultrasound [111]. They achieved a biodiesel yield of 70 % after one minute of sonication. This yield was only achieved after 60 minutes in the stirred reactor. Chen et al. produced biodiesel from ultrasound-assisted transesterification of palm oil [80]. Calcium oxide CaO catalyzed the reaction. They screened the effect of the following factors on the yield of biodiesel at a fixed temperature of 60 °C: (1) Ultrasound amplitude (30-80%), (2) reaction time (1-3 h), (3) oil/methanol molar ratio (1:3 - 1:15), (4) catalyst loading (9-10%). They obtained a maximum yield of 92.7 % after 1 h of reaction with an amplitude of 60 %, an oil/methanol molar ratio of 1:9, and 8 wt% of the catalyst. Boffito et al. improved biodiesel production in continuous and batch ultrasonic reactors [111]. After 18 seconds of sonications, the biodiesel yield was 90 %, with a reaction 300 times faster than in a conventional mixing reactor.

Data on ultrasound-assisted biolubricant production are still very limited. Only these five works applied ultrasound to synthesize lubricants: 1) Patience et al. esterified trimethylene glycol with oleic acid in the presence of Amberlyst®15 using 750 W and 500 W ultrasonic horns [140]. They formed a diester biolubricant with a two hours faster stoichiometric reaction than the traditional process. 2) Arumugam and co-authors produced a pentaerythritol ester lubricant in 81.4 % yield using ultrasound with 60 % amplitude and at 100 °C [141]. 3) Almasi and co-authors transesterified rapeseed methyl ester and TMP with ultrasound. They obtained 82 % lubricant after 1 h of reaction [142].4) Gawas and Rathod synthesized a cosmetic biolubricant by ultrasound-assisted biocatalyzed esterification of 2-ethylhexanol and stearic acid [143]. They obtained a conversion of 96 % with a molar ratio of 2:1 between 2-ethylhexanol and stearic acid, 2 wt% of enzyme (Fermase), an ultrasonic power of 80 W, and a temperature of 50 °C in 3h. Knowing that the traditional reaction lasted 7 h to achieve the same conversion. 5) Chengareddy et al. used an ultrasound-assisted transesterification process to produce a rapeseed oil-based pentaerythritol ester, a potential biolubricant for alternative air compressors [144].

CHAPTER 4 ARTICLE 1: ELECTRON PARAMAGNETIC RESONANCE OF SONICATED POWDER SUSPENSIONS IN ORGANIC SOLVENTS

Héla Laajimi, Michela Mattia, Robin S. Stein, Claudia L. Bianchi, Daria C. Boffito

Article published in Ultrasonics Sonochemistry, available online 26 March 2021.

Abstract

The chemical effects of the acoustic cavitation generated by ultrasound translate into the production of highly reactive radicals. Acoustic cavitation is widely explored in aqueous solutions but it remains poorly studied in organic liquids and in particular in liquid/solid media. However, several heterogeneous catalysis reactions take place in organic solvents.

Thus, we sonicated trimethylene glycol and propylene glycol in the presence of silica particles (SiO_2) of different sizes (5-15 nm, 0.2-0.3 µm, 12-26 µm) and amounts (0.5 wt% and 3 wt%) at an ultrasound frequency of 20 kHz to quantify the radicals generated. The spin trap 5,5-dimethyl-1-pyrrolin–N-oxide (DMPO) was used to trap the generated radicals for study by electron paramagnetic resonance (EPR) spectroscopy. We identified the trapped radical as the hydroxyalkyl radical adduct of DMPO, and we quantified it using stable radical 2,2,6,6-tetramethyl-1-piperidinyloxy (TEMPO) as a quantitation standard. The concentration of DMPO spin adducts in solutions containing silica size 12-26 µm was higher than the solution without particles. The presence of these particles increased the concentration of the acoustically generated radicals by a factor of 1.5 (29 µM for 0.5 wt% of SiO_2 size 12-26 µm vs 19 µM for 0 wt%, after 60 min of sonication). Ultrasound produced fewest radicals in solutions with the smallest particles; the concentration of radical adducts was highest for SiO_2 particle size 12-26 µm at 0.5 wt% loading, reaching 29 µM after 60 min sonication. Ultrasound power of 50.6 W produced more radicals than 24.7 W (23 µM and 18 µM, respectively, at 30 min sonication). Increased temperature during sonication generated more radical adducts in the medium (26 µM at 75 °C and 18 µM at 61 °C after 30 min sonication). Acoustic cavitation, in the presence of silica, increased the production of radical species in the studied organic medium.

Keywords: *EPR, spin trapping; ultrasound; free radicals; solid particle; organic solvent; sonochemical activity quantification*

4.1 Introduction

Low-frequency ultrasound (US, 20 kHz to 100 kHz) finds applications as a process intensification technology in many fields such as chemical synthesis (in homogenous and heterogeneous systems) [100], [145], food industry [146], [147], pharmaceutical [148], [149], water treatment [150]–[152] biotechnology [153], polymer chemistry [154]. When combined with heterogeneous catalysis, US promotes and accelerates reactions, and increases the yield of organic syntheses through cavitation [155].

Acoustic cavitation is the formation, growth, and implosive collapse of bubbles in a liquid irradiated with ultrasound [156]. When sound waves pass through the liquid, they generate areas of compression (positive pressure) and expansion (negative pressure). At very low pressure in the expanding region, the intermolecular spaces exceed the critical molecular distance and voids or microbubbles form in the liquid [34]. The size of these vapor-filled cavities oscillates in phase with the compression and expansion cycles (stable cavitation), growing under the effect of the sound pressure field [35]. Over a few cycles, they grow and reach an unstable size and implode violently, releasing phenomenal energy over a very short period of time (100 ns): the pressure and the temperature reach locally about 1000 MPa and 3000 °C, respectively [16–18]. At these conditions, the molecules trapped in the cavitating bubbles dissociate and generate radical plasma. In addition, cavitation induces local turbulence and microcirculation of the liquid thereby improving heat transfer locally and mass transfer both microscopically and macroscopically [125]. The combination of the chemical and mechanical effects of cavitation initiates and propagates chemical reactions [159]. Furthermore, ultrasonic cavitation creates small droplets of two immiscible or partially immiscible phases, which significantly increases the surface available for the reaction between two phases and accelerates the reaction rate [81].

Various sonochemical dosimetry methods measure the acoustic activity by detecting hydroxyl radicals; such as the terephthalate dosimeter (which reacts with hydroxyl radicals to generate 2-hydroxyterephthalate) [19, 22], the Fricke dosimeter (whereby hydroxyl radicals oxidize Fe^{2+} in acid solution) [23–25] and the Weissler dosimeter (where molecular iodine forms from a series of reactions involving iodide and hydroxyl radicals) [15, 26, 27]. Rajamma et al. [131] recently reviewed the Weissler [160], Fricke [161] and terephthalic acid [162] methods. Under the same conditions, they observed that the first two methods detect a higher $^{\bullet}OH$ radical yield than the

terephthalic acid method. This was partially, but not fully, explained by the presence of additional hydroxylated products in the case of the first two methods. The reliability of the Weissler and Fricke dosimeters is therefore called into question because of the involvement of the hydroxylated product that can lead to an overestimation of the concentration of •OH radical generated during sonication. The authors conclude that, however, these dosimetry methods remain key to quantify the relative difference in acoustic activity of a system working at different operating conditions. The application of these dosimeters is limited to water and only quantifies hydroxyl radicals.

There are other methods for quantifying other radicals, such as sonoluminescence [163], subharmonic analysis [164], laser holography [165], and electron spin resonance (ESR) or electron paramagnetic resonance (EPR) [35]. EPR spectroscopy utilizes microwave absorption of paramagnetic species in a magnetic field to characterize and quantify them. Free radicals are often key intermediates in chemical reactions, but their high reactivity means shorter lifetimes and low average concentration detectable by EPR [122]. The spin trapping method is a technique employed to stabilize the short-lived radicals; the radical reacts with the spin trap forming a more stable covalent paramagnetic adduct (spin adduct), which is EPR observable. The EPR spectra of the spin adducts allow the quantification and the identification of the spin trapped radicals [123], [124].

In addition, the spin-trapping technique increases the chance of detecting radicals due to the integrative nature of the spin-trapping process: the rate of spin adduct formation is much higher than the rate of spin adduct decay, and therefore there is a gradual build-up of trapped radicals [167].

Various cyclic nitrones such as 5,5-dimethyl-1-pyrrolin–N-oxide (DMPO) have been successfully exploited in spin trapping experiments [167]–[169]. DMPO is effective in trapping alkyl *(*R•*)*, hydroxyl (•OH) and alkoxy (•OR*)* radicals (Figure 4.1), because the presence of the two β-methyl groups hinders the disproportionation of the resulting spin adducts, thus rendering them more stable [170], [171].

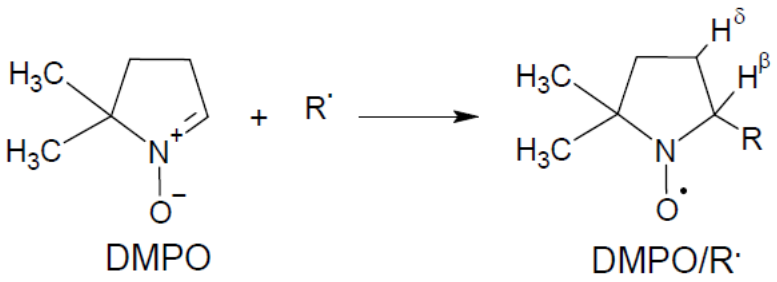

Figure 4.1: DMPO spin trapping

In the literature, most sonolysis studies by EPR have been conducted in water. Xu et al. identified reactive radicals ($SO_4^{\bullet-}$ and $^{\bullet}OH$) with EPR using DMPO spin trapping to analyze the mechanisms of interactions between ultrasound and peroxymonosulfate on the degradation of pollutants in water [172]. Wei and coworkers applied EPR to examine the kinetics and mechanism of ultrasonic activation of persulfate [173]. They measured the hydroxyl radical ($^{\bullet}OH$) and sulfate radical anion ($SO_4^{\bullet-}$) yield using DMPO as a spin trap. Migik and Riesz identified radical intermediates formed during the sonolysis of some organic liquids and aqueous solutions [167]. In organic liquids, they adopted nitrosodurene and 2,4,6-tri-tert-butylnitrosobenzene as nitroso spin traps. Castellanos et al. investigated the sonolysis of water and ethylene glycol, methanol, and chloroform by EPR-spin trapping at 20 kHz and 475 kHz [174]. The nature of the detected radicals spin adducts was dependent on the sonication time or ultrasound frequency.

Despite ultrasound as a process intensification technique being increasingly applied to mixtures containing solids, especially catalysts, there is a lack of literature on the quantification of chemical effects of ultrasound in the presence of powders. Quantifying these effects would aid in identifying synergies in process intensification and catalysis, maximizing yields and selectivity, and decreasing energy requirements [175].

Barchouchi et al. recently investigated the effect of the presence of solids (glass beads) on acoustic activity at frequency from 20 kHz to 1135 kHz [176]. The glass beads were used in concentrations ranging from 3.2×10^{-3} to 80 $g\cdot L^{-1}$ and with sizes between 8-12 and 6000 µm in diameter. While the calorimetric quantification (measurement of the power rate dissipated in the solution) did not seem affected by the particles, the chemical activity (Weissler method) sharply decreased beyond a certain surface area value. Barchouchi et al. also reviewed previous work done on the

determination of the acoustic activity in heterogeneous media. All these data were gathered in water and still, the literature on the subject remains limited [176].

In this work, we assessed for the first time the chemical effects of acoustic cavitation by identifying and quantifying the free radicals generated when bubbles implode in organic slurry solutions. In this research, EPR quantified the acoustically generated radicals, trapped by DMPO, in organic solvents (propylene glycol and trimethylene glycol) and in the presence of solids (SiO_2) of different particles size (5-15 nm, 0.2-0.3 µm, 12-26 µm). We chose these two organic solvents because in subsequent work we will transesterify vegetable oils with propylene-glycols to produce diester biolubricants. Our goal is to relate the acoustic yield to the conversion and selectivity towards biolubricants to minimize energy requirements.

We chose EPR because of its high sensitivity, specificity, and the simplicity of sample preparation. Moreover, it requires small aliquots of sample [177]. For instance, Abbas et al. could detect a concentration of radicals between 2 and 3 µM for a 25 µL sample, using conventional X-band with a frequency of about 9.4 GHz [178], [114]. Besides investigating the acoustic activity in the two different solvents in the presence of SiO_2, we also quantified the effects of the ultrasonic power and the temperature, in order to identify the optimal conditions to intensify the heterogeneous reaction associated with ultrasound.

4.2 Materials and methods

4.2.1 Sonolysis experiments

A 500 W nominal power ultrasonic processor (Sonics & Materials, Inc., Newtown, USA) and a solid probe (1.3 cm tip diameter, 25.4 cm length) sonicated a 50 mL of trimethylene glycol or propylene glycol (Sigma-Aldrich , St. Louis, Mo, USA). The glycol solution was at a concentration of 8 mM of the spin trap 5,5-Dimethyl-1-pyrroline N-oxide (≥97.0% DMPO, Fisher Scientific, Waltham, MA, USA). The processor operated at a fixed frequency of 20 kHz. The sonolysis experiments occurred in a 100 mL jacketed glass reactor (inner diameter = 4 cm, height = 10 cm) in the presence of SiO_2 particles (Sigma-Aldrich) of various sizes (5-15 nm, 0.2-0.3 µm, 12-26 µm) and concentration (0.5 wt% and 3 wt%). A Fisher Brand™ (Ottawa, Ontario) thermostatic bath with water circulation connected to the jacket of the reactor maintained the temperature constant

(62 ± 1 °C or 74 ± 1 °C). The irradiation time was 60 min with continuous ultrasonic irradiation. We sampled 40 µL of solution every 10 min for EPR measurement.

4.2.2 Calorimetry

We measured the actual power delivered to the solution with calorimetry, which is a standard method in dosimetry used both to measure power rates in various radiation fields and to calibrate standard and routine dosimeters [23,51]. The quantification of the temperature rise in calorimetric dosimeters provides a direct measurement of the absorbed power. A thermocouple (K type) measured the rise in temperature and we calculated the ultrasonic power dissipated in the solution by (Eq. 4.1):

$$Power\ (w) = \left(\frac{dT}{dt}\right) C_P m \quad (4.1)$$

Where C_p, m and (dT/dt) are respectively the specific heat capacity of the liquid ($J \cdot g^{-1} \cdot K^{-1}$)), the mass of the liquid (g) and the temperature difference per second ($K \cdot s^{-1}$).

This expression derives from the global calorimetric power dissipation after neglecting some parameters (Eq. 4.2): Calorimetric power dissipation = (Energy utilized to raise the temperature of bulk liquid) + (Energy absorbed by reactor walls and transducers) + (Energy lost to ambient air by convection) [180]:

$$P_{cal} = (mC_P\Delta T)_{liquid} + (m_i C_{pi}\Delta T)_{inner\ reactor\ wall} + (hA\Delta T) \quad (4.2)$$

Where m is the mass of liquid (g), m_i is the mass of the reactor/transducers (g), $C_p$is specific heat of liquid at constant pressure ($J.g^{-1}.K^{-1}$), C_{pi} is the specific heat of the material of the reactor ($J.g^{-1}.K^{-1}$), ΔT is the change in temperature (K), h is the convective heat transfer coefficient ($W.m^{-2}.K^{-1}$) and A is the area of the heat transfer (m^2).

We did not consider heat dissipated by the reactor walls and transducers, or the loss of energy in the ambient air due to convective heat transfer. Working at the laboratory scale with a volume of a few mL and small contact surface (liquid-wall, liquid-air), we can assume that heat losses by convection and conduction represent a negligible fraction of the global energy. These approximations result in about 5 % error on the measurement [17,52].

4.2.3 Electron paramagnetic resonance measurements and TEMPO calibration

We analyzed all the samples immediately after the sonication experiment, to avoid spin adduct decomposition. We transferred the 40 µL samples to 4 mm quartz EPR tubes to avoid paramagnetic impurities. A Bruker Elexsys E580 X-band EPR Spectrometer with 100 kHz modulation frequency and a microwave power level of 6.5 mW were used to record spectra. All spectra were recorded at room temperature. Each EPR measurement was repeated three times. Further parameters are given in Table 4.1. We used the SpinFit module in the Bruker Xepr software to simulate the spectra observed and thereby measure the hyperfine coupling constants to nitrogen (a_N) and hydrogen (a_H), which give information about the nature of trapped radicals.

We created a calibration curve from solutions of the stable radical 2,2,6,6-tetramethyl-1-piperidinyloxy (TEMPO) in trimethylene glycol to quantify spin adduct concentration. We prepared a 6-point calibration curve of TEMPO (Figure 4.2). We expressed the spin adduct yields in concentration units by double integration of the simulated spectra and compared them with the double integrals of TEMPO peak areas at known concentrations (1 µM, 10 µM, 50 µM, 100 µM, 250 µM).

Table 4.1: Electron paramagnetic resonance experimental parameters.

Parameter	Unit	Value
Microwave frequency	GHz	9.7
Modulation frequency	kHz	100
Attenuation	dB	15
Microwave power	mW	6.5
Modulation amplitude	G	3
Time constant	s	1.28
Sweep time	s	83.89
Number of scans	-	3
Center field	G	3510.00

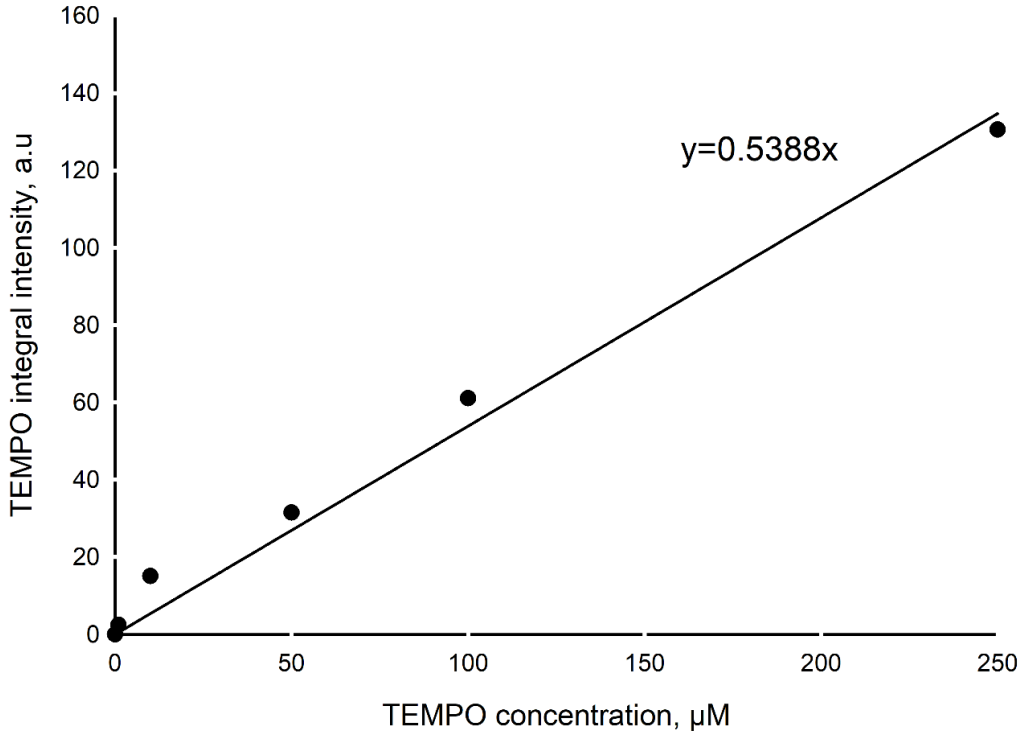

Figure 4.2: Standard curve relating double integrated intensity of TEMPO signal to concentration of TEMPO.

4.3 Results and discussion

4.3.1 EPR spectra and identification of radical adducts

The fragmentation of trimethylene glycol occurs mainly by breaking the C-C or C-O bonds. The possible radicals are: $^{\bullet}CH_2OH$, $^{\bullet}CH_2CH_2OH$, $^{\bullet}CH_2CH_2CH_2OH$ and $^{\bullet}OH$. The EPR spectrum (Figure 4.3) of the DMPO adduct generated in trimethylene glycol contains six lines as a result of hyperfine coupling to nitrogen (I=1, a_N=1.522 mT) and hydrogen (I=1/2, a_H^{β} = 2.171 mT) in the β position with respect to the nitrogen. The coupling to hydrogen is greater than that to nitrogen, indicating that the trapped radical is centred on a carbon atom [37,45]. Therefore, we excluded the detection of the hydroxyl radical $^{\bullet}OH$ (a_N=1.42 mT and a_H^{β} = 1.16 mT in 1-octanol [53,54]). Moreover, the main information on the nature of the radicals trapped by DMPO comes from the value of the β hydrogen hyperfine coupling constant (a_H^{β}). Specifically, for alkyl radical adducts,

$a_H^\beta \geq 2.0$ mT, while $0.6 \geq a_H^\beta \geq 0.8$ mT for alkoxy radicals [169], [182], [183], [184], [185]. This confirms the absence of an alkoxy radical. The values of the hyperfine coupling constants match those reported for the DMPO /Hydroxyalkyl radical adduct (Table 4.2) [170], [186]. Therefore, we conclude that the spectra observed correspond to a Hydroxyalkyl radical.

Table 4.2: EPR Spectral Parameters for DMPO/ Hydroxyalkyl Radicals adduct

Radical	**Solvent**	a_N **,mT**	a_H^β**, mT**	**g**	**References**
$^\bullet$ROH	Trimethylene glycol	1.52	2.17	2.006	This work
$^\bullet CH_2OH$	Ethylene glycol	1.56	2.10	-	[174]
$^\bullet CH_2OH$	Water/methanol	1.59	2.26	2.0055	[170][186]
$^\bullet CH_2OH$	Water	1.58	2.23	2.0056-2.0062	[187]
$^\bullet CH_2OH$	Methanol	1.52	2.14	2.00563	[188]
$^\bullet CH_2CH_2OH$	water	1.598	2.28	2.0057	[182][184]
$^\bullet CH_2CH_2CH_2OH$	water	1.56	2.56	-	[189]

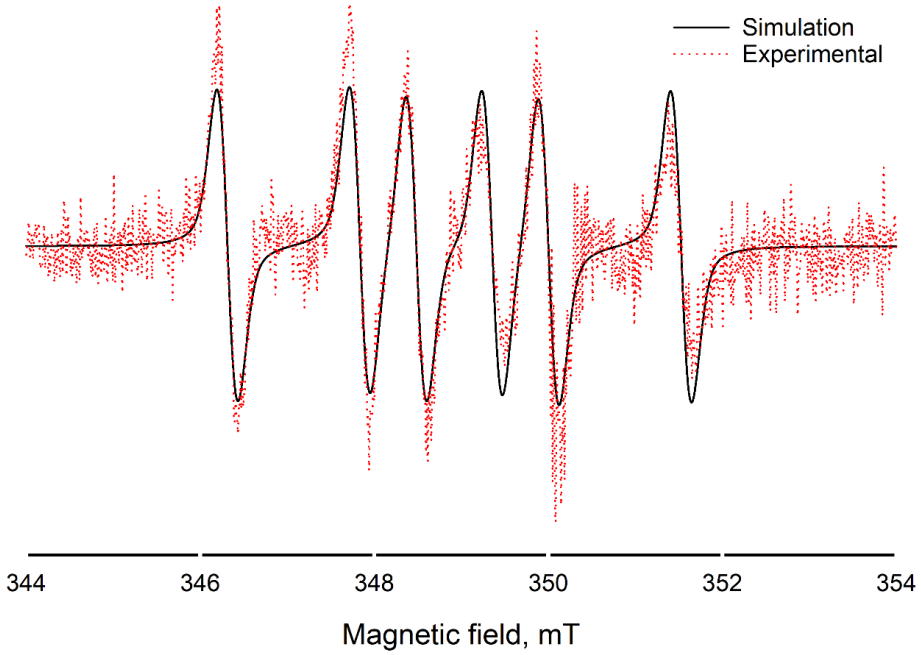

Figure 4.3: Comparison of simulated and experimental data (60 min of sonication in trimethylene glycol). Simulation parameters: a_N = 1.521 mT, a_H^β= 2.171 mT, g= 2.006.

4.3.2 Effect of SiO_2 particle size and concentration

When sonication starts, radicals form in our experimental conditions. We can detect radical adducts after 5 min of sonication and their concentration in the media increases with time (Figure 4.4). The concentrations reach a plateau between 30 min and 40 min of sonication (Figure 4.5 and 4.6), indicating that formation and decomposition of adducts are in equilibrium [190]. In a separate experiment, we tracked the decomposition rate of the radicals after sonication (lasted 60 min) stopped. After 105 min, there are no more radicals in the solution in the absence of solids (Figure 4.7).

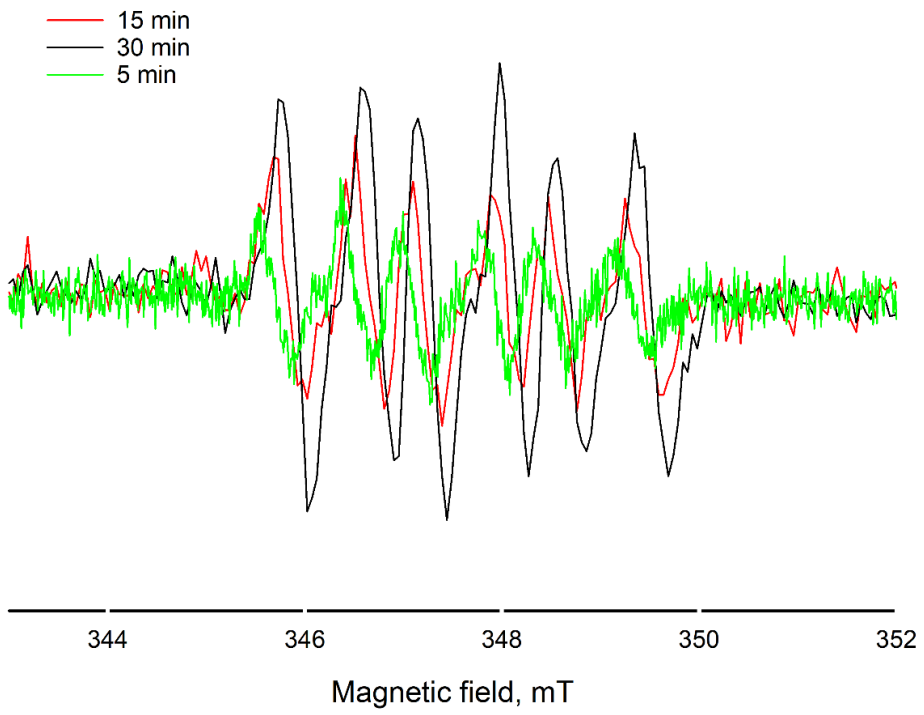

Figure 4.4: EPR spectra of radical adduct generated in trimethylene glycol. Spectra were acquired immediately after sonication for the period of time indicated in the figure legend. (US power= 24.7 W, T= 61 °C, particle diameter= 12-26 µm, 3 wt%).

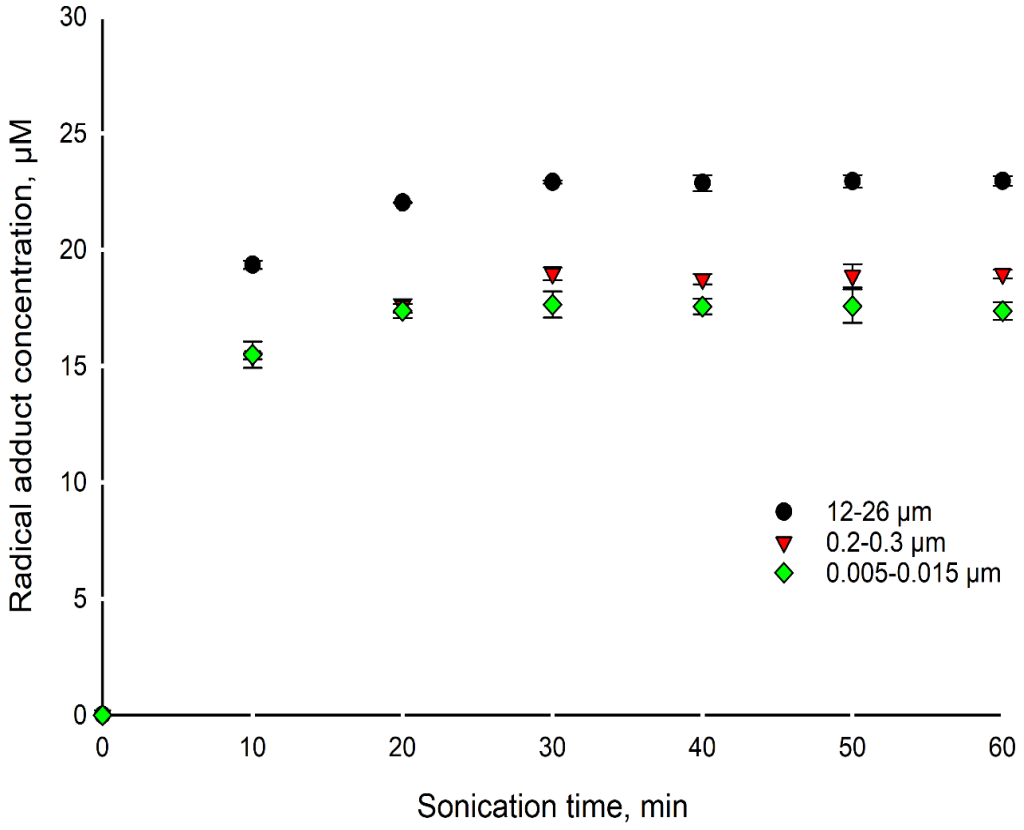

Figure 4.5: SiO_2 size effect with 3 wt% of solid and different particle size (in trimethylene glycol, US power= 24.7 W, T= 61 °C), error bars represent the sample standard deviation.

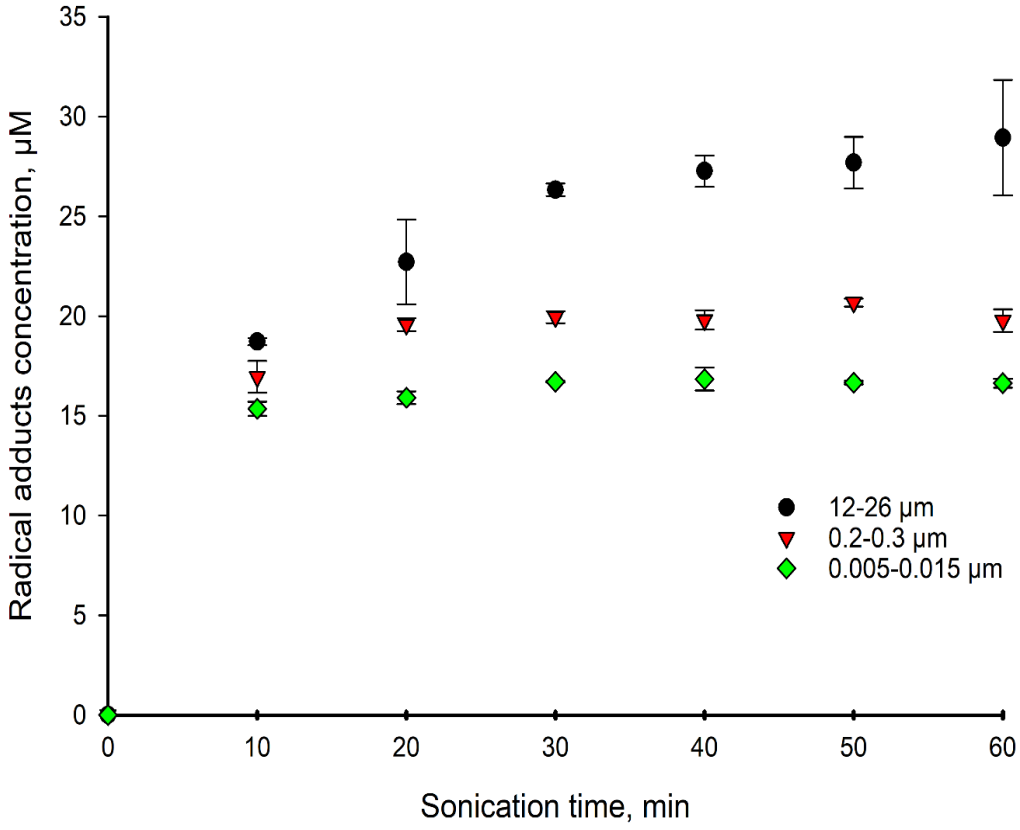

Figure 4.6: SiO_2 size effect with 0.5 %wt of solid and different particle size (in trimethylene glycol, US power= 24.7 W, T= 61 °C), error bars represent the sample standard deviation.

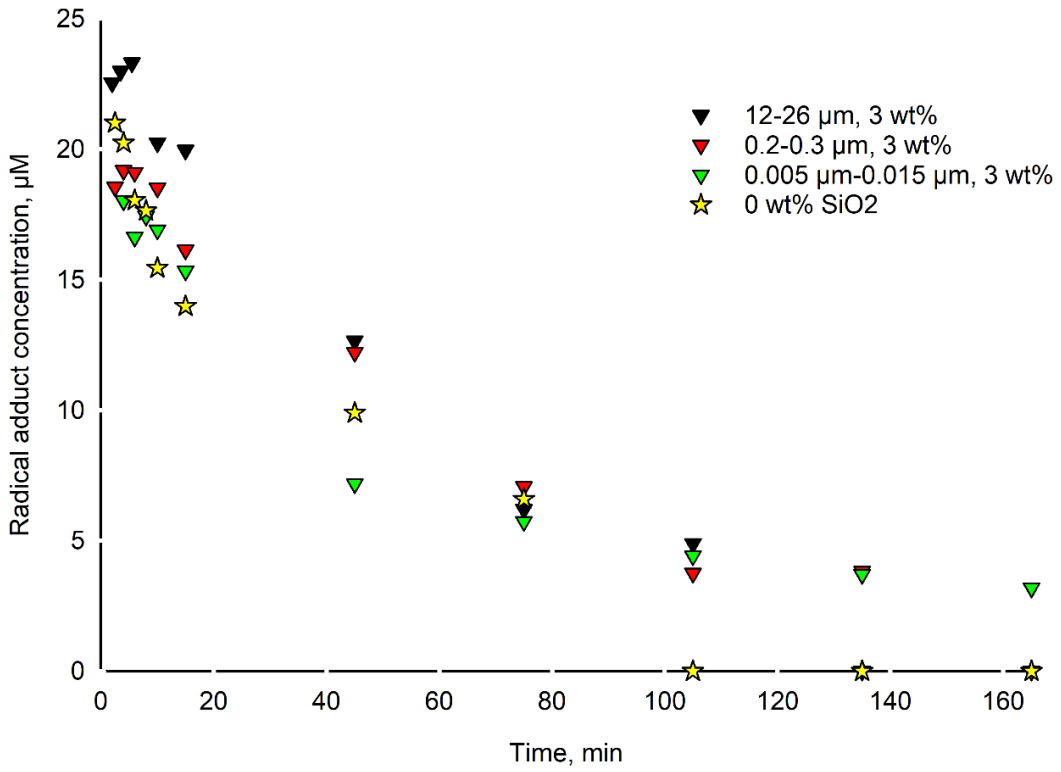

Figure 4.7: Radical adduct decomposition in the presence of SiO_2 particles of different sizes and at different concentrations following 60 min sonication in trimethylene glycol. In the plot, time t=0 indicates the end of the sonication period.

The size effect results (Figures 4.5 and 4.6) for both loadings of silica particles (3 wt% and 0.5 wt%) show that the concentration of radical adduct increases with particle size. For example, after 60 min sonication, the radical adduct concentration was twice as high for 12-26 µm than for 5-15 nm particles (for 0.5 wt% solids, 29 µM versus 16 µM, respectively). This can be rationalized in that the number of nucleation sites on the surface of the particles increases with an increase in their size, which produces more cavitation bubbles and subsequently more radicals. This is consistent with the results of Shanei, Tuziut and their coworkers [191] , [192]. They explained that the low chemical cavitation yield at the smallest size of particles is due to the fact that these particles and the fluid surrounding the bubbles were in motion together and that the particles do not necessarily act as a rigid wall against the bubble implosion to cause an asymmetric collapse, leading to the generation of a large number of bubbles and subsequently a high number of radicals. In the case

of particles in the nanometer range, the implosion of the acoustic bubbles creates micro-sized shear flows in different directions, whose diameter is larger than that of the solid particles. The solid particles are then surrounded by the jets of fluid, which scatter them in different directions. The greater the amount of solids in the solution, the higher the surface area available for nucleation and the higher the concentration of radicals formed. An increase in the surface area provides nucleation sites of bubbles active for cavitation. However, in our case, we obtained the opposite; for particle size of 12-26 μm and 0.2-0.3 μm, the concentration of 0.5 wt% produced more radical adducts than 3 wt% (Figure 4.8). Except for those with a diameter of 5-15 nm, there is no significant difference between the two concentrations. This is attributed to the high number of particles in the solution which can act as obstacles and slow down the propagation of ultrasound. A large concentration of solid particles dissipates the sound waves, which decreases the focused energy transferred into the system. Shanei [191] investigated the effect of the amount and size of gold nanoparticles on the acoustic cavitation activity to find a way for improving therapeutic effects on tumors. They found that the acoustic activity increases with the number of particles in the solution but beyond a certain amount (from 60 mg corresponding to 5 wt%), the activity begins decreasing. Barchouchi et al. [176] observed the same: the acoustic activity decreased sharply beyond a critical value between 0.01 and 0.03 m^2, depending on the size of the glass beads. Tuziuti et al. [192] considered the particle size effect on the absorbance of an aqueous KI solution with alumina particles (Al_2O_3) following sonolysis. When the added amount of particles increased beyond 20 mg, the absorbance became lower. They concluded that this is caused by the substantial prevention of ultrasound propagation due to the increase in the number of particles.

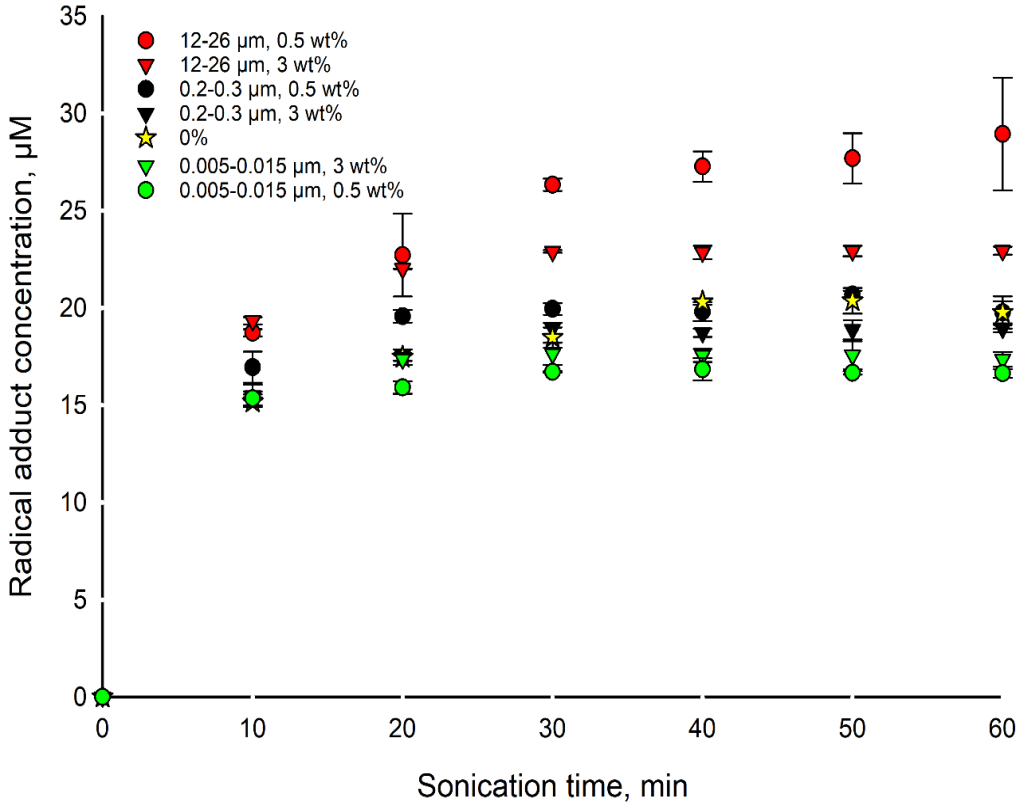

Figure 4.8: Effect of SiO2 size and particle concentration (T= 61°C, US power= 24.7 W), error bars represent the sample standard deviation.

4.3.3 Solvent effect

We find that the concentration of the radical adduct follows the same trend for both trimethylene glycol and propylene glycol (Figure 4.9). We are not therefore able to conclude which solvent has the best acoustic activity. However, theoretical studies indicated that liquids having a lower vapor pressure elicit a higher radical concentration [180], [193]. As the vapor pressure of the liquid increases, so does the vapor content of the cavity, thus lowering the energy released during the collapse. Thus the net cavitational effects will be lower for liquids with higher vapor pressure (vapor pressure of trimethylene glycol at 20 ºC = 0.006 kPa versus 0.011 kPa for propylene glycol) [180]. Also, liquids with higher surface tension, generally result in higher cavitational intensity

(surface tension at 20 °C of trimethylene glycol= 41.1 mN/m versus 38.0 mN/m for propylene glycol). Therefore, we chose trimethylene glycol to complete the rest of the experiments.

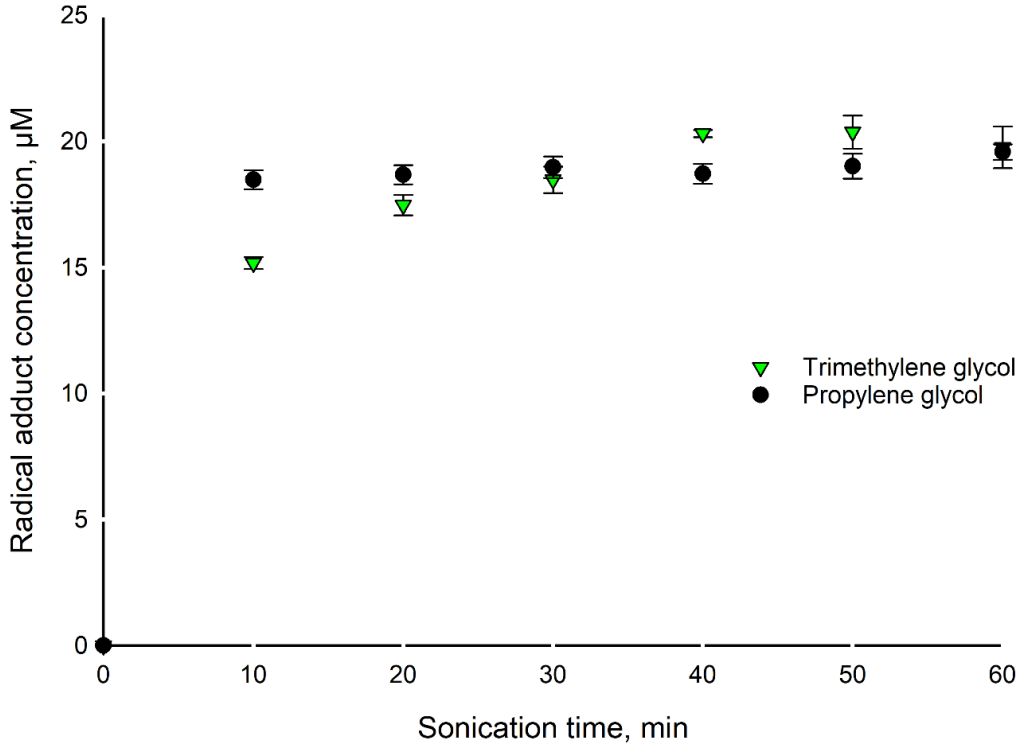

Figure 4.9: Comparison of the radical adduct concentration in trimethylene glycol and propylene glycol as a solvent (US power =24.7 W, 0% solid and T=61 °C), error bars represent the sample standard deviation.

4.3.4 Ultrasound power effect

The power delivered by the 500 W horn at 20 % and 40 % amplitude was 24.7 W and 50.6 W, respectively, according to the calorimetric calibration. As expected, the cavitation activity increases with the power of the sonication (Figure 4.10). With an increase in the intensity of irradiation, the collapse pressure increases, leading to enhanced cavitational effects. The size of the cavity increases with the intensity of the irradiation; therefore, a more cavitationally active volume is achieved with a longer lifetime of the cavity [194], [195].

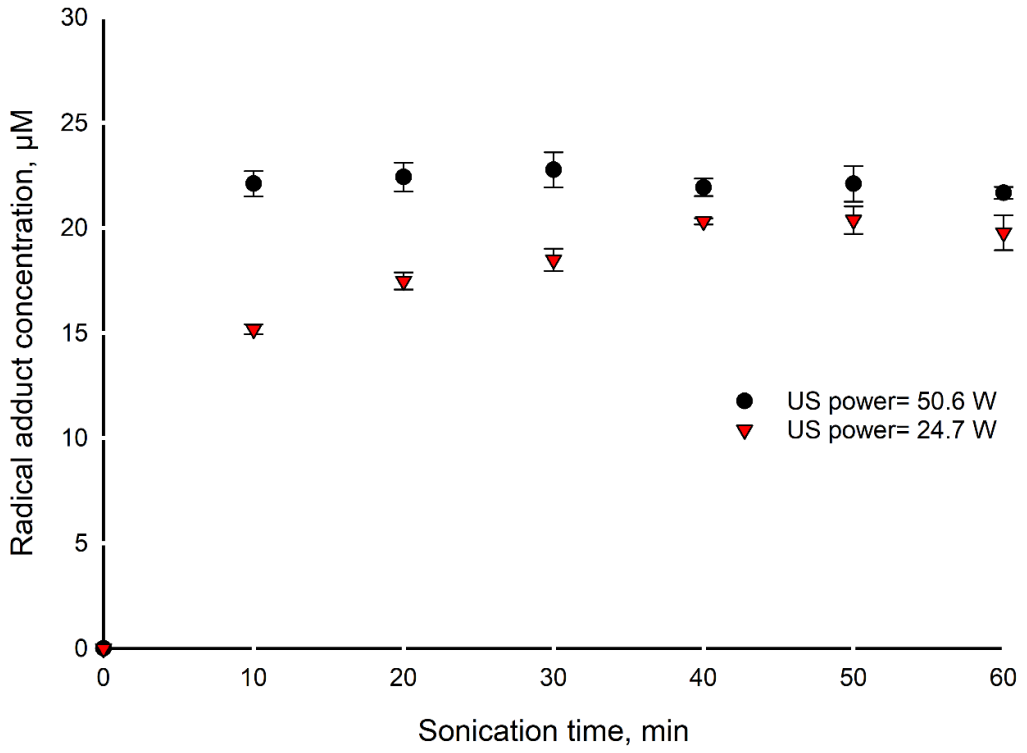

Figure 4.10: Ultrasound power effect (0% solid, T= 61 °C). Error bars represent the sample standard deviation.

4.3.5 Temperature effect

We expect the cavitational activity to decrease at higher operating temperature in the reactor. Price et al. [196] and many other [180], [194], [195], [197] interpret the cavitational activity in relation to the vapor pressure of the solvent, whereby there is a higher active gas nuclei concentration in the presence of solvents with a higher boiling point. This amortizes the collapse and reduces the shock waves. However, we obtained the opposite; we produced more radical adducts working at 75 °C than at 61 °C (27 µM vs 19 µM after 50 min of sonication) (Figure 4.11). This is attributed to the fact that higher operating temperature increases the vapor pressure inside the bubble, which in turn leads to a higher concentration of chemical species inside the cavitation bubble thereby generating much higher amounts of free radicals in the system [194]. This increases reaction rates, which is of interest to our case, where chemical reactions will be occurring so we have to find an optimum operating temperature.

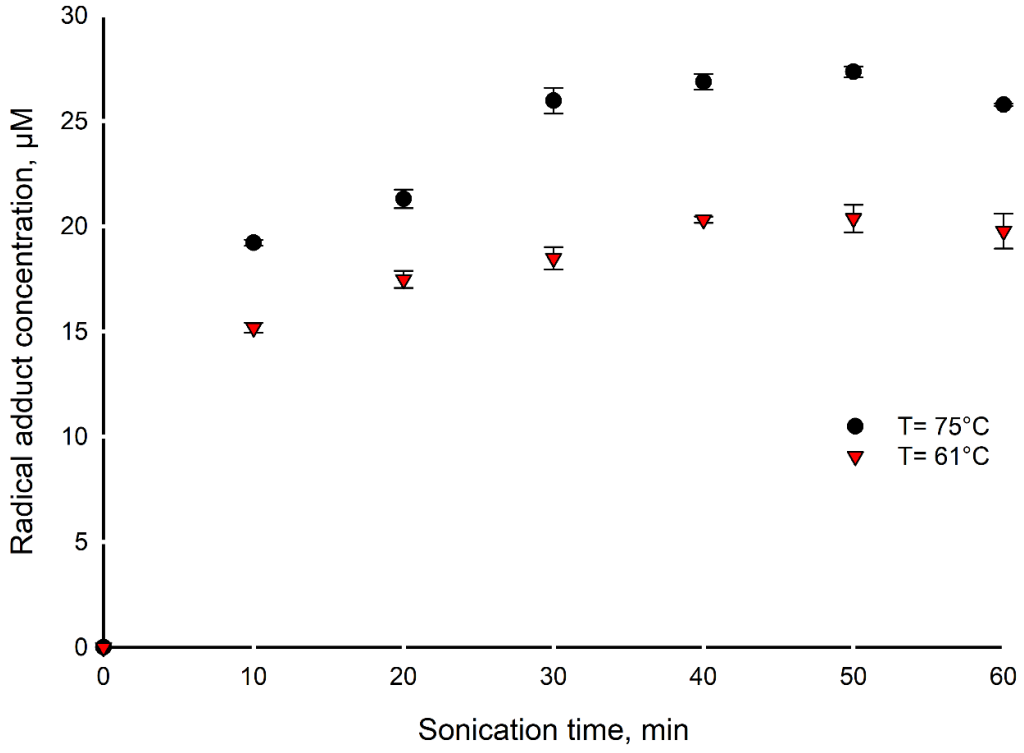

Figure 4.11: Temperature effect (US power= 24.7 W, 0% solid).

4.4 Conclusion

EPR is an effective tool for measuring the chemical effect threshold of the acoustic cavitation in organic solvents (trimethylene glycol and propylene glycol) and in the presence of SiO_2 particles with varying particle diameter and varying concentration. Pyrolysis in collapsing cavitation bubbles produced hydroxyalkyl radicals. Particles with 12-26 µm diameter produced the highest radical concentration (29 µM). The 0.5 wt% SiO_2 concentration gave higher cavitation activity than 3 wt% because a large number of particles can slow down the propagation of ultrasound. These findings proved that adding particles of appropriate size and concentration has the potential to enhance the radical yield, and likely the overall acoustic pressure in selected reactor zones in sonochemical reactions. These findings have applications in the field of heterogeneous catalytic reactions, solid and particle processing, food and metal extractions, as well as for sonoprocessing in general.

CHAPTER 5 ARTICLE 2: CAO / SIO_2 CATALYZES THE ULTRASONIC BIODIESEL TRANSESTERIFICATION TO PRODUCE LUBRICANT

Héla Laajimi, Mahmoud Yosry Zorainy, Dalma Schieppati, Daria C. Boffito

Article submitted to Biomass and bioenergy on April 15, 2022.

Abstract

The growth of the machinery and automotive industry drives interest towards the production of bio-lubricants due to their better lubricating properties and their low carbon footprint compared to petroleum-based lubricants. However, their traditional synthesis is long and energy-intensive.
We intensified the production of biolubricants from canola oil methyl esters by ultrasound. NaOH catalyzed the transesterification of two polyalcohols (propylene and trimethylene glycols). We varied the ultrasound power, temperature, the type of alcohol and the alcohol:biodiesel molar ratio. Trimethylene glycol produced 90 % ± 1.9 % of biolubricant at 80 °C and 62 W with a molar ratio of 0.25. Calcium oxide supported on silica (CaO/SiO_2) also catalyzed the reaction at the optimal conditions. We surveyed the loading of CaO over SiO_2, the catalyst loading in the reactor, and its leaching and reusability. A mass percentage of 50 % CaO to SiO_2 yielded 46 % ± 3.2 % lubricants at 3% by weight of the reactants' total mass. After three reaction cycles, the ultrasound did not alter the particle size (e.g. mean diameters of fresh and used catalysts were 31 µm and 32 µm, respectively), but it leached the active sites, which reduced the activity of the catalyst for successive uses.

KEYWORDS: *Biolubricant, Biodiesel, Transesterification, Ultrasound, Heterogeneous Sonocatalysis, CaO/SiO_2*

5.1 Introduction

Lubricants find application in many sectors, such as foundry, metal forming, energy, plastics, food industry, automotive and machining. The United States market research and consultancy firm Grand View Research valued the global lubricants market at USD 130 billion in 2021 and forecast an annual growth rate of 3.7 % by 2028 [198]. This expansion is a consequence of rapid

industrialization and the growth of automobile sales. The automotive sector dominated the global lubricants market with a share of more than 57% in 2020 [199]. The growing demand for lubricants and the depletion of fossil fuels in the world is spurring the exploitation of bio-based lubricants.

Vegetable oil-based lubricants (e.g., soybean, sunflower, canola, rapeseed, palm) exhibit better properties than mineral oil-based ones, such as biodegradability, lower greenhouse gas emissions, high viscosity indexes (e.g., 246 for soybean oil versus 96 for mineral oil [23]), high thermo-oxidative stability, and lower volatility [200], [201]. This results in better lubrication even at higher temperatures and a reduced risk of toxicity to humans and the environment. These characteristics are driving the growth of the global biolubricants market, which is expected to reach USD 2.93 billion by 2024 at an annual growth rate of 5.2 %. North America monopolized the biolubricants market in the world with a 36.6 % share in 2019 [202]. This is due to increasing regulatory intervention from the US government which requires a minimum renewable content for various products.

Biolubricants are prepared from biomass by esterification of free fatty acids or by transesterification of vegetable oils or waste oils [49], [203]–[206]. Traditional processes for synthesizing biolubricants are energy intensive, operate at reduced pressures and high temperatures (> 120 °C) and require long reaction times (> 6 h) [207], [208]. Gul et al. produced cottonseed oil-based biolubricants at 144 °C under vacuum (25 mbar) for 10 h [209]. Zaccheria and co-authors esterified free fatty acids (FFAs) with trimethylolpropane (TMP) to produce biolubricants at 200 °C for 6 h [210]. Gunam et al. converted jatropha methyl ester to biolubricant (47 % conversion) at 200 ˚C under 10 mbar for 3 h of reaction [211]. Menkiti et al. synthesized a biolubricant by transesterification of fluted pumpkin methyl esters and TMP. $Ca(OH)_2$ catalyzed the reaction. They produced 81% of biolubricant at 160 °C after 6 h reaction [212]. Chang et al. synthesized TMP triesters from high oleic acid palm oil [213]. They transesterified high oleic acid palm oil methyl esters with TMP and obtained 98% of triesters under 170 °C, at 50 mbar in 8 h, with calcium methoxide as a catalyst. Ivan-Tan and co-authors reported a direct conversion of palm oil methyl ester into a biolubricant on a basic catalyst (5 % by weight of SrO on CaO) [51]. The reaction yielded 88% triesters at 180 °C, 2 mbar vacuum pressure and 4 h reaction time.

To get around these long reaction times and drastic reaction conditions, we utilized ultrasound (US) to intensify the production of biolubricants. The energy density of US is 10 to 30 times higher than

that of a conventional process and its power consumption is 45 % to 65 % lower [11]. Since our goal is to establish an environmentally friendly and economically viable process, we evaluated the synergistic effect of heterogeneous catalysis with US to synthesize lubricants from biodiesel.

There are several literature data available on US-assisted transesterification or esterification. For instance, Boffito et al. intensified the biodiesel production through the application of US in batch and continuous reactors [111]. The biodiesel yield was 90 % after 18 seconds of pulsed US, with a reaction that was 300 times faster than the traditional mixing process. Patience and co-authors used 750 W and 500 W ultrasonic horns to esterify 1,3-propanediol with oleic acid in the presence of Amberlyst®15. They produced a diester biolubricant with a stoichiometric reaction that was 2 h faster than the conventional method [140]. Almasi et al. transesterified rapeseed methyl ester and TMP with a US amplitude of 82 %. They produced a bio-lubricant with a yield of about 82 % after 1 h [142]. Arumugam and co-authors produced 81.4% yield of pentaerythritol ester lubricant with ultrasound (60 % amplitude) and at 100 °C [141]. Data on the US-assisted production of biolubricants is still very limited. As per 2022, the Web of Science Core Collection indexes only five articles on the topic of "ultrasound" and "biolubricant" [140]–[144].

Furthermore, the polyalcohols used in these works are either TMP or pentaerythritol. Here we are the first to sonicate a polyalcohol that can be potentially derived from biomass (propylene and trimethylene glycol synthesized from glycerol) with canola oil fatty acid methyl esters (FAME) to produce diester (DE)-biolubricant. We studied the effect of the type of alcohol, of different US powers (22 W and 62 W), three alcohol to biodiesel molar ratios (1:1, 1:2 and 1:4), and we varied the reaction temperature (80 °C and 100 °C). After having optimized the reaction conditions in the presence of a homogeneous catalyst (NaOH), we tested them with calcium oxide supported on silica (CaO/SiO_2). The choice of this catalyst is justified by the fact that CaO is among the base metal oxides most commonly used in US-assisted transesterification and because of its availability and low cost [132], [133], [214]–[216]. We investigated the influence of the catalyst load on the total mass of the reactants and the effect of the CaO concentration on the support. We also considered leaching and reusability of the catalyst.

5.2 Materials and methods

5.2.1 Preparation of CaO/SiO_2

We prepared three catalysts with a mass fraction of 24 %, 34 %, and 50% of CaO supported on SiO_2 by incipient wetness impregnation. We adopt this nomenclature throughout the manuscript: $24CaO/SiO_2$, $34CaO/SiO_2$, and $50CaO/SiO_2$. An aqueous solution of the precursor calcium nitrate tetrahydrate (Sigma Aldrich) is added dropwise to the dried SiO_2 support (12-26 µm, MP Biomedicals), while stirring. We impregnated the support in a rotary evaporator at 25 °C for 24 h. Then the water evaporated at 60 °C and under 0.2 bar for 8 h. A furnace dried the catalyst at 80 °C overnight, then calcined it at 550 °C (ramp of 2 °C min^{-1}) for three hours to oxidize and fix the CaO on the surface of the support.

5.2.2 Catalyst characterization

A N_2 physisorption instrument (Quantachrome Autosorb-1) analyzed the porous texture of the catalysts after impregnation by recording N_2 adsorption and desorption isotherms at -196 °C. The pore size distribution and the pore volume were calculated according to the Barrett-Joyner-Hallender (BJH) method and the Brunauer-Emmett-Teller (BET) method determined the specific surface area. Before each measurement, about 0.2 g sample degassed under vacuum at 250 °C overnight to remove moisture and impurities from the sample.

A laser diffractometer (Horiba, LA950) characterized the particle size distribution (PSD). We reported the d_{10}, d_{50}, d_{90}, and the mean diameter $D_{4,3}$.

A Thermo Scientific Nicolet iS5 Fourier-transform infrared (FTIR) spectrometer with an ATR iD7 accessory identified the functional groups on the catalyst surface. The solid was dried in an oven at 80 °C for 12 h prior to the analysis. A single beam scanned the samples 60 times with a resolution of 2 cm^{-1} in a spectral range from 3600 cm^{-1} to 600 cm^{-1}.

A Bruker D8 Advance X-ray diffractometer scanned the catalyst samples with a Cu-Kα source (λ = 1.5406 Å at 40 kV and 40 mA) over 2θ = 3º-100º to identify the crystalline metal phases on the support.

A scanning electron microscope (SEM, Benchtop Hitachi TM 3030 Plus) equipped with an energy-dispersive X-ray (EDX) characterized the surface morphology and the elemental distribution on the catalyst samples (fresh and used).

An Epsilon 4 Benchtop Energy Dispersive X-ray Fluorescence (EDXRF) spectrometer quantified the CaO and SiO_2 in the samples. The spectrometer is a non-destructive analyzer with a silver anode x-ray tube, 50 kV excitation capabilities, a maximum current of 2 mA, and a maximum power of 10 W.

5.2.3 Catalytic activity

We esterified commercial canola oil with methanol (99.8%, Sigma-Aldrich) to produce biodiesel and utilized it for all of the biolubricant synthesis experiments. We followed the biodiesel synthesis protocol of Boffito et al. [111]. All experiments took place in a 100 mL jacketed glass reactor (4 cm internal diameter, 10 cm height). We loaded the reactor with 40 g of biodiesel and we preheated it at the reaction temperature at 400 rpm agitation. We dissolved sodium hydroxide (99.9%, Alfa Aesar) in propylene glycol (PG) or trimethylene glycol (TG) (Sigma-Aldrich, St. Louis, Mo, USA) with a mass fraction of 1 %, and then we added the mixture to the biodiesel and we started the sonication. The alcohol is added to the mixture at an alcohol:biodiesel molar ratio of 1:1, 1:2 or 1:4. A Sonics & Materials, Inc 500 W (20 kHz) nominal power ultrasonic processor and a solid probe (1.3 cm tip diameter, 25.4 cm length) sonicated the solution for 3 hours with a duty cycle of 2 s on and 2 off . A thermostatic bath maintained the reactor temperature constant at 80 °C or 100 °C (Table 5.1). A K type thermocouple measured the temperature inside the solution and we determined the actual power conveyed to the solution by calorimetric method [179].

Table 5.1: Experimental condition and diester yield after 3 h of reaction catalyzed by NaOH (mass fraction of 1% relative to the total mass of the reagents). Uncertainty refers to the sample standard deviation.

Run #	**Alcohol**	**US power (W)**	**Alcohol:biodiesel molar ratio**	**Temperature (°C)**	**DE yield (%)**
1	PG	62	1:4	100	28 ± 1.5
2	TG	62	1:4	100	43 ± 2.6

3	TG	62	1:1	80	52 ± 2.6
4	TG	22	1:1	100	4 ± 3.9
5	PG	62	1:1	80	10 ± 1.2
6	TG	62	1:2	80	70 ± 2.8
7	PG	22	1:4	80	14 ± 1.5
8	PG	22	1:1	100	3 ± 2.4
9	PG	22	1:1	80	5 ± 2.5
10	PG	62	1:4	80	30 ± 2.1
11	TG	62	1:1	100	12 ± 2.2
12	TG	22	1:4	80	61 ± 2.9
13	TG	22	1:2	80	52 ± 3.5
14	TG	62	1:4	80	90 ± 1.9
14 (r1)	TG	62	1:4	80	93 ± 1.1
14 (r2)	TG	62	1:4	80	92 ± 2.3
15	PG	22	1:2	80	7.4 ± 2.8
16	TG	22	1:2	100	5 ± 3.5
17	PG	62	1:2	80	9 ± 1.6
18	TG	62	1:2	100	41 ± 1.7
19	TG	22	1:4	100	15 ± 2.7
20	PG	22	1:4	100	10 ± 1.9
21	PG	62	1:2	100	6 ± 2.4
22	PG	22	1:2	100	6 ± 3.2
23	TG	22	1:1	80	47 ± 1.2
24	PG	62	1:1	100	6 ± 1.7
25	TG	0	1:4	100	16 ± 1.9

We varied the type of alcohol, US power, alcohol to biodiesel molar ratio and the reaction temperature (Table 5.1) to identify parameters to achieve maximum biolubricants yield. In the rest of the manuscript, the uncertainty refers to the standard deviation of the sample and arises from three repeated analyses of the biolubricant sample.

After optimizing the reaction conditions in the presence of NaOH, we evaluated the effect of the three solid catalysts 24CaO/SiO_2, 34CaO/SiO_2, and 50CaO/SiO_2 on the transesterification reaction (Table 5.2). We tested three mass fractions of the catalyst: 1, 3 and 5 % relative to the total weight of the reactants. We also tested a heterogeneously catalyzed transesterification without US.

The reusability of the catalyst was investigated by running three reaction cycles at the optimal conditions. After each reaction cycle, we separated the catalyst from the reaction mixture and rinsed it with n-hexane. An oven dried the catalyst at 60 ° C for 24 h before a new transesterification cycle.

Table 5.2: Experimental condition and diester yield of heterogeneously catalyzed transesterification at optimized parameters: T= 80 °C, alcohol:biodiesel molar ratio = 1:4, US power = 62 W. The catalyst loading is the mass fraction of catalyst relative to the total mass of reactants. Uncertainty refers to the sample standard deviation.

Run #	**Catalyst**	**Catalyst loading (%)**	**US power (W)**	**Yield (%)**
1	24CaO/SiO_2	3 %	62	8 ± 1.8
2	34CaO/SiO_2	3 %	62	18± 2.0
3	50CaO/SiO_2	3 %	62	46 ± 3.2
4	50CaO/SiO_2	1 %	62	27 ± 2.8
5	50CaO/SiO_2	5 %	62	11 ± 2.5
6	50CaO/SiO_2	3 %	No US	3 ± 1.8
Cycle 1	50CaO/SiO_2	3 %	62	35 ± 2.3
Cycle 2	50CaO/SiO_2	3 %	62	30 ± 1.6
Cycle 3	50CaO/SiO_2	3 %	62	22 ± 2.5

A Scion 436 GC and an Rtx-Biodiesel TG Column (fused silica, 15 m × 0.32mm ID × 0.10 μm) equipped with an FID analyzed the biodiesel and the biolubricant at the end of each test. The operating conditions of the GC and the preparation of the samples are performed according to the D6584 standard [217]. We used 1,2,4-*butanetriol* and tricaprin as internal standards (ISTD). The n-heptane was the solvent and the N-Methyl-N-(trimethylsilyl) trifluoroacetamide (MSTFA) was the silylating reagent.

The GC analysis of the biodiesel used as a feedstock indicated the presence of methyl palmitate (C16)(10.9 % ± 1.9 % of the biodiesel total mass), methyl oleate (C18:1) (58 % ± 1.8 %), methyl linoleate (C18:2) (19 % ± 1.14 %) and methyl linolenate (C18:3) (3.8 % ± 1.0 %), which agrees with the known composition of canola oil [218]. The transesterification of this biodiesel with glycol (after 3 h) produced monoester (ME) and diester (DE) biolubricant (Figure 5.1). An Agilent 7890A GC-MS and a DB-Wax column (30 m x 0.250 mm x 0.25 µm) characterized both reactants and products through detection with a 5975C VL MSD with Triple-Axis Detector. We quantified the diester yield by calculating the relative response factor (RRF) by the effective carbon number (ECN) method (Eq. 5.1 and 5.2) [219]–[222]. We used this method since pure DE standards are not commercially available. The mass and the yield of the diester are determined from (Eq. 5.3 and 5.4).

$$RRF = \frac{A_{ISTD} \times m_{DE}}{A_{DE} \times m_{ISTD}} \quad (5.1)$$

$$RRF = \frac{ECN_{ISTD} \times M_{DE}}{ECN_{DE} \times M_{ISTD}} \quad (5.2)$$

$$m_{DE} = \frac{RRF \times A_{DE} \times m_{ISTD}}{A_{ISTD}} = \frac{ECN_{ISTD} \times M_{DE}}{ECN_{DE} \times M_{ISTD}} \times \frac{A_{DE} \times m_{ISTD}}{A_{ISTD}} \quad (5.3)$$

$$Yield = \frac{Amount\ of\ DE\ produced}{\max of\ DE\ would\ be\ produced} \quad (5.4)$$

A_{DE} = area of the diester

A_{ISTD} = area of internal standard

m_{DE} = mass of diester

m_{ISTD}= mass of internal standard

ECN_{ISTD} = Effective carbon number of the internal standard

ECN_{DE} = Effective carbon number of the DE

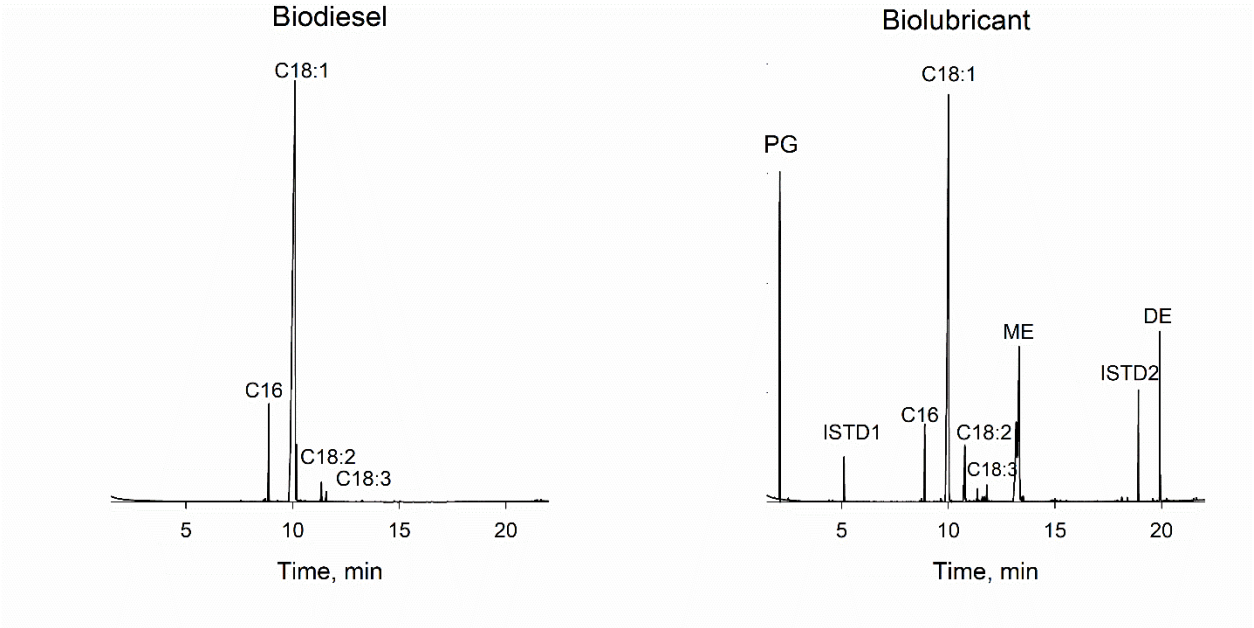

Figure 5.1: Chromatograms of the biodiesel used as a feedstock and the biolubricant.

5.2.4 Properties of biodiesel and biolubricant

An ANTON PAAR DMA 4500 measured the density of the canola oil, biodiesel and biolubricant at 20 °C. A Thermo Scientific rheometer HAAKE Viscotester iQ Air evaluated their apparent viscosity.

Acid-base titrations quantified the amount of FFAs in the canola oil. This step is important before any synthesis of biodiesel to avoid the reaction of the FFAs with the basic catalyst, which forms soap thus altering the quality of the biodiesel and subsequently the lubricant. According to the American standard specification for biodiesel (ASTM D-6751), FFAs concentration should not exceed 0.80 mgKOH/g [223], [224].

A Karl Fischer titrator (METTLER TOLEDO, model V20S) quantified the water content of the biodiesel and lubricant. The reagent utilized for the titration was HYDRANAL^{TM} Composite 5 (Honeywell) and the solvent was dry methanol (HYDRANAL^{TM}, Honeywell).

5.3 Results and discussion

5.3.1 Catalyst characterization

XRD and XRF

The three diffraction patterns of SiO_2 impregnated with different concentrations of CaO show the amorphous structure of SiO_2 with a broad peak at 2θ of 22° (Figure 5.2). The 24CaO/SiO_2 diffraction pattern doesn't exhibit any crystalline feature. However, a peak corresponding to the CaO phase appears at a 2θ of 32° for the 34CaO/SiO_2. The 50CaO/SiO_2 pattern confirms that the calcined catalyst was mainly CaO (at 2θ equal to 32°, 38° and 64°) with calcium carbonate $CaCO_3$ (2θ of 28°, 44 ° and 48°) and calcium hydroxide $Ca(OH)_2$ (21°). The existence of these phases confirms the deposition of calcium on the SiO_2 surface. $Ca(OH)_2$ and $CaCO_3$ are subsequent products of the absorption of the atmospheric moisture and carbon dioxide. These results agree with those of Lani et al. [32]. They reported characteristic peaks of crystalline CaO at 2θ of 32.2, 37.4 and 65.5. Chen et al. [225] identified identical CaO peaks at a 2θ of 32.1°, 37.2° and 64.2°.

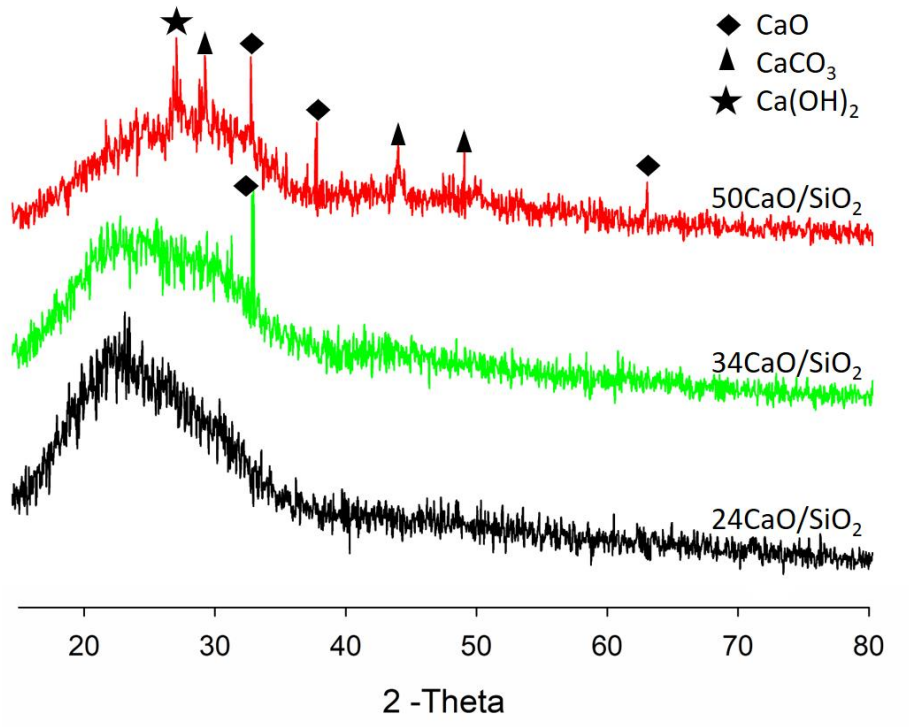

Figure 5.2: XRD diffraction patterns of the catalysts calcined at 550 °C.

The XRF results confirm the deposition of calcium on SiO_2 and the formation of CaO during the calcination of the catalysts (Table 5.3).

Table 5.3: XRF analysis of the catalysts (% are on a weight basis).

Catalyst	% Elements		% Oxides	
	Si	**Ca**	**CaO**	**SiO_2**
24CaO/SiO_2	57.9	41.2	24.3	75.3
34CaO/SiO_2	47.2	52.3	33.9	65.8
50CaO/SiO_2	32.4	67.1	49.8	49.7

FTIR

The FTIR spectrum of the three catalysts (Figure 5.3) shows bands at 1050, 1364 and 1734 cm^{-1}, corresponding, respectively, to the asymmetric stretching of Si-O-Si from the SiO_2 of the support, asymmetric stretching of O-C-O and the C=O stretching of the carbonyl group (CO_3^{2-}) [32], [226], [227]. The CO_3^{2-} group refers to of calcium carbonate $CaCO_3$ phase produced by the chemisorption of atmospheric CO_2 on the CaO surface. The 786 cm^{-1} band, in the spectrum of the catalysts 24CaO/SiO_2 and 34CaO/SiO_2, indicates the Si-O-Si symmetric stretching of the SiO_2. In the 50CaO/SiO_2 spectrum, the 875 cm^{-1} band is the out-of-plane band vibration mode of the CO_3^{2-} group [228], [229]. The absorption band at 1456 cm^{-1} is ascribed to the asymmetric stretch of CO_3^{2-} group [230], [231]. A peak at 3649 cm^{-1} corresponds to the angular folding of O–H water molecules bound to the Ca atom, which ascribes to $Ca(OH)_2$, deriving from the adsorption of atmospheric moisture on the CaO surface [228], [226].

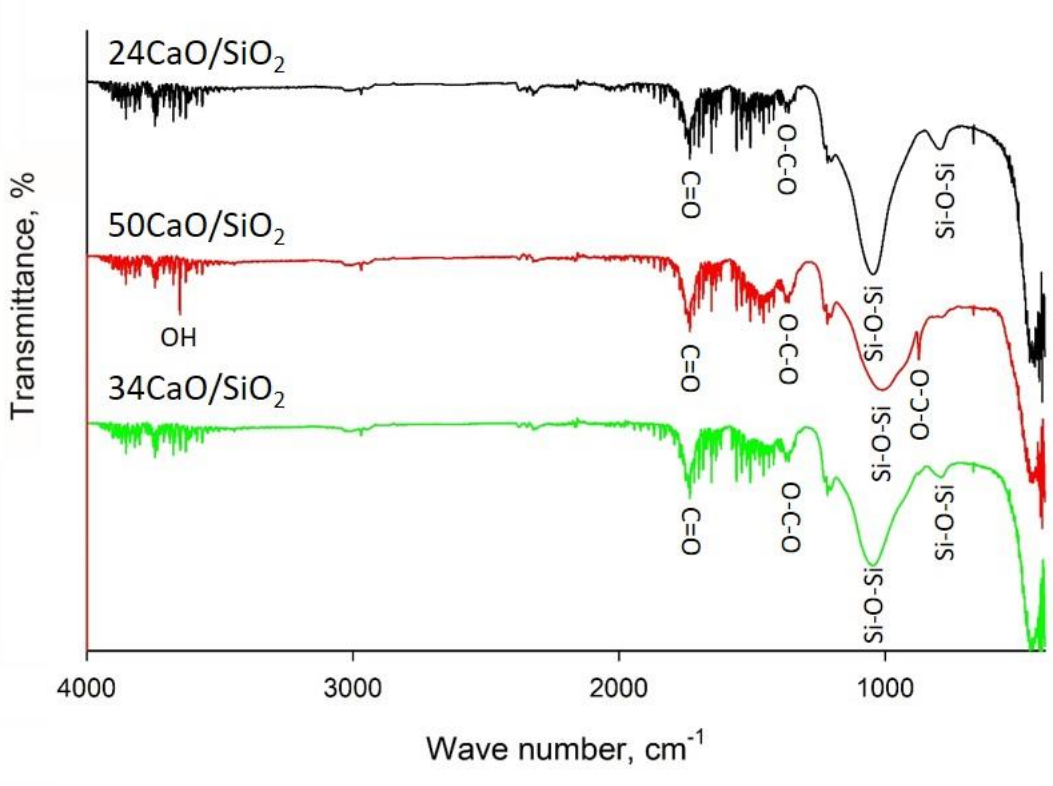

Figure 5.3: FTIR spectrum of the CaO/SiO_2 catalysts calcined at 550 °C.

PSD and BET

All catalysts after impregnation roughly display similar mean ($d_{4,3}$) and d_{50} (Table 5.4) upon PSD analysis. They also maintain the same particle size after the US-assisted transesterification reaction. Indicating that the sonication did not affect the particle diameter. Fresh and used catalysts ($50CaO/SiO_2$) also have the same particle distribution (Figure 5.4). The particles after impregnation lie from 22 and 48 µm and the shapes of the curves are symmetrical. However, CaO loading decreased the particle diameters (d_{50}, d_{90} and $d_{4,3}$) and narrowed the particle size distribution (Figure 5.4).

Table 5.4: Particles diameters of the catalysts and the support.

	SiO_2	**$24CaO/SiO_2$**	**$34CaO/SiO_2$**	**$50CaO/SiO_2$ (fresh)**	**$50CaO/SiO_2$ (used)**
d_{10} (μm)	22.8	26.2	26.5	26.5	26.9
d_{50} (μm)	36.2	33.2	31.3	31.3	33.3
d_{90} (μm)	53.7	38.5	36.6	36.5	38.4
$d_{4,3}$ (μm)	37.4	31.8	31.1	31.1	32.4

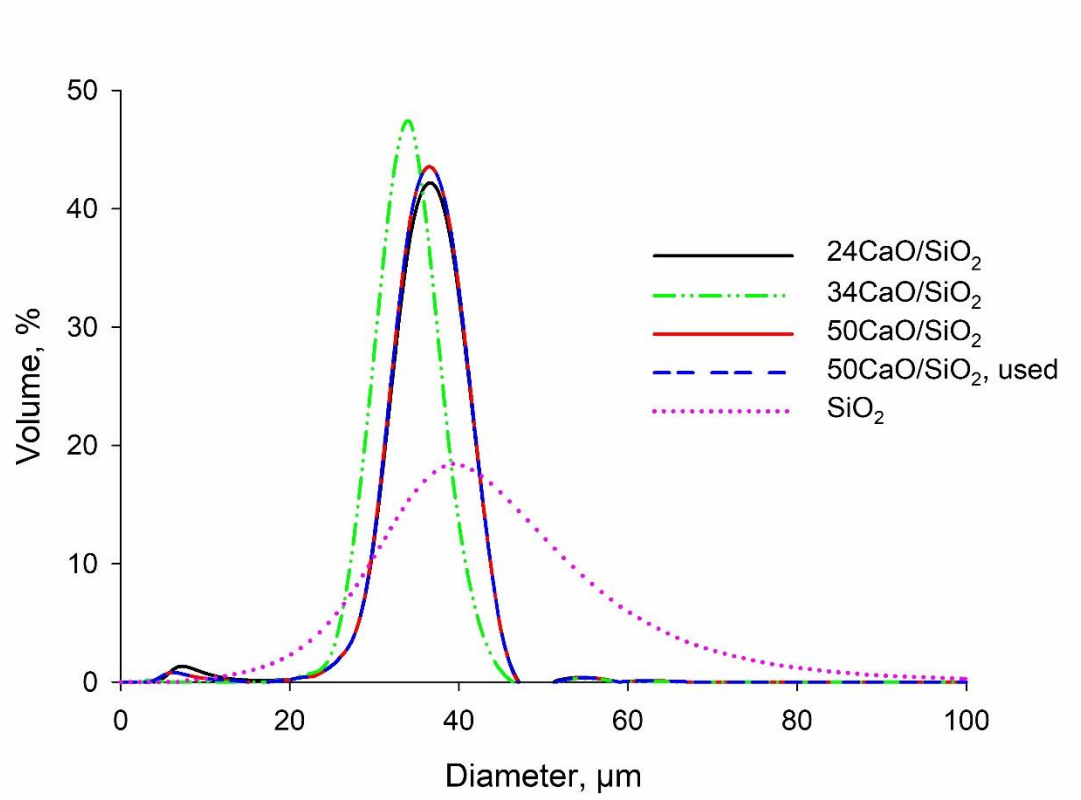

Figure 5.4: Particle size distribution of the CaO/SiO_2 catalysts.

The BET data indicates that increasing the active component loading, decreases both the area and the diameter of the pores, as more CaO occupies the internal pores (Table 5.5). Despite the high CaO loading, we were able to retain SSA beyond 200 $m^2\ g^{-1}$. All the catalysts after impregnation have a microporous structure since their pore diameter is less than 20 Å. However, FAMEs are sterically hindered molecules, so they do not penetrate inside the micropores of synthesized catalysts. Boffito et al. demonstrated that these reactions occur mainly on the outer surface of the catalyst rather than inside the pores [197]. Therefore, we assume that the active sites located on the external surface of the catalyst are the ones responsible for the transesterification reaction.

Table 5.5: Surface area and pore diameter of the catalyst. The accuracy of the instrument is ± 0.11 %.

Catalyst	S_{BET} (m^2/g)	Average pore diameter (Å)
SiO_2	453	40
$24CaO/SiO_2$	324	20
$34CaO/SiO_2$	298	13
$50CaO/SiO_2$	233	10

SEM- EDX

The EDX analysis gave similar results to those of the XRF and they confirm the CaO deposition on the surface of the SiO_2 support (Table 5.6). After three reaction cycles with the $50CaO/SiO_2$ catalyst, the CaO is still present on the SiO_2 surface, however, its quantity decreased by 20%. Elemental mapping of the fresh and used $50CaO/SiO_2$ indicated that the Ca was uniformly distributed on the support (Figure 5.5 and 5.6). Even after three cycles under US treatment, the catalyst particles retained their shape and size (Figure 5.7). The homogeneous dispersion of CaO over the surface of SiO_2 grants a highly active surface thereby enhancing the catalytic activity.

Table 5.6: EDX and XRF analysis of the catalyst composition in terms of Ca and Si (% are on a weight basis). The standard deviation of the samples measured with EDX was between 0.6 % and 0.8 % and that with XRF was less than 0.01%.

	EDX		**XRF**	
	% Ca	**% Si**	**% Ca**	**% Si**
$24CaO/SiO_2$	23.3	76.7	24.3	75.3
$34CaO/SiO_2$	34.2	65.8	33.9	65.8
$50CaO/SiO_2$	50.1	49.9	49.8	49.7
$50CaO/SiO_2$ (after 3 cycles)	40.2	52.8	39.1	51.8

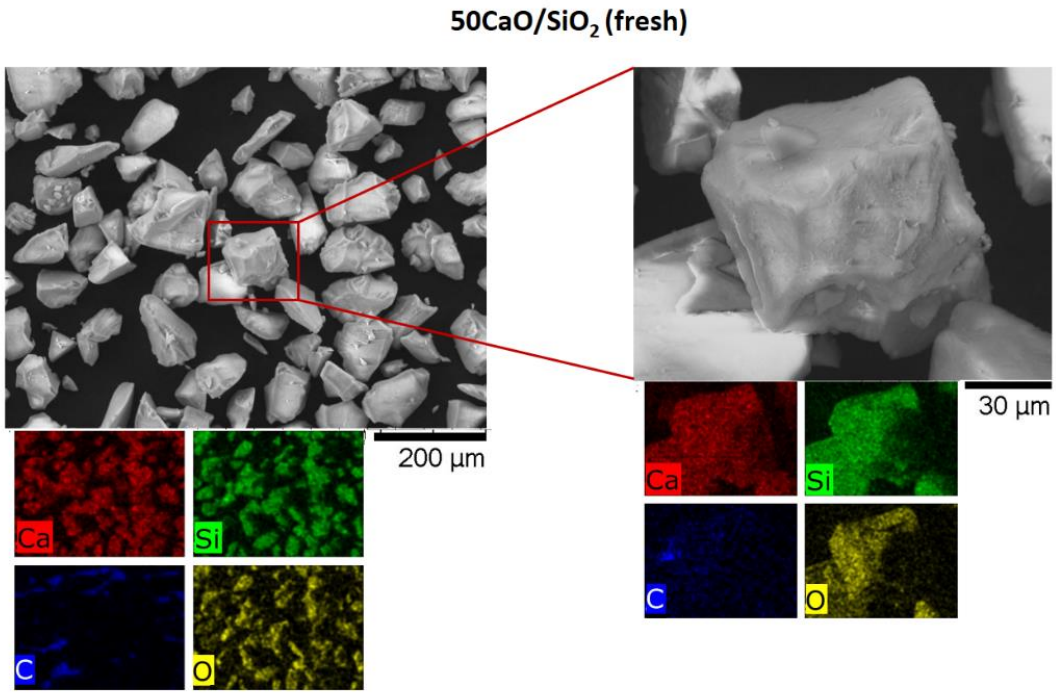

Figure 5.5: Element map of the freshly synthesized catalyst.

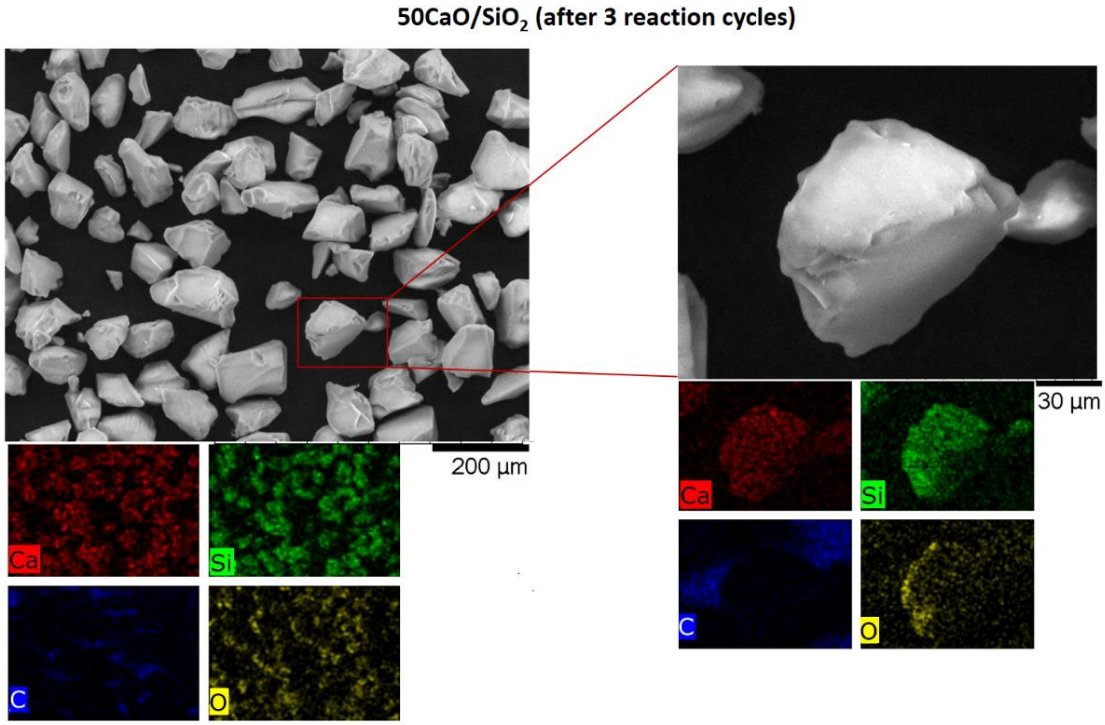

Figure 5.6: Element map of the catalyst after three reaction cycles.

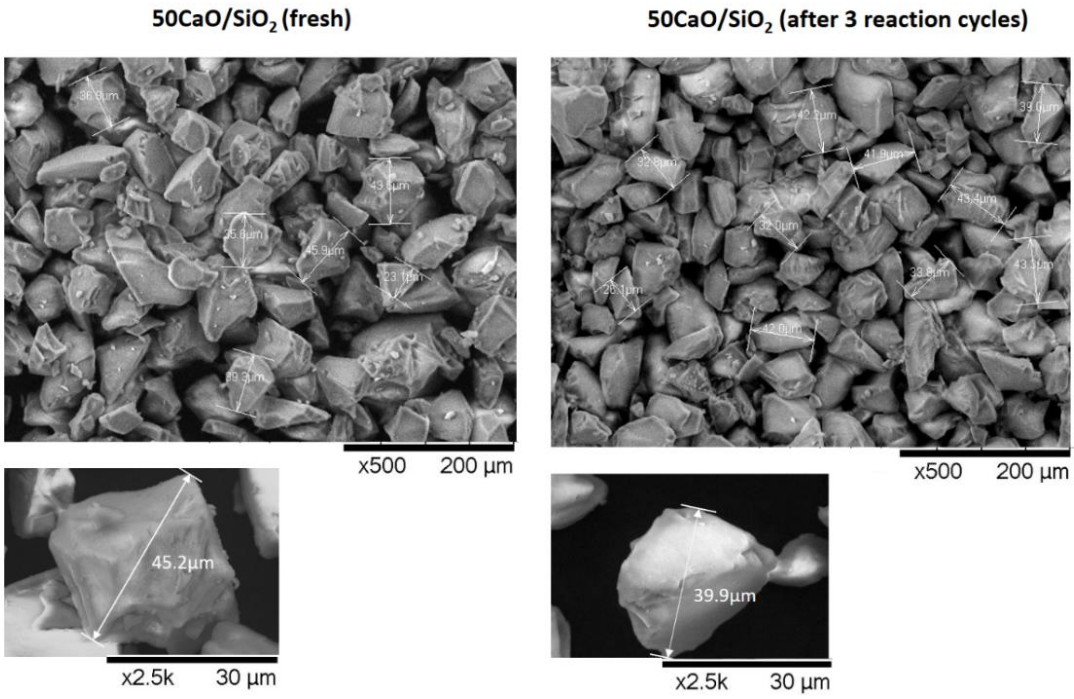

Figure 5.7: SEM images of fresh and used catalyst.

5.3.2 Activity tests

The biolubricant produced by both homogeneous and heterogeneous catalysis met the specifications required for industrial lubricating oil type ISO VG 32 (Table 5.7).

Table 5.7: Canola oil, biodiesel and biolubricant proprieties.

Proprieties	**Canola oil**	**Biodiesel**	**Biolubricant**	**ISO VG 32 [232], [233]**
Yield wt.%	-	< 96.6	90	-
Density at 20 °C, g/cm^3	0.9126	0.8810	0.9021	0.860
Viscosity at 40 °C, cSt	50.10	7.23	32.24	28.8-35.3
Total acid number, mg KOH/g	0.55	0.37	-	-
Water content (volume(%))	-	0.040	0	-

Optimization of experimental parameters

- **Effect of the type of alcohol**

We compared trimethylene glycol (TG) and propylene glycol (PG) under fixed conditions of temperature, US power and alcohol: biodiesel molar ratio (Figure 5.8). Regardless of the conditions, TG produced more DE than the PG. TG has a higher surface tension (41.1 mN m^{-1} for TG and 38.0 mN m^{-1} for PG, at 20 °C) and lower vapor pressure than PG (0.006 kPa for TG versus 0.011 kPa for PG, at 20 °C), which results in a higher cavitational intensity and higher radical concentration [180], [234].The increase of alcohol vapor pressure concentrates the vapor inside the bubble, thus reducing the energy released during the collapse. A higher concentration of free radicals in the medium also favors the transesterification reaction and increases the production of DE (e.g. TG yielded 90 % ± 1.9 % of DE compared to 30% ± 2.1 % for PG, at 80°C, 62W and 1:4 (mol alcohol:mol biodiesel)).

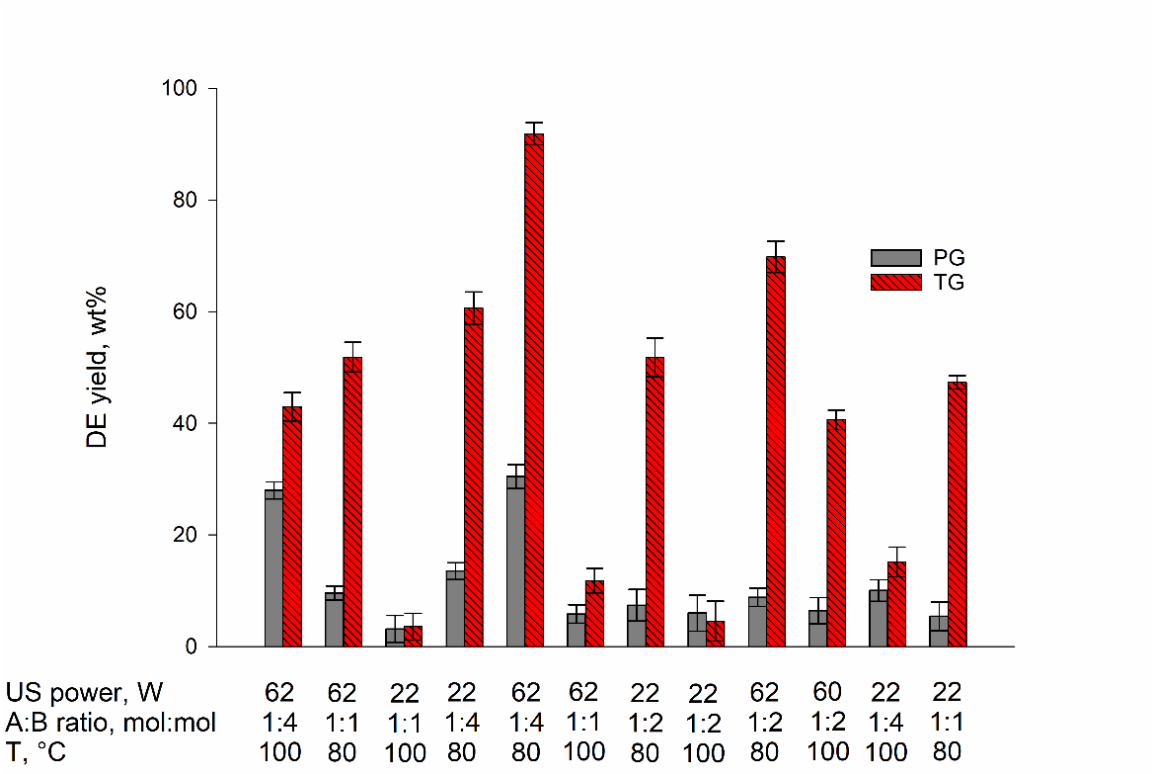

Figure 5.8: Comparison of alcohols at fixed US power, temperature and alcohol (A): biodiesel (B) ratio. NaOH with a mass fraction of 1 % catalyzed the reaction for 3 h. Error bars indicate the sample standard deviation.

- **Temperature Effect**

For both alcohols, working at a lower temperature gave a higher DE yield, e.g., for TG, operating at 80 °C gave 90 % ± 1.9 % of DE compared to 42% ± 2.5 % at 100 °C (Figure 5.9). At high temperatures the alcohol evaporates and the concentration of the vapor in the cavitation bubble increases, which dampens the collapse of the acoustic bubbles, and weakens the shock waves: fewer radicals are produced in the system [196]. Furthermore, vaporization results in a reduced contact of the alcohol with the biodiesel leading to a lower biolubricant yield.

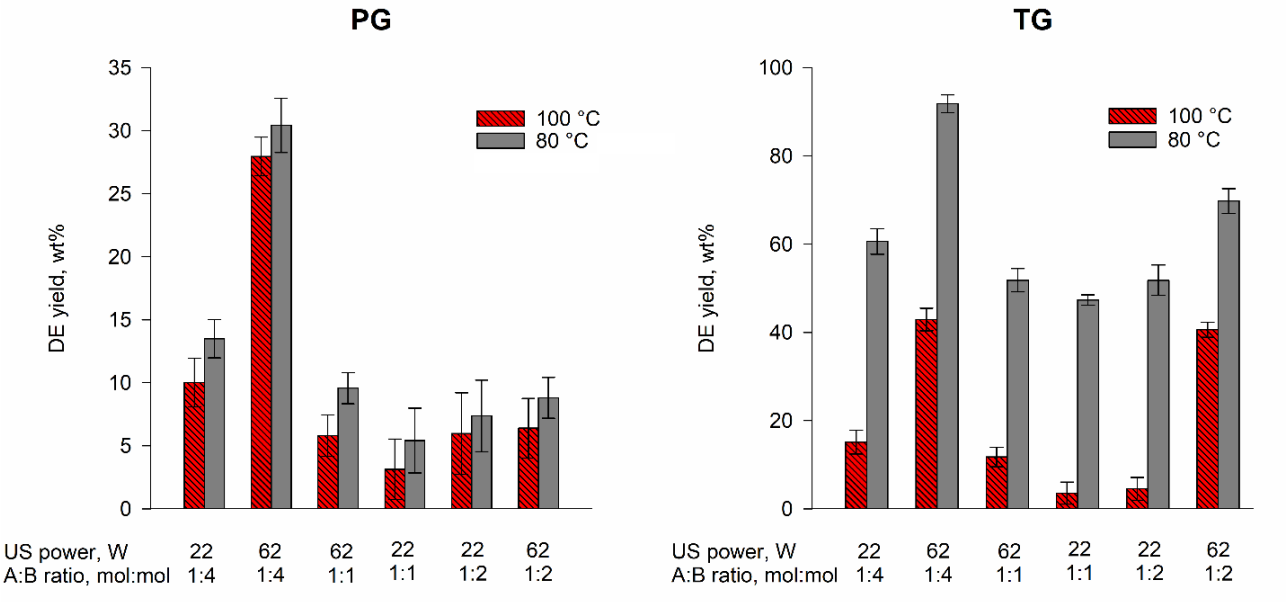

Figure 5.9: Effect of the temperature for PG and TG at constant US power and alcohol : biodiesel (A:B) ratio. 1 % of NaOH (mass fraction) catalyzed the reaction for 3h. Error bars indicate the sample standard deviation.

- **Ultrasound power**

Keeping other conditions constant, increasing the US power from 22 to 62 W enhanced the DE production for both alcohols. For example, by setting the molar ratio at 1: 4 and the temperature at 80 ° C, the yield increased by 30% ± 2.3 % for TG and by 15% ± 1.8 % for PG (Figure 5.10). Boffito et al. produced biodiesel by US [111] and observed a rise in FAME yield as the power increased. High-power dissipation induces a more violent collapse of cavitation bubbles. This

improves mixing and miscibility of alcohol and biodiesel, which increases the contact surface between the two reactants, thus improve mass transfer and promotes the reaction.

We did not increase the power further in order to avoid side effects such as shielding and acoustic decoupling effects [235]. When the power conveyed to the system exceeds an optimal value, a large number of cavities form clouds of bubbles around the surface of the transducer hence the shielding effect [101]. Bubbles clusters absorb or scatter the sound waves, thus attenuating the sound field. The decoupling arises from the variation of the acoustic impedance of the sonicated medium when the concentration of bubbles increases. This reduces the efficiency of energy transfer to the system with the consequent reduction in the reaction yield.

The optimum power depends on the reaction conditions, reactor geometry, and the ultrasonic system to achieve maximum yields before reaching a point of diminishing return [111]. Hingu et al.[236] reported the optimum power density for the transesterification reaction to produce biodiesel. When the ultrasonic power increased from an optimum of 200 W to 250 W, the conversion decreased by about 30%. Gandhi [237] reported the data on the ultrasonically assisted transesterification to produce biodiesel from mahua oil. The yield increased by 74 % when the US power increases from 20 W to 120 W. A further increase of power to 150 W did not elicit an additional increase in yield.

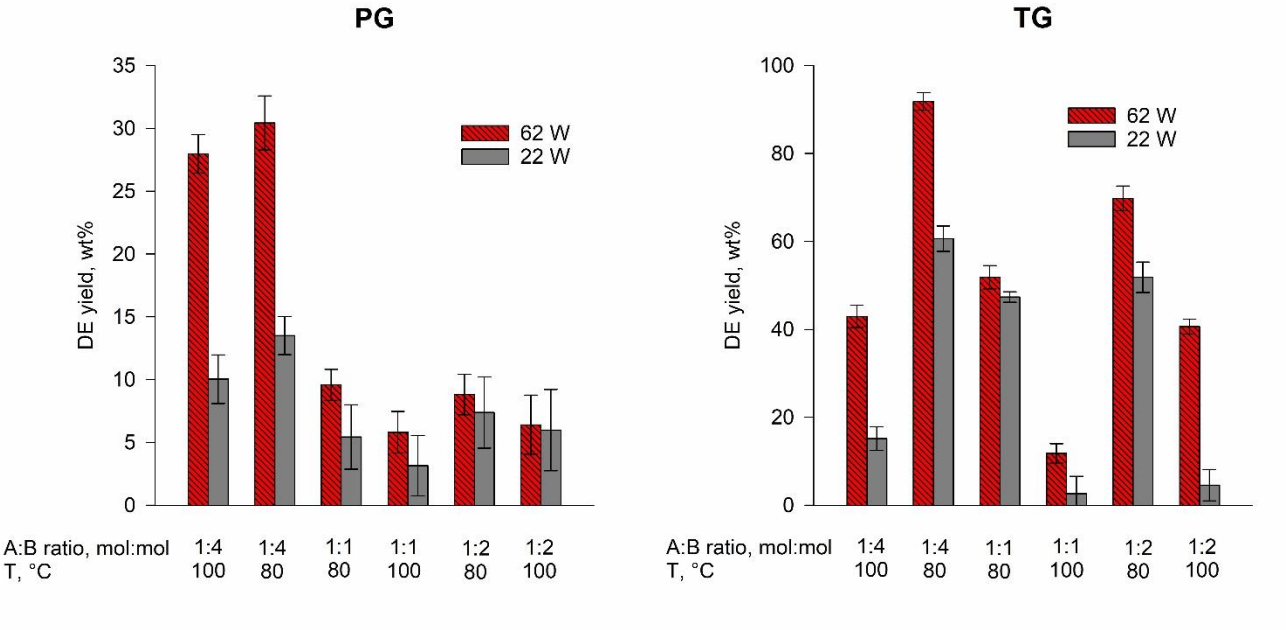

Figure 5.10: Effect of the power for PG and TG at constant temperature and alcohol : biodiesel

(A:B) ratio. 1 % of NaOH (mass fraction) catalyzed the reaction for 3 h. Error bars indicate the sample standard deviation.

- **Alcohol/Biodiesel Molar Ratio Effect**

An excess of FAME directs the reversible transesterification reaction in the forward direction which maximizes the production of diesters. The 1:4 Alcohol/biodiesel molar ratio produced higher DE than 1:2 and 1:1 (Figure 5.11). By setting the temperature and ultrasonic power conditions constant at 80 ° C and 62 W, decreasing the alcohol:biodiesel molar ratio from 1:1 to 1:4 raised the yield from 10% ± 1.2 % to 30% ± 2.1 % for PG and from 52% ± 2.6 % to 90% ± 1.9 % for TG. Indeed, the excess of biodiesel drives the equilibrium of the reaction towards the products.

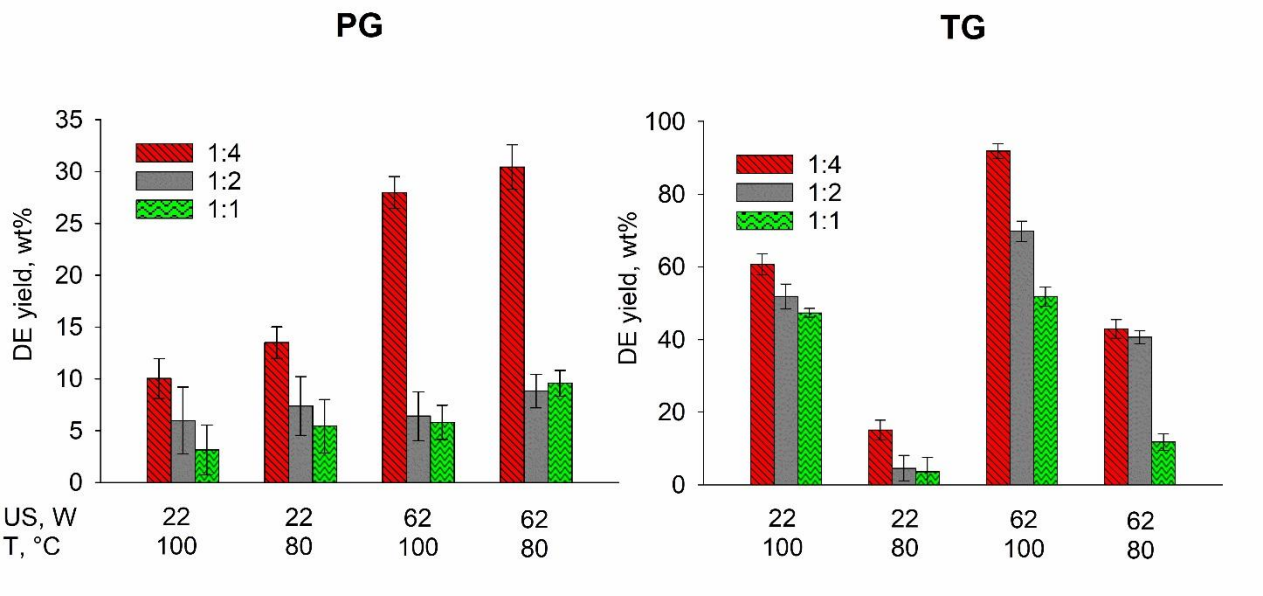

Figure 5.11: Effect of the molar ratio at fixed US power and temperature. A mass fraction of 1 % of NaOH catalyzed the reaction for 3h. Error bars indicate the sample standard deviation.

CaO/SiO_2 activity in the US-assisted transesterification

- **Effect of CaO concentration and catalyst loading**

After optimizing the reaction conditions by NaOH (US= 62W, T= 80°C, TG : biodiesel ratio= 1:4), we tested the activity of the three solid catalysts $24CaO/SiO_2$, $34CaO/SiO_2$ and $50CaO/SiO_2$. The increase in the CaO content corresponds to the increase in the quantity and strength of the basic sites, which favored the production of DE. After three hours of sonication, the reaction catalyzed

by $50CaO/SiO_2$ produced 46 % ± 3.2 % of DE against 18 % ± 2.0 % DE for $34CaO/SiO_2$ and 8% ± 1.8% DE for $24CaO/SiO_2$ (Figure 5.12). The higher number of active sites lowers the activation energy for the transesterification reaction.

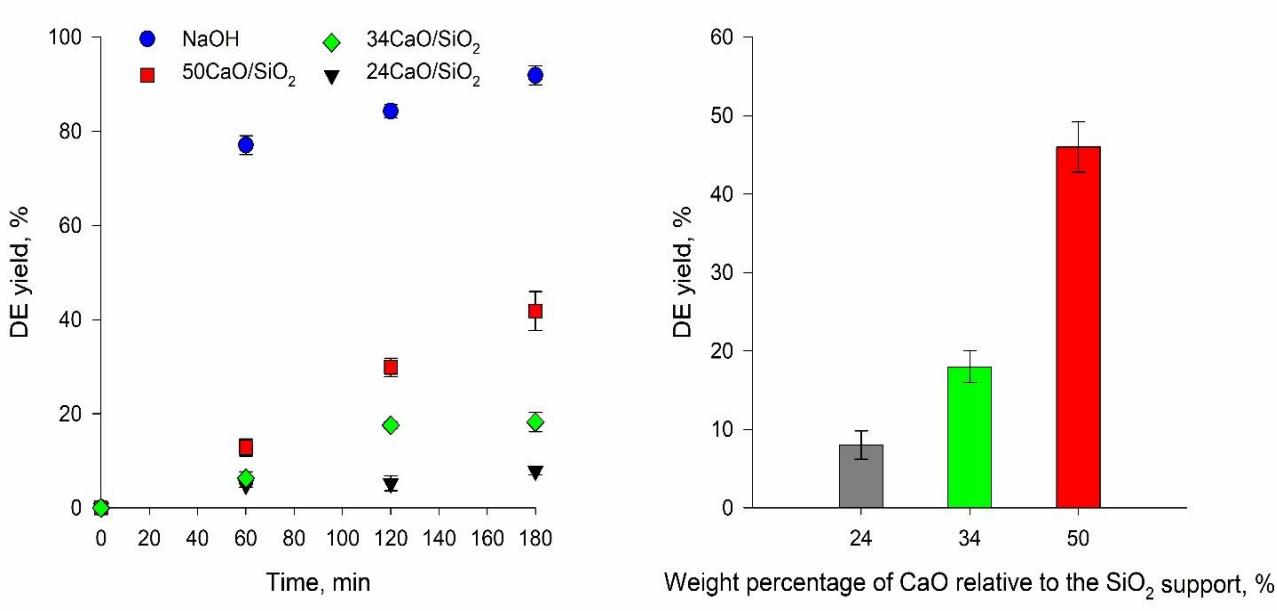

Figure 5.12: Effect of the CaO concentration on the biolubricant yield. 3 h of reaction at: US power= 62 W, T= 80 °C, TG : biodiesel ratio= 1:4. Error bars represent the sample standard deviation.

We investigated the effect of the catalyst loading on the biolubricant yield at 1 %, 3 % and 5 % by weight of the total mass under these conditions; catalyst: $50CaO/SiO_2$, alcohol:biodiesel molar ratio of 1:4, temperature of 80 ° C, reaction duration of 3 hours, and US power equal to 62 W. We chose 50CaO/SiO2 as catalyst because this concentration of CaO (50% on SiO_2) produced the highest lubricant yield. Increasing the catalyst loading resulted in a higher amount of active sites available for the transesterification reaction. However, the DE concentration decreased when the loading of catalyst reached 5 % by weight (46 % ± 3.2 % DE obtained with the mass fraction of 3 % versus 11 % ± 2.5 % of DE with 5 %) (Figure 5.13). A larger amount of catalyst particles act as a barrier and slows down the propagation of US in the reaction medium, which dampens the rates of mass transfer around the particles. The bubble collapse near the catalyst's surface generates high-speed micro-jets of liquid striking the solid particles. The micro-jets and the shock waves improve the

mass transfer between the liquid and the solid, thereby increasing the reaction rate. This might as well increase the surface area of the catalyst [159].

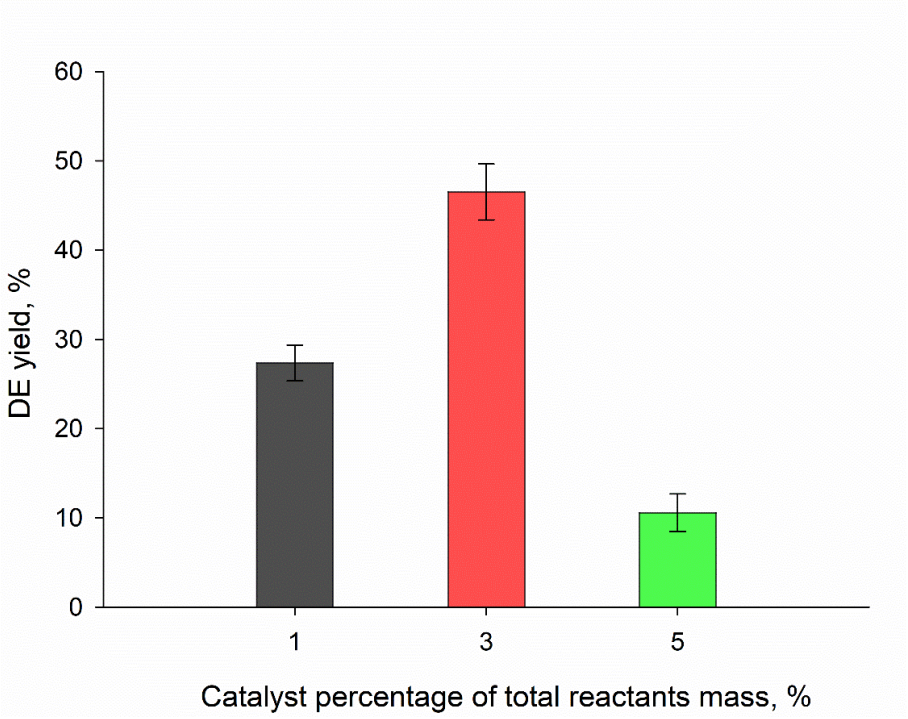

Figure 5.13: Effect of catalyst loading relative to total reactant mass on the biolubricant yield. 3 h of reaction with the catalyst 50CaO/SiO_2, alcohol:biodiesel molar ratio= 1: 4, temperature: 80 ° C and US power: 62 W. Error bars indicate the sample standard deviation.

- **Ultrasound vs. Mechanical Stirring**

We performed the experiments at the optimized parameters (3 % of 50CaO/SiO_2 relative to the total weight of the reagents, with the alcohol:biodiesel molar ratio= 1: 4, temperature: 80 ° C and US power: 62 W) to compare the results obtained under US with conventional stirring and utilizing both heterogeneous and homogenous catalysts. The sonicated and homogeneously catalyzed reaction produced 90 % ± 1.9 % of biolubricant yield against 16 % ± 1.9 % for the conventionally stirred reaction (Figure 5.14). The heterogeneously catalyzed one yielded 46 % ± 3.2 % DE after 180 min of sonication, however, it produced only 3 % ± 1.8 % DE with mechanical stirring. Transesterification is limited by mass transfer due to the immiscible nature of the reactants and the catalyst. US intensifies these reactions through acoustic cavitation, by forming microemulsions between the immiscible phases so that the interfacial surface area increases. This results in higher

yields in the US-assisted process. These findings are consistent with those of Boffito et al. [136]. They produced methyl esters from vegetable oils. An ultrasonic reactor transesterified 90 % of the feed in 5 min, whereas it took 90 min in a conventional batch reactor. Furthermore, in another work [159], they obtained a conversion of free fatty acids by US three times higher than with conventional mechanical stirring. Koutsouki et al. [238] demonstrated that the transesterification under mechanical stirring of rapeseed oil produced a 40 % lower yield than that of sonication under similar operating conditions.

Typically, in presence of a heterogeneous catalyst, the reaction requires a longer reaction time than with a homogeneous one to obtain the required product yields. In heterogeneous catalysis, the reaction mixture constitutes a three-phase system and the diffusion of reactants to the surface of the catalyst and the diffusion of products from the surface can be rate determining.

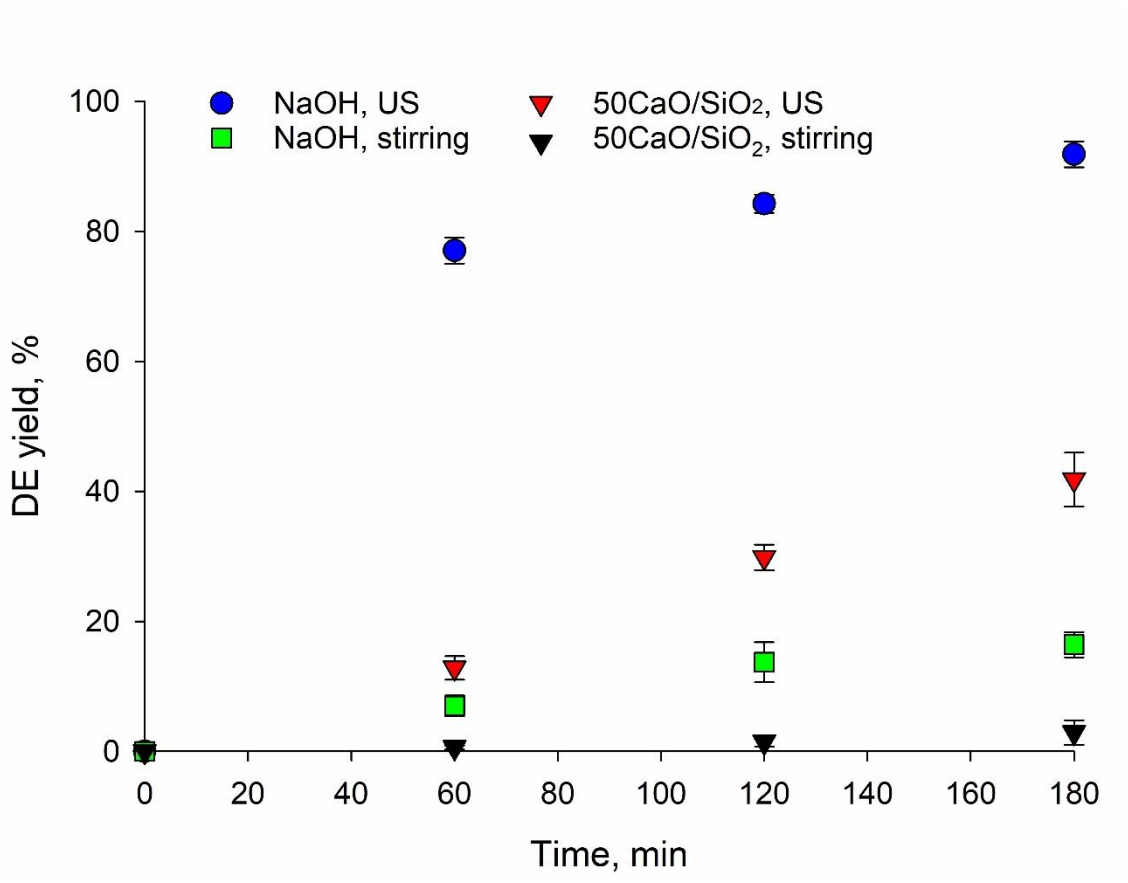

Figure 5.14: US Vs. mechanical stirring for homogeneous and heterogeneous catalysis. Error bars indicate the sample standard deviation.

- **Reusability Study of CaO/SiO_2 for the Synthesis of Biolubricants**

We investigated the reusability of the catalyst by repeating transesterification cycles under the optimal conditions of the US-assisted reaction. After each activity test, we separated the catalyst from the product mixture. After washing the catalyst with n-hexane to remove eventual impurities, an oven dried it at 60 °C for 24 h before being used for further reaction. The catalyst was still active after three reaction cycles with a DE yield greater than 20 % ± 2.5 % (Figure 5.15). However, its activity decreases over the cycles (it decreases by about 20 % after each cycle.). The reduction in activity can be attributed to the CaO leaching due to sonication.

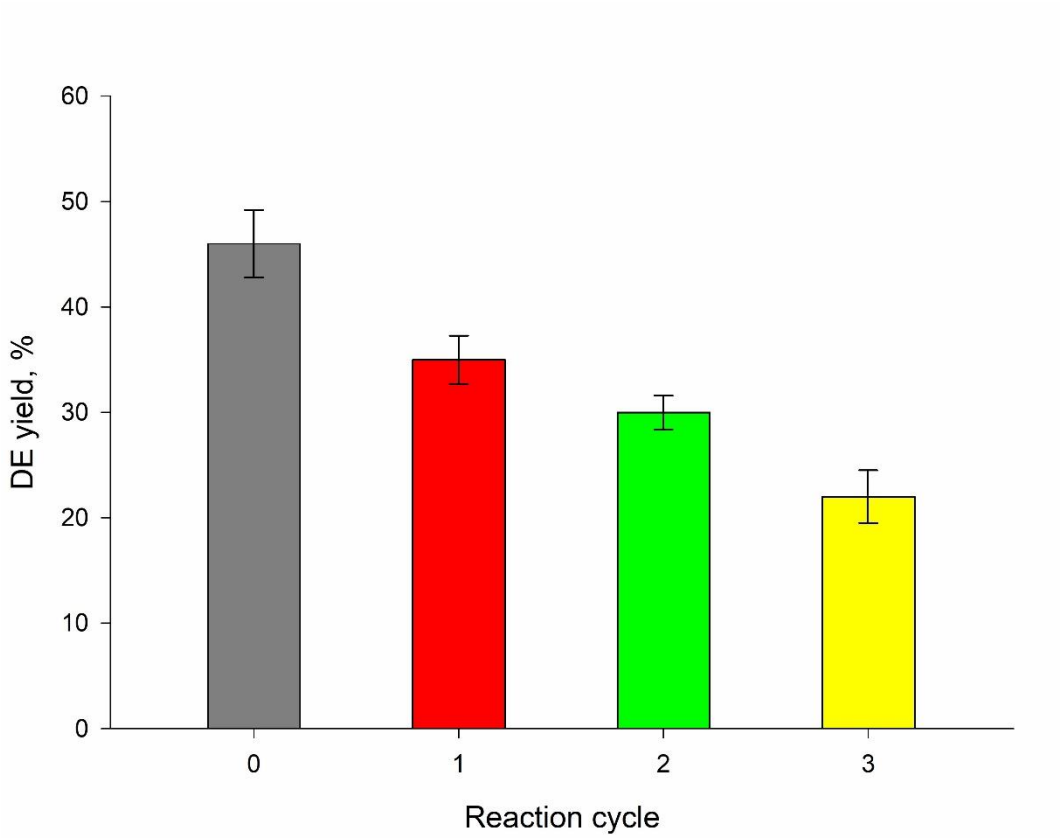

Figure 5.15: Reusability test of CaO/SiO_2.

We analyzed the biolubricant by XRF after each cycle (Table 5.8). XRF reveals CaO leaching as the catalyst is reused. The cavitation occurring near the surface of the catalyst leached the active species. This confirms that US lessened the activity of the catalyst throughout the reusability cycles.

Table 5.8: XRF analysis of the biolubricant after three cycles. The standard deviation of the measures was less than 0.01%

Test	Ca (ppm)
0	210.7
Cycle 1	191.5
Cycle 2	147.2
Cycle 3	103.9

5.4 Conclusions

We intensified the transesterification of canola FAME to synthesize lubricants. US resulted in a DE yield six times greater than the one obtained with the conventional process transesterification. The biolubricant produced is comparable to the commercial industrial oil ISO VG32 in terms of viscosity. The higher surface tension of TG and its lower vapor pressure compared to those of PG, promote cavitation, resulting in higher diester yield. A mild reaction temperature produced more DE yield (90 % ± 1.9 % of DE at 80 ° C vs. 42% ± 2.5 % at 100 ° C). The increase of the US power from 22 W to 62 W heightened the DE yield by 32 %. Reducing the alcohol:biodiesel molar ratio from 1:1 to 1:4 doubled the DE production. With a view to developing a cleaner synthesis process, we manufactured and tested an heterogeneous catalyst (CaO on SiO_2) on the transesterification reaction. A mass fraction of 50 % CaO relative to SiO_2 gave the highest DE yield (46 % ± 3.2 %) at a concentration of 3 % of the total reactants mass. After three reaction cycles, the catalyst retains its morphology and particle size. However, its activity decreases by 20% after each reuse. XRF analyzes confirmed leaching of the active phase, hence its instability to ultrasound. The yield of the reaction catalyzed by CaO/SiO_2 is two times lower than that achieved by NaOH, which is due to the limited mass transfer at the outer surface of the catalyst.

We combined heterogeneous catalysis with ultrasound to produce lubricants from biodiesel under mild reaction conditions. US is a valuable emerging green technology that plays a momentous role in sustainable chemistry.

CHAPTER 6 ARTICLE 3: NUMERICAL INVESTIGATION OF THE ULTRASOUND-ASSISTED BIODIESEL TRANSESTERIFICATION WITH A POLYALCOHOL

Héla Laajimi, Kobra Fattahi, Daria C. Boffito

Article submitted to Chemical Engineering and Processing: Process Intensification on April 15, 2022.

Abstract

Ultrasound elicits chemical and physical effects that drive and intensify chemical reactions. It can assist esterification and transesterification reactions for biomass conversion. There is extensive experimental data on the literature that highlight the effects of ultrasound on these reactions, but their numerical investigations are very few. In this work, we simulated an ultrasound-assisted biodiesel transesterification to produce lubricants. We studied the acoustic reactive flow by coupling acoustic, fluid dynamics, and chemical reaction models via the finite element software COMSOL Multiphysics. The acoustics interface in COMSOL computed the pressure field and the Reacting Turbulent Flow interface simulated the fluid velocity and the lubricant concentration profiles inside the reactor. After validating the numerical model with experimental results, we investigated the effect of the probe immersion depth and diameter on lubricant production. The probe immersion depth at mid-height level (at 3 cm depth) was the optimal position. It produced a higher lubricant yield than the 1 cm and 4 cm depths (94 % versus 86 % at 4 cm and 81 % at 1 cm). A 1.9 cm diameter probe yielded more lubricant than a 1.3 cm probe, maintaining the ultrasound power constant (e.g., 96 % lubricant versus 87 %, at 62 W).

Keywords: *Biolubricant, Ultrasound; Sonochemical reactor; Transesterification; Multiphysics modelling*

6.1 Introduction

To enrich its portfolio while being environmentally friendly, the bio-based chemical industry has turned to the implementation of process intensification (PI) technologies. PI significantly shrinks the size of a chemical plant (over 100 times smaller) while retaining production targets [155]. It accounts for energy and cost savings of 20 to 80 %, and 10 to 1000 times lower chemical discharges [239], [240]. PI technologies for chemical processing applications include intensified separations [155], [241], [242], static mixers [243], [244], microwave-assisted synthesis [245], [246], membrane separation [247], [248], and cavitational reactors such as sonochemical reactors [99], [249], [250]. In this work, we consider an ultrasound-assisted process as an approach to PI that we studied numerically to intensify the conversion of biodiesel into lubricants. This study complements previous work and aims to optimize the performance of the sono-reactor [251].

Through acoustic cavitation, ultrasound induces the generation of a radical plasma, local turbulence, and micromixing of a liquid in a reactor [96], [101]. These combinations of chemical and physical effects enhance heat and mass transfer and thus initiate and propagate chemical reactions [159]. The acoustic cavitation effects are entirely dependent on the operating parameters and reactor design [101]. A proper geometric configuration of the sono-reactor is crucial to ensure the efficiency of the ultrasonic process. Available literature data include the influence of geometric parameters on the performance of bath [252]–[254] or probe [255]–[257] reactors types, mainly at the experimental level. For instance, Son and co-authors investigated experimentally (by calorimetry, dosimetry KI, and sonochemiluminescence) the effects of the probe position, liquid height, and the ultrasound power on sonochemical oxidation reactions [119]. Hihn et al. mapped out the acoustic activity by dosimetry, electrochemistry, particle image velocimetry, and calorimetry [258].

Numerical simulation is a fundamental tool to assist and advance the design and scale-up of ultrasonic reactors. It provides additional numerical data that facilitates the understanding of acoustic activity and the optimization of functional parameters and geometry, by either replacing or complementing expensive experimental analysis [259]. Several research works reported the numerical simulation of the acoustic pressure and velocity distribution [260]–[263], the optimization of the cavitational activity by modifying the geometry and the probe position [255], [264]–[266], and the operating conditions of the ultrasonic reactor [180], [267]–[269]. For instance,

Niazi et al. assessed the acoustic pressure distribution and active zones numerically in an ultrasonic reactor for crude oil upgrading [261]. Klíma and co-authors optimized a sono-reactor geometry through an experimental and numerical investigation of the cell dimensions, the probe position, and the liquid volume [264]. Girard et al. carried out a numerical model to identify the optimum geometry, and probe position to improve the dispersion of a cellulose nanocrystals suspension [265]. The off-centred and halfway-up probe positions ensured the best suspension dispersion.

Ultrasound intensifies several types of chemical reactions, among which esterification and transesterification [111], [132], [140], [143], [215]. Here, we evaluate, through numerical simulation, the performance of the ultrasound-assisted transesterification of biodiesel with trimethylene glycol to produce a biolubricant. We implemented a COMSOL model to study the effect of ultrasound power and probe position and diameter. The literature on the simulation of ultrasound-assisted reactions and in particular on the coupling of acoustic pressure and reactive flow is very limited. Jordens and co-authors studied the thermal degradation of carbon tetrachloride with ultrasound in a tubular milliscale reactor [259]. They applied a COMSOL model to optimize the ultrasound power, frequency, and reactor diameter. To our knowledge, only Hussain and coauthors applied multiphysics simulation to characterize ultrasound-assisted transesterification for biodiesel production. They assessed the effect of the ultrasound frequency and power, the methanol to oil molar ratio and temperature on biodiesel yield [270]. Hussain and Janajreh modelled a continuous sonoreactor for biodiesel production [271]. They investigated the effects of the reactor length (20, 50, and 100 cm) and the number of transducers (single or dual). In a 20 cm length reactor, a single transducer generated higher acoustic pressure and greater biodiesel yield than two transducers placed opposite to each other. Single and dual transducer designs produced similar biodiesel yields at higher reactor lengths (50 and 100 cm).

In this work, for the first time, we simulate reactive acoustic streaming in an ultrasonic batch reactor, with COMSOL Multiphysics, to produce lubricants from the reaction between methyl esters (biodiesel) and a polyalochol. The model calculated the acoustic pressure distribution, the velocity field, and the lubricant concentration profile inside the reactor for probes of different diameters and varied immersion depths. We determined the reaction rate by considering the combined effect of sonication and flow agitation in the reactor. We assessed the accuracy of our

model by comparing it to the experimental results of previous work [251]. We investigated the effects of the probe diameter and immersion depth on the sono-reactor performance.

6.2 Methodology

We selected three different modules to simulate the reaction in COMSOL Multiphysics 5.5 software: 1) *the pressure acoustics, frequency domain module*; 2) *the turbulent flow, k-ℰ*; and 3) *the transport of concentrated species*. Our system was a batch reactor where a trimethylene glycol transesterified canola biodiesel to produce a lubricant. We verified the accuracy of our model by comparing it to the experimental results of previous work [251]. We performed these experiments utilizing a 500 W nominal power Sonics & Materials, Inc. ultrasound processor (VCX 500). The probe emitter operates at 20 kHz. The solid probe sonicated a mixture of trimethylene glycol and biodiesel (at alcohol:biodiesel molar ratio of 1:4) at powers of 22 and 62 W for 3 hours at 80 °C. All experiments took place in a jacketed glass reactor 4 cm in diameter and 10 cm in height. The probe was immersed in the solution to a 1 cm depth. Sodium hydroxide catalyzed the reaction with a mass fraction of 1 %.

In terms of simulations, we ran them under the same conditions as the experiments (62 W and 22 W, 80°C and molar ratio of 1:4) to ensure the accuracy of our model.

After validating the model, we studied the effect of different probe diameters (1.3 cm and 1.9 cm) and immersion depths (1, 3, and 4 cm) on lubricant production. We chose the 1.9 cm and 1.3 cm diameters because they are among the most marketed probes and they are suitable for our reaction volume (they are adapted for volumes between 50 and 500 mL) [272].

6.2.1 Numerical model

The modelling process consists of three steps (Figure 6.1):

1) *The pressure acoustics, frequency domain module* solves the acoustic field and acquires the vibration velocities and the acoustic pressure.
2) *The turbulent flow model (k-ℰ)* simulates the acoustic flow and calculates the fluid velocity.
3) *The transport of concentrated species* module calculates the concentration of the produced biolubricant after coupling the reaction rate due to sonication and flux.

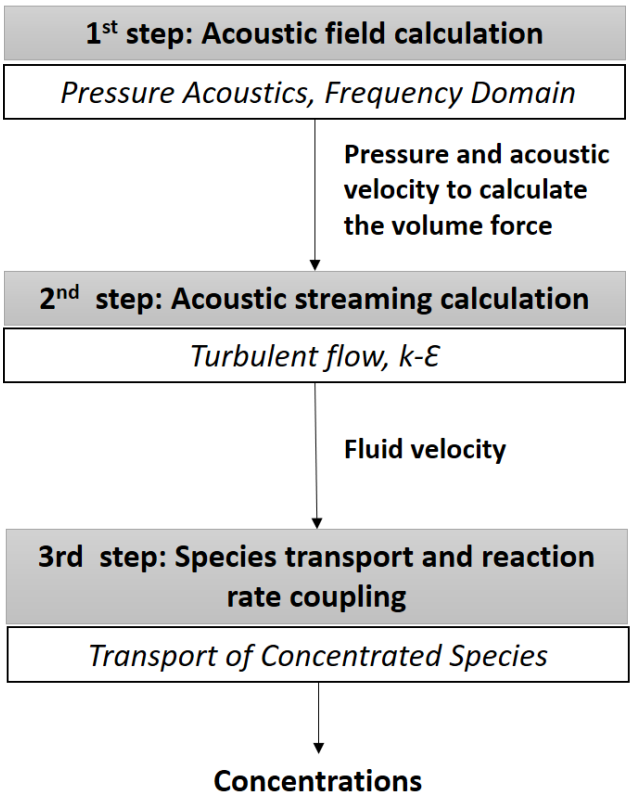

Figure 6.1: Modeling steps.

Acoustic pressure field

The *pressure acoustics, frequency domain* physic in COMSOL solves the Helmholtz equation (Eq. 6.1) for the propagation of sound waves to calculate the acoustic pressure *P* distribution [273].

$$\nabla^2 P \frac{1}{\rho} - \frac{\omega^2}{\rho s^2} P = 0 \quad (6.1)$$

Where ω is the angular frequency (equal to $2\pi f$), f is the ultrasound frequency (20 kHz), ρ is the biodiesel density and s is the speed of sound (Table 6.1). We designated the material as biodiesel because it is the majority product and will not change the density of the mixture significantly.

The linear absorption coefficient (α), of the sonicated medium , is equal to (Eq. 6.2):

$$\alpha = \frac{8\mu\pi^2 f^2}{3\rho s^3} \quad (6.2)$$

Where μ is the biodiesel dynamic viscosity.

Table 6.1: Biodiesel properties [251], [274].

Input parameter	Value
Density, ρ	881 kg m^{-3}
Viscosity, μ	0.014 Pa·s
Sound speed, s	1211.48 m s^{-1}
Absorption coefficient, α	9.4 10^{-5} m^{-1}

Acoustic streaming

The COMSOL physic *turbulent flow (k-ε)* modelled the steady acoustic streaming (Eq. 6.3) and calculated the flow velocity field, from the ultrasonic vibration velocity and the acoustic pressure (determined from the pressure acoustic module) [260], [275].

$$\rho(u.\nabla)u = \nabla\left[-P_{\mathrm{T}}I + (\mu + \mu_{\mathrm{T}})(\nabla u + (\nabla u)^{\mathrm{T}}) - \frac{2}{3}(\mu + \mu_{\mathrm{T}})(\nabla u)I - \frac{2}{3}\rho kI\right] + F \quad (6.3)$$

Where u is the acoustic streaming velocity, P_{T} is the total pressure, I is turbulent intensity, μ_T is the turbulent viscosity, k is the kinetic energy, and F is the volume force of the acoustic flow (Eq. 6.4). The indices i and j designate the direction of the flow and the bar means the average value over a period [276].

$$F_j = -\frac{\partial(\overline{\rho u_i u_j})}{\delta x_i} \quad (6.4)$$

Lubricant concentration

The *transport of concentrated species* module simulated the reaction within the flow. To calculate the concentrations of the products, we defined the order of the reaction as pseudo-first-order from a kinetic study (section 2.2). We solved the equation rate by coupling rates from the sonication and flow agitation (Eq. 6.5) [271], [277], [278]:

$$-R_{rx} = [(P > P_{Blake})\beta k_{son} C] + [(1-\beta)k_1 C] \quad (6.5)$$

Where R_{rx} is the reaction rate, P is the acoustic pressure, P_{Blake} is the threshold pressure (above which the cavitation bubble implodes and it is of the order of 0.1 MPa), β is the cavitation volume fraction, C is the concentration, k_{son}=A$e^{\frac{-E_a}{RT_{max}}}$ and k_1 are the reaction constants with and without ultrasound, $T_{max} = \frac{T_{liq}P(\gamma-1)}{P_v}$ is the temperature at a point of cavitational collapse, T_{liq} is the liquid

temperature, and P_v is the solvent vapor pressure. We determined the rate constant and the activation energy from a kinetic study (section 2.2).

Geometry and boundary conditions

We modelled the sonoreactor in the 2-D domain with an axisymmetric geometry (Figure 6.2). The computational domain consists of a big rectangle that represents the reaction mixture (with a height, H = 6 cm, and an internal diameter, D = 4 cm). We assumed that the material is biodiesel at the reaction temperature of 80 °C. The small rectangle represents the ultrasound probe (with a tip diameter, d_p = 1.3 cm and operating at 20 kHz) immersed in the liquid at different depths (1, 3, and 4 cm) from the top side of the beaker.

The air-liquid interface was a sound soft (acoustic pressure is zero) boundary condition for the acoustic pressure field, and it was a zero normal stress and an open boundary condition for the velocity and the concentration calculations. We defined a normal acceleration a_0 at the probe tip surface (Eq. 6.6) [265]:

$$a_{0z} = -4\pi^2 f^2 A_m \quad (6.6)$$

where a_{0z} is the acceleration in the z-direction and A_m is the amplitude of ultrasound and calculated from (Eq. 6.7) [279]:

$$P_{US} = \frac{1}{2}\rho c {A_m}^2 S_A (2\pi f)^2 \quad (6.7)$$

Where P_{US} is the ultrasound power, ρ is the liquid density and S_A is the ultrasound emission surface area.

For the other domain boundaries, we defined sound hard (the normal component of the acceleration is zero), no-slip (zero velocity), and no flux boundary conditions.

The Fluid Flow module generated automatically the mesh size by linear elements. After performing a mesh dependency analysis, we found the fine element size to be optimal. The computation time was 12 min.

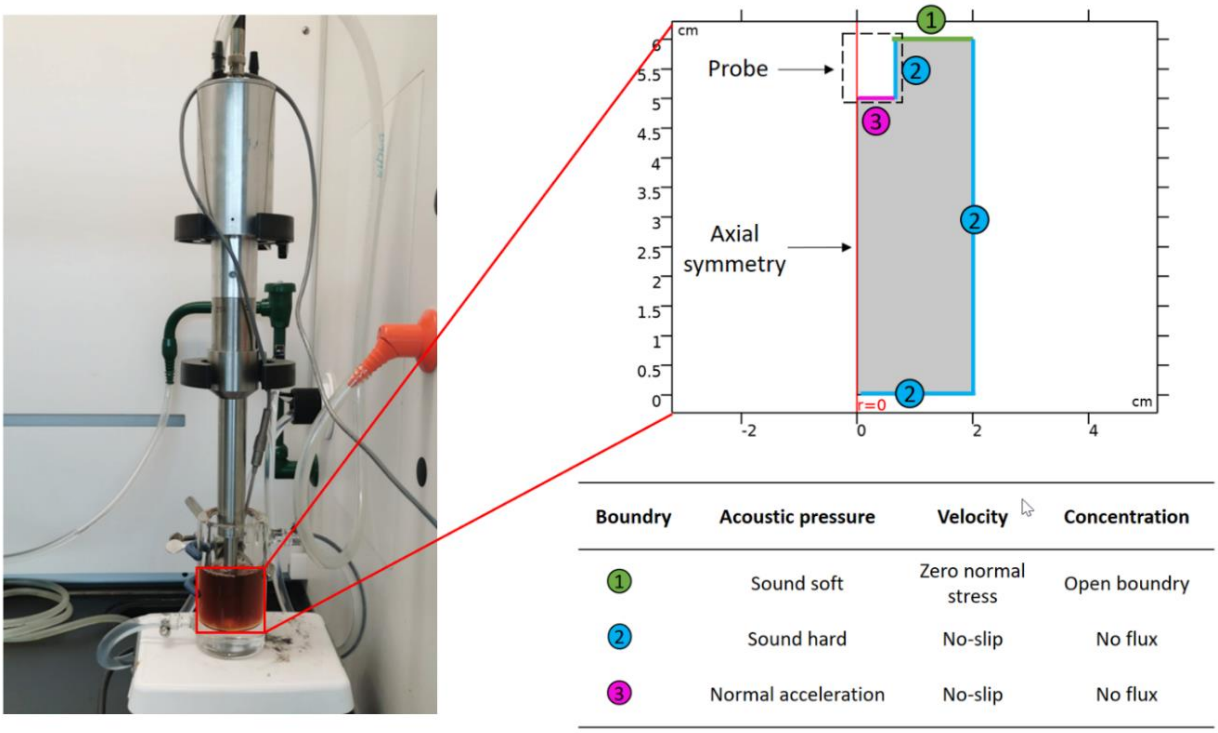

Figure 6.2: 2-D axisymmetric geometry and boundary conditions of the ultrasonic probe immersed in the reaction mixture.

6.2.2 Kinetic study

Here, we aimed to determine the kinetic constant and the activation energy as input parameters in the reaction model. Canola fatty acid methyl esters (FAME) transesterified trimethylene glycol (TG) to produce diester (DE) –lubricant and methanol (MeOH) (Eq. 6.8). NaOH (with a mass fraction of 1 % from the total reactant weight) catalyzed the reaction at 80 °C, 100 °C, and 120 °C.

$$2\,FAME + TG \overset{NaOH}{\longleftrightarrow} DE + 2\,MeOH \quad (6.8)$$

Excess biodiesel (a TG:biodiesel molar ratio of 1:4) and continued removal of methanol are used to drive the reaction forward. We analyzed the concentration of the limiting reagent (TG) to identify the reaction order and the kinetic parameters (rate constant and activation energy). We took samples every 10 min and we stored them in the fridge to quench the reaction prior to a GC analysis. A Scion 436 gas chromatograph (GC), with a flame ionization detector, and an Rtx-Biodiesel TG Column (fused silica, 15 m × 0.32mm ID × 0.10 μm) analyzed the products. We studied the kinetics

during the first 60 min of the reaction. We assumed pseudo-first-order (Eq. 6.9) and second-order kinetic models (Eq. 6.10). The pseudo-first-order kinetic equation is:

$$ln\frac{[TG_0]}{[TG]} = k_1 t \quad (6.9)$$

[TG₀] and *[TG]* are the initial concentration of trimethylene glycol and its concentration at time t, respectively, and k_1 is the pseudo-first-order rate constant.

The second-order kinetic equation is:

$$\frac{1}{[TG]} - \frac{1}{[TG_0]} = k_2 t \quad (6.10)$$

With $k_2$is the second-order rate constant.

We investigated the pseudo-first-order and the second-order kinetic models by plotting $ln\frac{[TG_0]}{[TG]}$ and $\frac{1}{[TG]}$ against t (Figure 6.3).

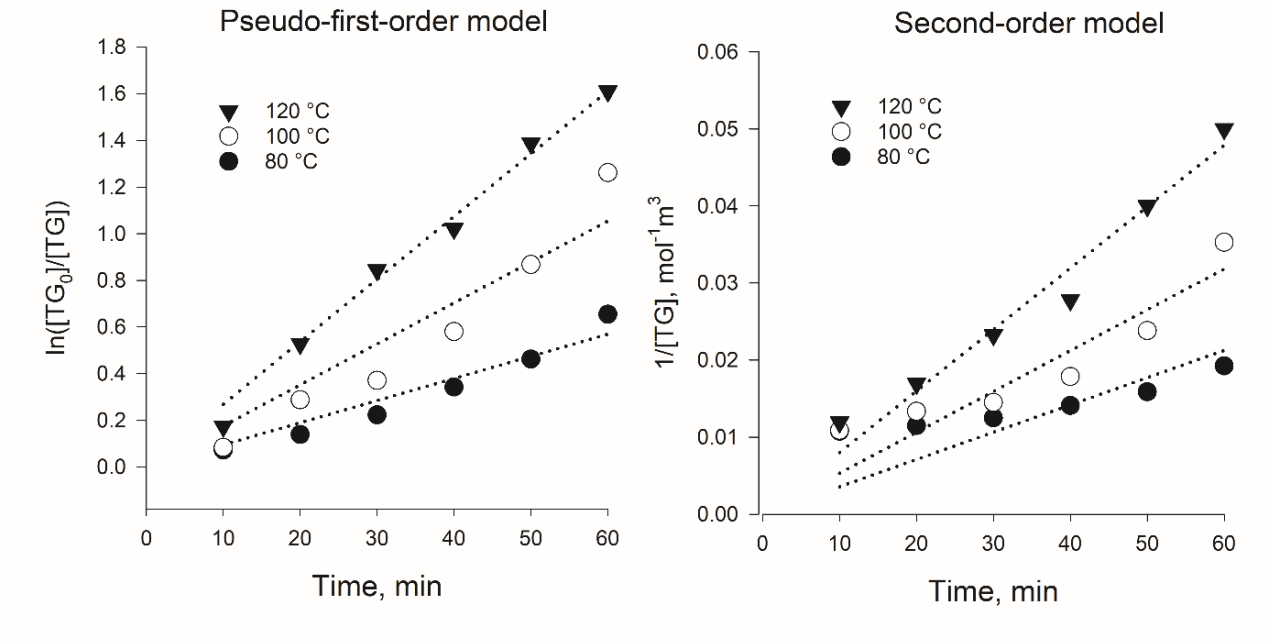

Figure 6.3: Pseudo-first and second-order kinetic models for the synthesis of biolubricant at 80 °C, 100 °C, and 120 °C. [TG0] and [TG] are the initial concentration of trimethylene glycol and its concentration at time t, respectively.

We assessed the consistency of the models with the experimental data according to the magnitudes of the linear correlation coefficient (R^2) [211], [280], [281]. During the first 60 minutes of reaction, at all three temperatures, the reaction follows a pseudo-first-order kinetic model (Table 6.2).

Table 6.2: Rate constants and regression values of the pseudo-first and second-order kinetic models at different temperatures (80 °C, 100 °C, and 120 °C). We regressed the data with normalization to minimize error. The mean squared errors were 6.2×10^{-9} for the first order and 1.6×10^{-11} for the second order.

Temperature	**Pseudo-first order**		**Second-order**	
(°C)	**k_1, 10^{-4} [s^{-1}]**	**R^2**	**k_2, 10^{-6} [$mol^{-1}\ m^3\ s^{-1}$]**	**R^2**
80	1.9	0.9686	3.3	0.9329
100	3.2	0.9515	5.7	0.8622
120	5.4	0.9929	9.4	0.9667

We calculated the activation energy, E_a from the slope of the plot of $\log_{10} k_1$ versus 1/T (Figure 6.4) from the Arrhenius equation (Eq. 6.11)

$$\log_{10} k_1 = \frac{-E_a}{2.303\mathrm{R}T} + \log_{10} A \quad (6.11)$$

R is the gas constant (8.314 J mol^{-1} K^{-1}). *T* is the temperature and A is the pre-exponential factor.

We selected the pseudo-first-order kinetic model to simulate the transesterification reaction of canola biodiesel with TG. The rate constant at 80 °C was 1.9×10^{-4} s^{-1} and the activation energy was Ea= 30.11 kJ mol^{-1}.

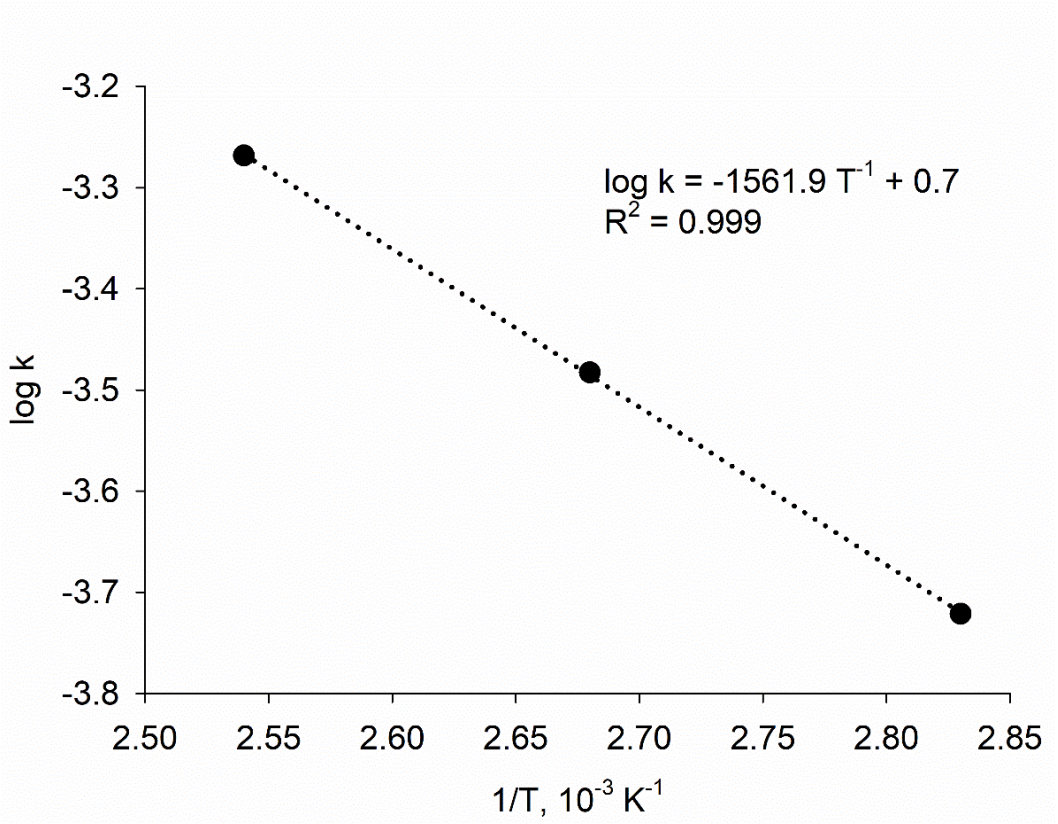

Figure 6.4: Normalized pseudo-first-order rate constant as a function of temperature.

6.3 Results and discussion

6.3.1 Model validation

We simulated the reaction under the same conditions of the previous experiments: at powers of 62 W and 22 W, 80°C, trimethylene glycol to biodiesel ratio equal to 1:4, the probe was 1.3 cm in diameter and immersed at a 1 cm depth. Modeling and experimental results were comparable (Table 6.3). The difference between modelled and experimental lubricant yield was less than 11 %. The result of the simulation at an ultrasound power of 62 W differs from the experimental result by 10 % and the difference was 3 % at 22 W. The variation is likely due to experimental errors during sampling or to GC analysis (the analytical method standard deviation was 0.28 and relative error was 22 % [222]). The model integrated the lubricant concentration in the entire volume of the reactor, whereas during experiments we took samples from the middle of the reactor, and despite continuous stirring, the solution might not have been completely homogeneous.

Table 6.3: Experimental and simulated lubricant yields at 62 W and 22 W. The error of the experimental results corresponds to the sample standard deviation.

Ultrasound power, W	**Biolubricant yield (simulation), %**	**Biolubrticant yield (experimental), %**
22	58	61 ± 2.9 %
62	81	91 ± 1.9 %

62 W of sonication generated a higher velocity field and lubricant concentration compared to 22 W (Figure 6.5). The velocity magnitude and the lubricant concentration reached, respectively, maximum values of 1.38 m s^{-1} and 0.26 mol m^{-3} at 62 W and of 0.39 m s^{-1} and 0.23 mol m^{-3} at 22 W. A power of 62 W generated a higher acoustic volume force, which drove a greater flow field to the bottom of the reactor. Tsochatzidis and co-authors investigated the influence of the ultrasound power and they recorded a quasi-linear increase in velocity with ultrasound power input [282]. At low power input, the flow jet vanishes near the reactor bottom. However, by increasing the power, it extends and reaches the bottom (velocity magnitude at the bottom of the reactor was greater than 0.4 m s^{-1} at 62 W and it was less than 0.15 m s^{-1} at 22 W). Higher velocity improves the mixing and miscibility efficiency of trimethylene glycol and biodiesel, which increases the contact surface between the two reactants, thereby improving mass transfer and promoting the reaction. These findings are consistent with those of our previous experimental work [234].

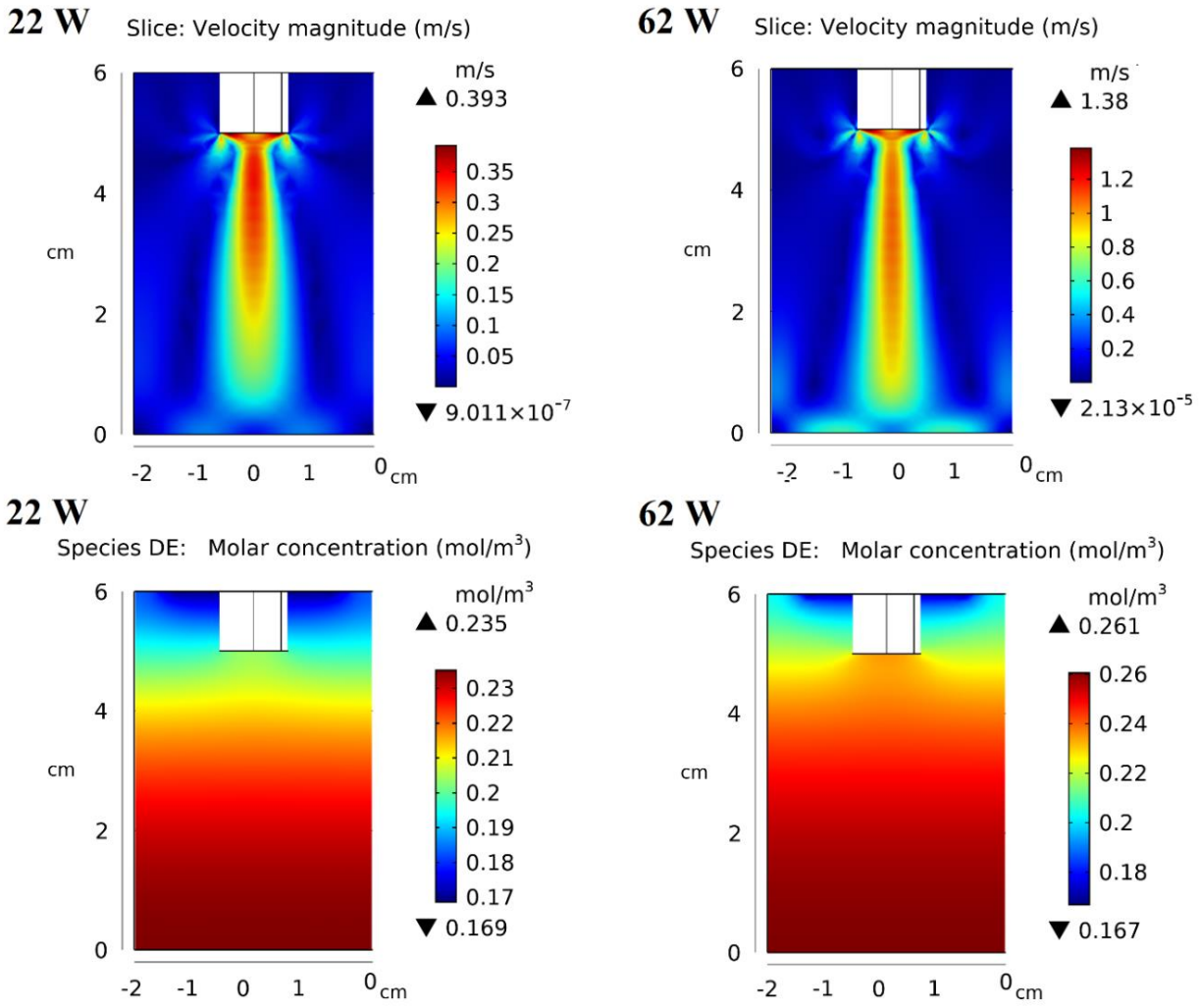

Figure 6.5: Velocity field and lubricant (DE) concentration profiles at different ultrasound powers 62 W and 22 W. The probe diameter was 1.3 cm and its immersion depth was 1 cm.

6.3.2 Effect of probe immersion depth

The acoustic flow arises from the probe tip and progresses towards the vessel's bottom (Figures 6.6 and 6.7). The flow changes its direction at the bottom of the reactor and moves upward along the inside wall. Changing the probe immersion depth affected the acoustic streaming inside the reactor. The area with low acoustic streaming (velocity amplitude less than 0.2 m s^{-1}) increases with the immersion depth of the probe (Figure 6.6). At 1 cm and 3 cm, the probe is located at a relatively greater distance from the bottom of the cell, which allows the flow rate to evolve thoroughly. These configurations offer enough space to create back-flows where the acoustic streaming can reach the

upper surface, which ensures uniform mixing in the reactor. The 3 cm depth generated the highest acoustic velocity value: 1.42 m s^{-1} against 1.38 m s^{-1} and 1.25 m s^{-1} for 1 cm and 4 cm depth respectively. At 3 cm depth, the acoustic vortex forms at the bottom of the cell and the flow continues to move upward forming two other additional acoustic vortices caused by the interaction with the down-flow and the inner wall (Figure 6.7). At 4 cm depth, the acoustic vortex forms in the lower regions of the cell and it is reduced at the upper regions. When the probe was near the bottom, the flow jet did not grow sufficiently and was blocked by the bottom wall of the vessel. This reduced the number of vortices generated due to the jet stream which decreased the mixing efficiency in the reactor.

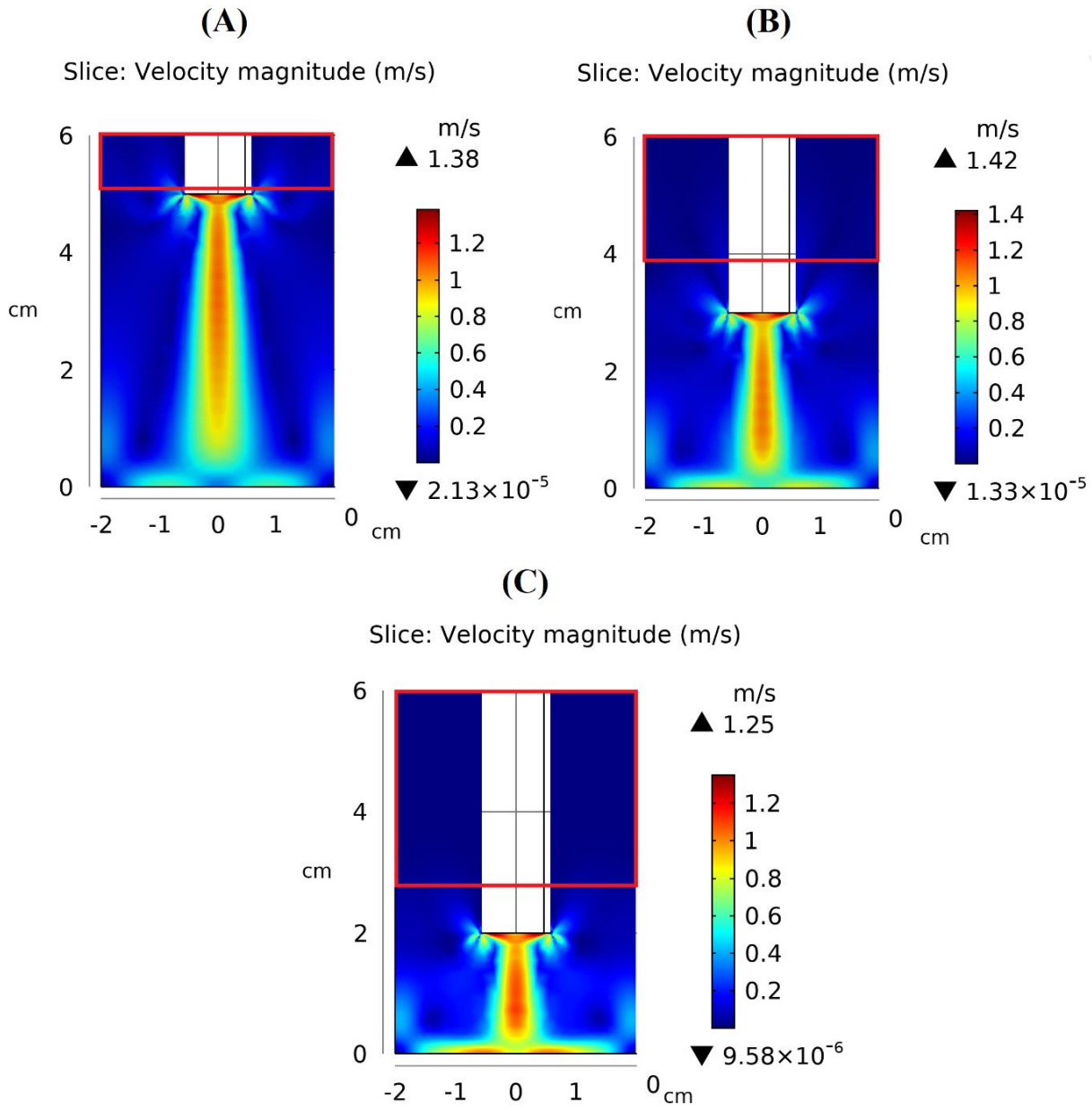

Figure 6.6: Velocity profiles at (A) = 1 cm, (B) = 3 cm and (C) = 4 cm immersion depths. The probe diameter = 1.3 cm and the ultrasound power = 62 W. The red box corresponds to the area where velocity magnitude is less than 0.2 m s^{-1}.

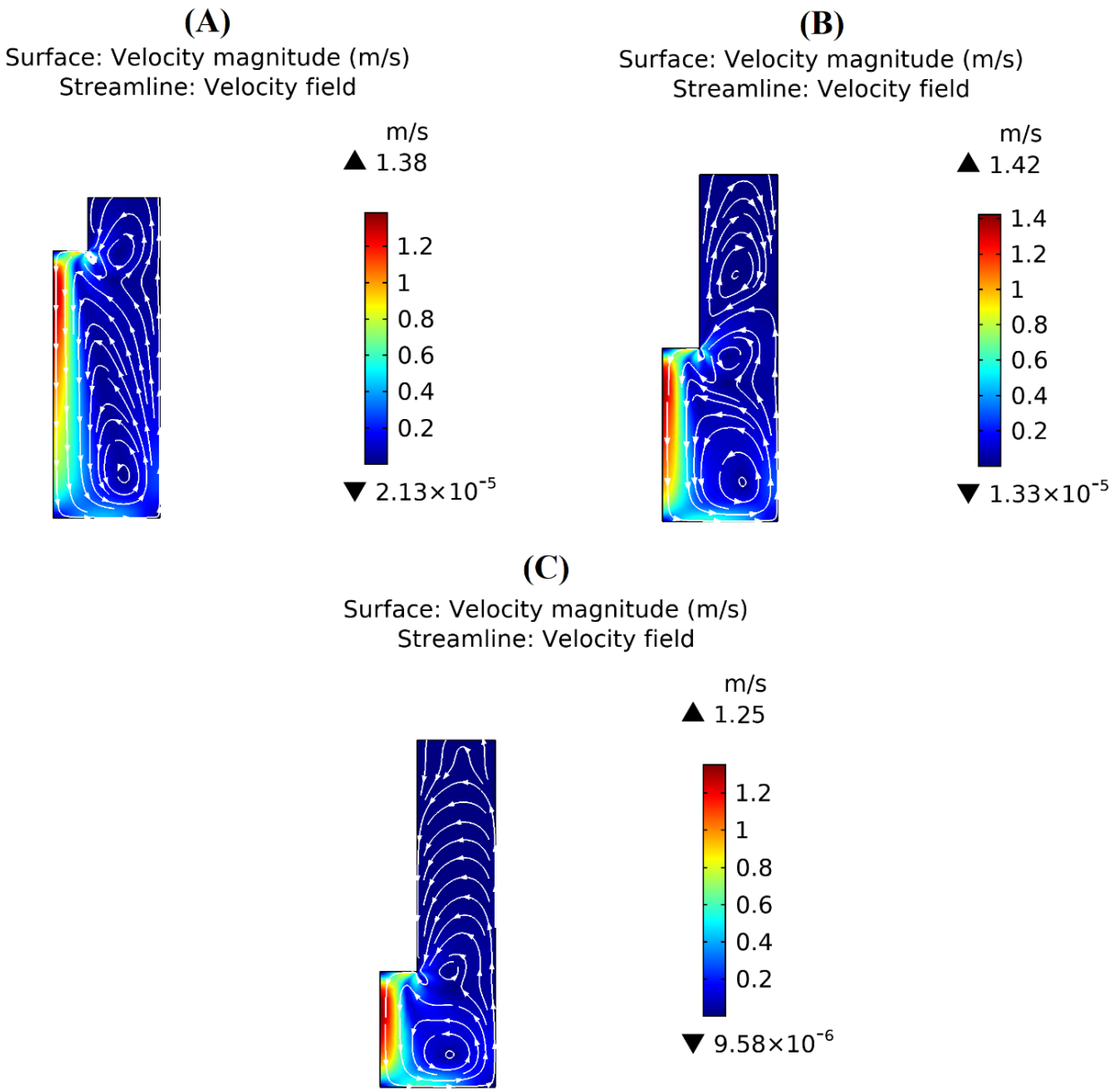

Figure 6.7: Acoustic streaming and streamlines at (A) = 1 cm, (B) = 3 cm and (C) = 4 cm immersion depths. The probe diameter = 1.3 cm and the ultrasound power= 62 W.

The COMSOL model calculated the average concentration in the entire volume of the reactor and then we calculated the lubricant yield (Figure 6.8). When the immersion depth increased from 1 cm to 3 cm, the lubricant yield increased from 81 % to 94 % and then decreased slightly to 86 % at 4 cm depth. The position of the probe at 3 cm depth produced the highest concentration of

lubricant (Figure 6.9). The maximum concentration at 3 cm depth was 0.3 mol m^{-3} compared to 0.28 mol m^{-3} and 0.26 mol m^{-3} at 4 cm and 1 cm, respectively. The middle position was optimal where the physical and chemical effects of acoustic cavitation come together. The middle position provides enough space for efficient and uniform mixing and is close enough to the reactor walls so that reflection of sound waves can occur and lead to the extension of active acoustic zones throughout the volume of the reactor and to the formation of hot spots which generate highly reactive radical species.

Figure 6.8: Probe immersion depth effect on the lubricant yield.

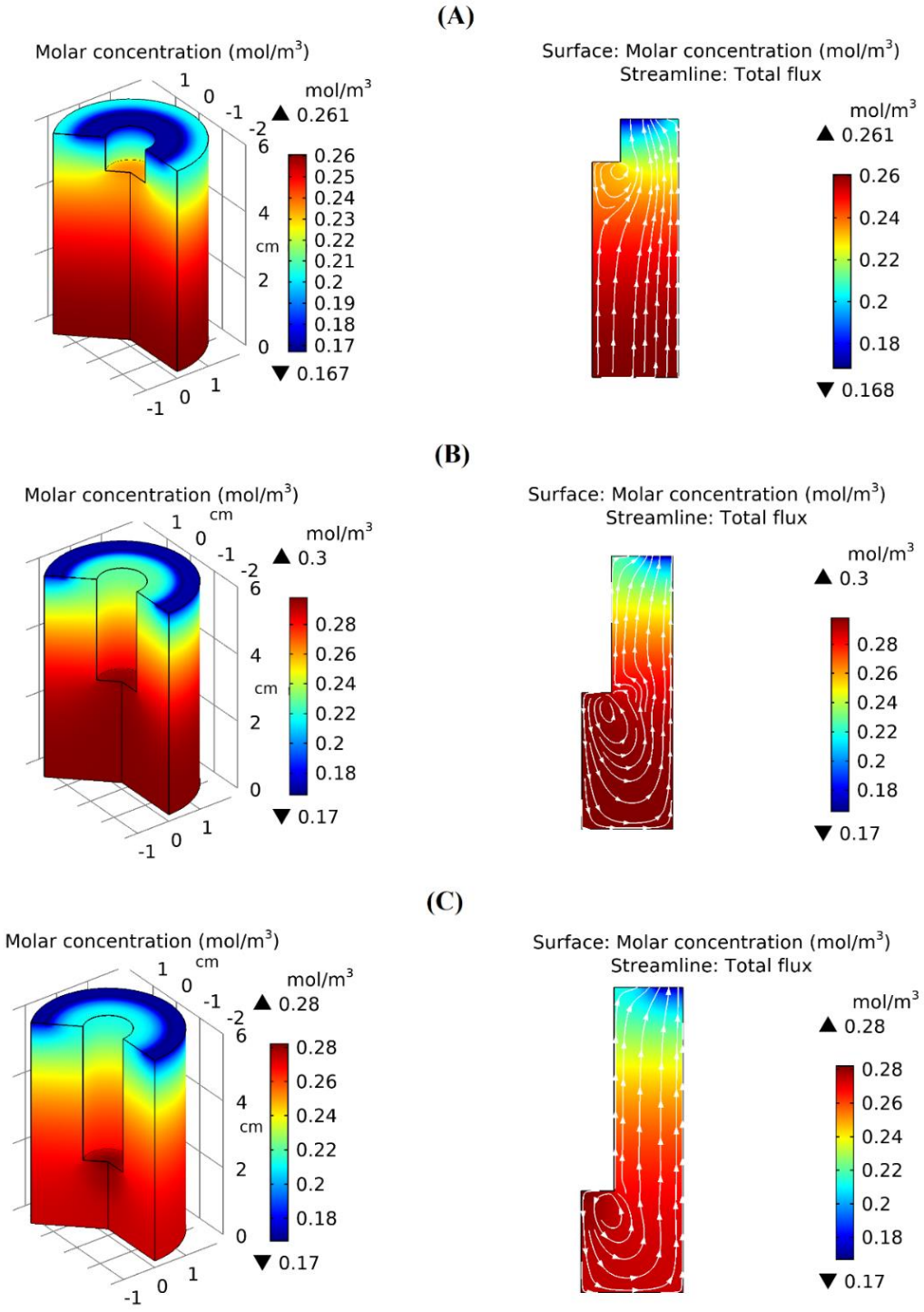

Figure 6.9: Lubricant concentration profile at different probe immersion depths (A = 1 cm, B = 3 cm and C = 4 cm). The white streamlines represent the total flux. The probe diameter was 1.3 cm and the ultrasound power was 62 W.

6.3.3 Effect of probe diameter

By setting the power to 62 W, the 1.9 cm diameter probe produced 96 % lubrication yield compared to 87 % obtained by the 1.3 cm probe. At 22 W, the 1.9 cm probe produced 12 % more lubricant than the 1.3 cm diameter (90 % vs. 78 %) (Figure 6.10). The larger the surface of the probe, the lower the intensity of the energy conveyed to the system, but the thickness of the flow jet is higher [283]. This boosted mixing efficiency in the reactor and thus produced more lubricant. These results agree with those of Hoffman and co-authors [284]. They investigated the impact of different probe diameters on the C-alkylation of benzyl cyanide. Abedi et al. surveyed the effect of ultrasonic probe size on the efficiency of ultrasonically assisted starch pre-gelatinization [285]. They reported that a larger surface area of the probe enhanced pre-gelatinization.

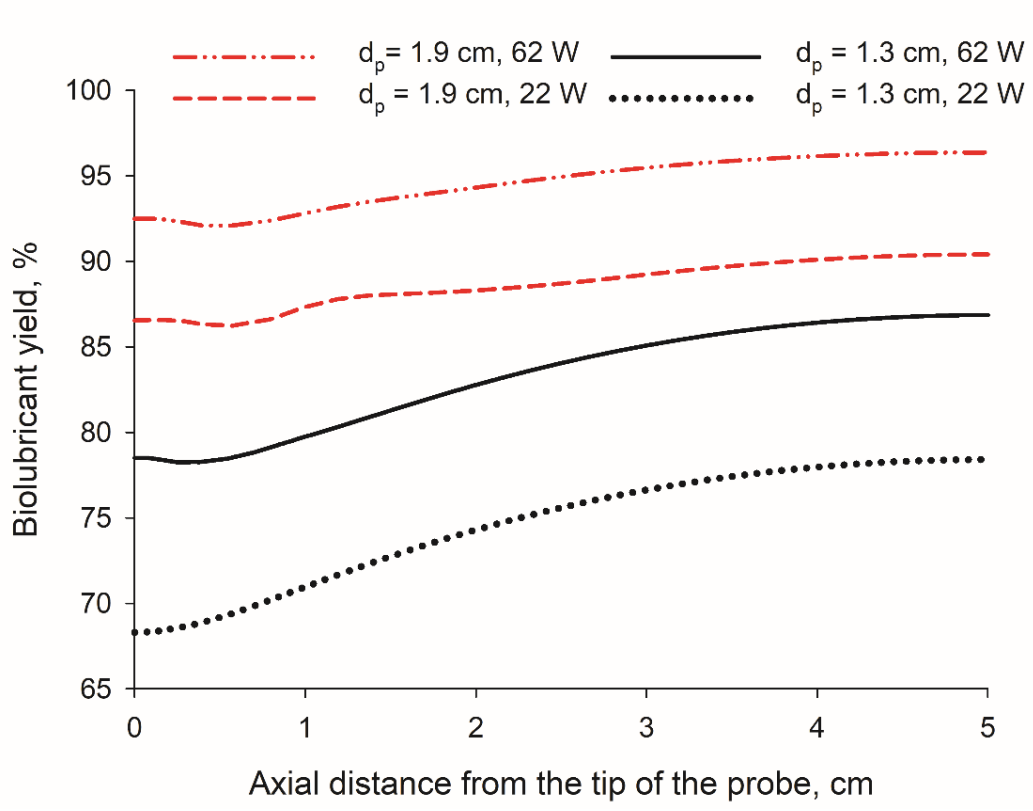

Figure 6.10: Lubricant yield as a function of the axial distance from the probe with a tip diameter (d_p) of 1.9 cm (red lines) and 1.3 cm (black lines) and an ultrasonic power of 22W and 62 W. The probe immersion depth in the reactor was 1 cm.

6.4 Conclusion

We simulated an ultrasound-assisted biolubricant synthesis to optimize the reactor's configuration. COMSOL calculated the acoustic pressure distribution and the steady acoustic streaming. A kinetic study defined the reaction as pseudo-first-order and determined the rate constant and the activation energy. We simulated the concentration profile after coupling the reaction rates with and without ultrasound. We validated our model with the experimental results to verify its accuracy. The simulated biolubricant yield differs from that obtained experimentally by less than 10 %. The probe immersion depth at mid-height of the reactor (at 3 cm depth) was the optimal depth where there was the highest velocity magnitude (1.42 m s^{-1} compared to 1.38 m s^{-1} and 1.25 m s^{-1} for 1 cm and 4 cm depth, respectively) and lubricant yield (94 % compared to 86 % at 4 cm deep and 81 % at 1 cm). This position granted efficient mixing and extension of the active acoustic zones throughout the reactor volume since the probe was close enough to the reactor walls for sound wave reflection to take place. At fixed ultrasonic power, a 1.9 cm diameter probe yielded more lubricant than a 1.3 cm probe (96 % biolubricant vs. 87 % at 62 W and 90 % vs. 78 % at 22 W). For future work, this methodology will be practical for assessing more reactor sizes and geometries, and other materials for process intensification by ultrasound of different reactions. A 3D model will allow to evaluate other positions (radial position or angle with respect to the vessel walls) of the ultrasonic probe, it would also be interesting to further develop this model to consider the reaction in presence of a heterogeneous catalyst.

CHAPTER 7 GENERAL DISCUSSION

This PhD project aimed to study experimentally and numerically an ultrasound-assisted transesterification of biodiesel with polyalcohols to produce a lubricant. In the first part of the project, we quantified the chemical effect threshold of the acoustic cavitation in the polyalcohols (trimethylene glycol and propylene glycol) and in the presence of SiO_2 particles. EPR spectroscopy detected the generation of hydroxyalkyl radicals from pyrolysis in collapsing cavitation bubbles. The study of the catalyst size effect demonstrated that the concentration of radicals in the medium increases with the particle size. For example, after 60 minutes of sonication, the concentration of radicals generated in the vicinity of 12-26 µm particles was twice as high as that of 5-15 nm particles. We attributed this to the fact that the larger the particle size, the more nucleation sites there are on the particle surface, producing more cavitation bubbles and thus more radicals. For nano-sized particles, the acoustic bubbles implosion generates shear flows of micro size, whose diameter is larger than that of the solid particles. These are then encircled by fluid streams, which disperse them in various directions. Hence the negligible effect of these nanoparticles on the acoustic cavitation. Furthermore, we investigated the effect of the solid quantity on radical production. The concentration of 0.5 % SiO_2 from the total mass generated more radicals than 3 %. The large number of particles in the solution behaves as obstacle and slows down the propagation of ultrasound. A dense solid particle concentration vanishes the sound waves, reducing the concentrated energy conveyed to the system. According to the literature, the formation of radicals increases with the concentration of particles in the solution but above a certain amount it decreases again. We did not rely on these results for the choice of the amount of catalyst in the following work but rather chose to further investigate the effect of the catalyst concentration on the reaction. The concentration of radical species in the medium increased with the ultrasonic power. Indeed, the cavity volume grows proportionally to the intensity of the irradiation, intensifying the collapse and leading to greater cavitation effects. As the temperature increased from 61 to 75 °C, the concentration of radicals in the medium increased (from 19 M to 27 M after 50 minutes of sonication). We ascribed this phenomenon to the rise in vapor pressure inside the bubble with

operating temperature. Therefore, the concentration of chemical species within the cavitation bubble is higher, leading to much more free radicals in the system. This accelerates chemical reactions, which is important in the following work where the biodiesel transesterification will take place and we need to set an optimal operating temperature.

The second part of the project focus mainly on the optimization of the ultrasound-assisted biodiesel conversion into lubricant. The biodiesel was produced from the esterification of commercial canola oil with methanol. We sonicated the biodiesel with polyalcohols in the presence of NaOH to optimize the reaction conditions. From the study of the effect of the type of polyalcohol, we confirmed that: the higher the surface tension and lower the vapour pressure of the polyalcohol, the more lubricant it produces. This is due to the fact that these properties induce more energy to be released during cavitation bubble collapse, resulting in a higher concentration of free radicals in the medium and thus promoting lubricant production (e.g., under similar reaction conditions, trimethylene glycol yielded 90 % ± 1.9 % of lubricants compared to 30 % ± 2.1 % for propylene glycol). A mild reaction temperature yielded more lubricant (90 % ± 1.9 % of lubricant at 80 ° C vs. 42% ± 2.5 % at 100 ° C). We previously (Article 1) established that increasing the temperature improves the reaction yield because more free radicals are present in the media. However, based on what we obtained in article 2, we assume there is an optimal temperature that should not be surpassed (in our case, 80 °C). At higher temperatures, the alcohol evaporates and the vapour content in the cavitation bubble rises, dampening the collapse of the acoustic bubbles and weakening the shock waves, leading to fewer radicals in the system. Furthermore, vaporization reduces the amount of alcohol in contact with the biodiesel, preventing the reaction from taking place. Lubricant production was doubled when we reduced the alcohol:biodiesel molar ratio from 1:1 to 1:4. Increasing the ultrasound power from 22 to 62 W improved lubricant yield (by 32 %) for both polyalcohols while keeping all other variables constant. High-power dissipation causes cavitation bubbles to collapse more violently. This improves alcohol and biodiesel mixing and miscibility, thereby increasing the area of contact between the two reactants, which improves mass transfer and speeds up the reaction. After identifying the parameters that maximize the performance of the lubricants (62 W, 80 °C and molar ratio of 1:4), we tested them on the CaO/SiO_2-catalyzed reaction. We prepared three catalysts with 24 %, 34 % and 50 % mass fraction of CaO supported on SiO_2 by incipient wetness impregnation. The catalyst was tested in three mass fractions: 1, 3,

and 5 % of the total reactant weight. The results of the article 2 were consistent with those of article 1 regarding the effect of the catalyst loading on the reaction performance. They confirmed that above a certain concentration, the catalyst starts to behave as a barrier, slowing the propagation of ultrasound and dampening the rates of mass transfer around the particles. 3 wt % of the catalyst to the total reagent mass was the optimal loading. After three reaction cycles, the catalyst particles retained their morphology and size but the CaO concentration on the SiO_2 support decreased by 20 %. Each cycle reduced the activity of the catalyst by about 20 %. This decrease in activity was ascribed to CaO leaching due to sonication. When catalyzed homogeneously, the sonicated reaction yielded six times more lubricant than the normally stirred reaction, and 15 times more lubricant when catalyzed heterogeneously. Ultrasonic process promotes mass and heat transfer between the reactants and the catalyst, which accounts for the greater yields of ultrasonic-assisted transesterification. They induce the formation of micro-emulsions between the immiscible phases, thus enlarging the interfacial area for the reaction. The lubricant produced by both homogeneous and heterogeneous catalysis, met the specifications for an ISO VG 32 industrial lubricating oil in terms of viscosity.

The third part of the project was devoted to a numerical study in order to optimize the geometric configuration of the sonoreactor and to maximize the lubricant yield. We investigated, via COMSOL Multiphysics, the effects of the ultrasound power, different probe diameters (1.3 cm and 1.9 cm) and immersion depths (1, 3 and 4 cm) on the lubricant production. The numerical model calculated the acoustic pressure distribution, velocity field, and the lubricant concentration profile inside the reactor. A kinetic modelling defined the reaction as pseudo-first-order and determined the rate constant and the activation energy. We considered the collective effect of sonication and flow agitation in the reactor to calculate the reaction rate. We verified the accuracy of our model by comparing it to the experimental results of previous work (Article 2). We ran the simulations under the same conditions as the experiments (62 W and 22 W, 80 °C and molar ratio of 1:4). The difference between the simulated and experimental lubricant yield was less than 10 %. A greater velocity magnitude was achieved with a 62 W ultrasonic power than with a 22 W, resulting in a higher lubricant yield (81 % with 62 W and 58 % with 22 W). A higher velocity improves the miscibility and mixing efficiency of the polyalcohol and biodiesel, increasing the contact surface between the two reactants and speeding up the reaction. These findings corroborate those acquired

experimentally in the second part of the project (Article 2). We also studied the effect of the probe immersion depth since it is considered as one of the essential geometrical parameters that significantly influence the sono-reactor's performance. Changing the probe immersion depth affected the acoustic streaming and the lubricant yield inside the reactor. The ultrasound probe placed halfway up the reactor (at 3 cm depth) produced more lubricant than when placed at 1 cm and 4 cm depths (the corresponding yields were 94 %, 81 % and 86 %). The middle position was ideal because it combined the physical and chemical effects of acoustic cavitation; It creates enough space for efficient and homogeneous mixing and is close enough to the reactor walls to allow the reflection of sound waves, resulting in the extension of active acoustic zones throughout the reactor volume and the formation of hot spots that generate highly reactive radical species. A 1.9 cm diameter probe yielded 10-12% more lubricant than a 1.3 cm probe. A probe tip with smaller surface area produces more intense cavitation, but the energy released is limited to a narrower, more concentrated field. In contrast, a larger area probe tip generates less intense cavitation but disperse the energy over a larger area and produce a thicker flow jet. This improves the mixing efficiency in the reactor, resulting in higher lubricant yield.

CHAPTER 8 CONCLUSION

8.1 Conclusion

Climate change is a major environmental concern of our time. The vision of this project is to contribute to the reduction of the carbon footprint by combining process intensification and biomass conversion. This doctoral project will advance research on green chemical production. My main objective is to implement a process intensification technology, a sonochemical reactor, to produce lubricant from canola biodiesel and biomass derived polyalcohols. The first part of the project focused on the quantification of the chemical effects of acoustic cavitation, in terms of free radical production. We examined the behavior of polyalcohol and solid catalyst towards ultrasound irradiation and their effects on the acoustic yield. Our goal is to connect this latter to lubricant selectivity in order to minimize energy requirements. The findings of the first article demonstrated that adding particles of the optimum concentration and size to a sonochemical process boost radical yield and, overall acoustic pressure in specific reactor zones. This work advances the knowledge in the field of food and metal extraction, solid processing, and especially in the area of catalysis and process intensification in general. Indeed, quantifying the chemical effects of ultrasound in an organic solvent and in the presence of solids will aid in identifying synergies of ultrasound and heterogeneous catalysis, in order to maximize yields and selectivity while reducing energy consumption.

The second part of the project (article 2) covered the ultrasonic production of lubricants from biodiesel under mild reaction conditions. A NaOH-catalyzed reaction yielded 90 % lubricant at 80 °C, with an ultrasonic power of 62 W, and with an alcohol:biodiesel molar ratio of 1:4. We synthesized and tested the activity of a solid catalyst CaO/SiO_2 on the reaction. Compared to the traditionally stirred reaction, the ultrasound-assisted one produced 15 times more lubricant (46 % lubricant versus 3 % lubricant obtained with mechanical stirring). However, ultrasound induced CaO leaching although its morphology and size were stable. Moreover, the activity of the catalyst decreased by 20 % as it was reused.

Since the acoustic cavitation effects are entirely dependent on the operating parameters and the design of the reactor, an appropriate geometrical configuration of the sono-reactor components is essential to ensure the efficiency of the process. It is in this context that we elaborated the third part of the project. This part provides a method to simulate the ultrasound-assisted lubricant synthesis

to optimize the reactor's configuration. We coupled, for the first time, acoustic pressure and reactive turbulent flow to simulate a sono-chemical reaction. We investigated the effects of the ultrasound power, different probe diameters and immersion depths on the lubricant yield. The proposed methodology is of importance for assessing other parameters, more reactor sizes and geometries, and materials to optimize operating conditions and identify areas for improvement on an industrial scale. The result of this work advances the research on process intensification, specifically combining multiphysics with kinetic modelling. It also proposes ways to valorize biomass, as well as to design reactors for sonoprocessing.

The results of this PhD project will have an implication in the process intensification scenario in general, and in particular in ultrasound-assisted processes involving heterogeneous catalysts. Such results will open up new reaction pathways to synthesize chemicals derived from biomass, thus contributing to the advancement of knowledge.

8.2 Limitation of the solution proposed

Ultrasound may have a positive or negative impact on the structures and performance of solid catalysts. Indeed, the physical and chemical effects exerted locally on a catalytic surface during the implosion of cavitation bubbles can be beneficial (e.g. to increase the specific surface area, deliver energy to the catalyst/reaction, activate or generate active sites in situ, or regenerate it) as well as detrimental (e.g. leaching or deactivation of the catalyst). In our case, the CaO/SiO_2 catalyst we synthesized was unstable under ultrasound exposure as the active phase leached and its activity decreased with each reuse, knowing that the maximum lubricant yield it generated did not exceed 46 %.

8.3 Recommendation for the future research

For future work, we suggest i) anchoring CaO on another support such as Al_2O_3 or mesoporous silica SBA-15 as it is possessed good hydrothermal and mechanical stability, or ii) stabilizing the active phase by preparing a mixture of calcium-based oxides such as CaO/MgO, CaO/ZnO or CaO-La_2O_3. Other base catalysts that have been shown to be ultrasonically stable in the literature, such as Zn-Mg-Al hydrotalcite, SrO and BaO, shall also be investigated.

We also propose further analysis of the biolubricant by determining the pour point, flash point, and oxidation stability and measuring its biodegradability.

We also recommend replacing the canola oil with a non-edible oil. Since Canada is a leader in the production of canola oil and rapeseed oil (with high erucic acid content), it would be preferable to replace canola oil with high erucic rapeseed oil as the latter is toxic to humans when consumed. The transition to a continuous process would also be interesting because it is more attractive at large scale. A techno-economic analysis would be necessary beforehand to ensure that the process can guarantee higher yields while minimizing costs and carbon footprint.

REFERENCES

[1] W. M. O. (WMO), W. M. O. (WMO), (UNEP) United Nations Environment Programme, (IPCC) Intergovernmental Panel on Climate Change, S. and C. O. (UNESCO); I. O. C. (IOC) United Nations Educational, and G. C. Project, *United In Science 2021*. Geneva: WMO, 2021.

[2] "The Paris Agreement | United Nations." https://www.un.org/en/climatechange/paris-agreement (accessed Mar. 29, 2022).

[3] P. Friedlingstein *et al.*, "Global Carbon Budget 2020," *Earth Syst. Sci. Data*, vol. 12, no. 4, pp. 3269–3340, Dec. 2020, doi: 10.5194/ESSD-12-3269-2020.

[4] "Renewable Power Generation Costs in 2019." https://www.irena.org/publications/2020/Jun/Renewable-Power-Costs-in-2019 (accessed Mar. 30, 2022).

[5] "Net Zero Coalition | United Nations." https://www.un.org/en/climatechange/net-zero-coalition (accessed Mar. 29, 2022).

[6] "2030 Plan for a Green Economy | Gouvernement du Québec." https://www.quebec.ca/en/government/policies-orientations/plan-green-economy (accessed Mar. 30, 2022).

[7] "An assessment of the opportunities and challenges of a bio-based economy for Agriculture and Food Research in Canada." https://atrium.lib.uoguelph.ca/xmlui/handle/10214/15052 (accessed Mar. 30, 2022).

[8] "Canola industry in Canada, from farm to global markets." https://www.canolacouncil.org/about-canola/industry/ (accessed Mar. 30, 2022).

[9] "Bio lubricants Market Size, Share | Global Report, 2020-2027." https://www.fortunebusinessinsights.com/bio-lubricants-market-104654 (accessed Apr. 13, 2022).

[10] "North America Accounts for 47.8% Global Bio Lubricants Market Share in 2021: Persistence Market Research."

https://www.persistencemarketresearch.com/mediarelease/biolubricants-market.asp (accessed Apr. 13, 2022).

[11] M. C. Bubalo *et al.*, "A comparative study of ultrasound-, microwave-, and microreactor-assisted imidazolium-based ionic liquid synthesis," *Green Process. Synth.*, vol. 2, no. 6, pp. 579–590, Dec. 2013, doi: 10.1515/GPS-2013-0086.

[12] "US7601677B2 - Triglyceride based lubricant - Google Patents." https://patents.google.com/patent/US7601677B2/en (accessed Apr. 19, 2022).

[13] L. E. Mirci and A. Pătrut, "Synthetic adipic complex tetraesters as eco-friendly lubricants," *Lubr. Sci.*, vol. 25, no. 5, pp. 339–350, Aug. 2013, doi: 10.1002/LS.1226.

[14] W. R. Murphy, D. A. Blain, and A. S. Galiano-Roth, "Benefits of synthetic lubricants in industrial applications," *J. Synth. Lubr.*, vol. 18, no. 4, pp. 301–325, Jan. 2002, doi: 10.1002/JSL.3000180406.

[15] E. O. Aluyor, K. O. Obahiagbon, and M. Ori-Jesu, "Biodegradation of vegetable oils: A review," *Sci. Res. Essay*, vol. 4, no. 6, pp. 543–548, 2009, Accessed: Apr. 19, 2022. [Online]. Available: http://www.academicjournals.org/SRE.

[16] T. M. Panchal, A. Patel, D. D. Chauhan, M. Thomas, and J. V. Patel, "A methodological review on bio-lubricants from vegetable oil based resources," *Renew. Sustain. Energy Rev.*, vol. 70, pp. 65–70, Apr. 2017, doi: 10.1016/J.RSER.2016.11.105.

[17] Y. M. Shashidhara and S. R. Jayaram, "Vegetable oils as a potential cutting fluid—An evolution," *Tribol. Int.*, vol. 43, no. 5–6, pp. 1073–1081, May 2010, doi: 10.1016/J.TRIBOINT.2009.12.065.

[18] J. A. Cecilia, D. B. Plata, R. M. A. Saboya, F. M. T. de Luna, C. L. Cavalcante, and E. Rodríguez-Castellón, "An Overview of the Biolubricant Production Process: Challenges and Future Perspectives," *Process. 2020, Vol. 8, Page 257*, vol. 8, no. 3, p. 257, Feb. 2020, doi: 10.3390/PR8030257.

[19] N. Salih and J. Salimon, "A Review on Eco-Friendly Green Biolubricants from Renewable and Sustainable Plant Oil Sources," vol. 11, no. 5, pp. 13303–13327, 2021, doi: 10.33263/BRIAC115.1330313327.

[20] H. M. Mobarak *et al.*, “The prospects of biolubricants as alternatives in automotive applications,” *Renew. Sustain. Energy Rev.*, vol. 33, pp. 34–43, May 2014, doi: 10.1016/J.RSER.2014.01.062.

[21] J. Van Rensselar, “Biobased Lubricants: Gearing up for a green world COVER STORY,” Jan. 2010, Accessed: Apr. 18, 2022. [Online]. Available: https://www.stle.org/images/pdf/STLE_ORG/BOK/LS/Base Oils/Biobased Lubricants_Gearing up for a Green World_tlt article_Jan10.pdf.

[22] J. Salimon, N. Salih, and E. Yousif, “Biolubricants: Raw materials, chemical modifications and environmental benefits,” *Eur. J. Lipid Sci. Technol.*, vol. 112, no. 5, pp. 519–530, May 2010, doi: 10.1002/EJLT.200900205.

[23] H. E. Henderson, “Re-Refined Base Oils,” *Synth. Miner. Oils, Bio-Based Lubr.*, pp. 379–386, Jan. 2020, doi: 10.1201/9781315158150-22.

[24] M. A. Hossain *et al.*, “Development of catalyst complexes for upgrading biomass into ester-based biolubricants for automotive applications: a review,” 2018, doi: 10.1039/c7ra11824d.

[25] W. Liew Yun Hsien, “Utilization of Vegetable Oil as Bio-lubricant and Additive,” pp. 7–17, 2015, doi: 10.1007/978-981-287-266-1_2.

[26] N. A. Zainal, N. W. M. Zulkifli, M. Gulzar, and H. H. Masjuki, “A review on the chemistry, production, and technological potential of bio-based lubricants,” *Renew. Sustain. Energy Rev.*, vol. 82, pp. 80–102, Feb. 2018, doi: 10.1016/J.RSER.2017.09.004.

[27] S. Z. Erhan, B. K. Sharma, Z. Liu, and A. Adhvaryu, “Lubricant Base Stock Potential of Chemically Modified Vegetable Oils,” *J. Agric. Food Chem.*, vol. 56, no. 19, pp. 8919–8925, Oct. 2008, doi: 10.1021/JF801463D.

[28] Y. Singh, A. Farooq, A. Raza, M. A. Mahmood, and S. Jain, “Sustainability of a non-edible vegetable oil based bio-lubricant for automotive applications: A review,” *Process Saf. Environ. Prot.*, vol. 111, pp. 701–713, Oct. 2017, doi: 10.1016/J.PSEP.2017.08.041.

[29] L. A. T. Honary and E. W. Richter, *Biobased lubricants and greases : technology and products*. Wiley, 2011.

[30] N. Salih and J. Salimon, “A Review on Eco-Friendly Green Biolubricants from Renewable and Sustainable Plant Oil Sources,” vol. 11, no. 5, pp. 13303–13327, 2021, doi: 10.33263/BRIAC115.1330313327.

[31] D. Liao, J. He, L. Mao, and Y. Xu, “Synthesis and lubricating properties of neopentyl glycol oligoesters based on rapeseed oil,” *Ind. Lubr. Tribol.*, vol. 67, no. 5, pp. 449–454, Aug. 2015, doi: 10.1108/ILT-02-2014-0010.

[32] N. S. Lani, N. Ngadi, and I. M. Inuwa, “New route for the synthesis of silica-supported calcium oxide catalyst in biodiesel production,” *Renew. Energy*, vol. 156, pp. 1266–1277, Aug. 2020, doi: 10.1016/J.RENENE.2019.10.132.

[33] V. B. Borugadda, A. K. R. Somidi, and A. K. Dalai, “Chemical/Structural Modification of Canola Oil and Canola Biodiesel: Kinetic Studies and Biodegradability of the Alkoxides,” *Lubr. 2017, Vol. 5, Page 11*, vol. 5, no. 2, p. 11, Apr. 2017, doi: 10.3390/LUBRICANTS5020011.

[34] K. S. Suslick and S. E. Skrabalak, “Sonocatalysis,” in *Handbook of Heterogeneous Catalysis*, Weinheim, Germany: Wiley-VCH Verlag GmbH & Co. KGaA, 2008, pp. 2007–2017.

[35] T. J. Mason and A. Tiehm, *Advances in Sonochemistry, Volume 6.* Elsevier, 2001.

[36] C. K. Ho, K. B. McAuley, and B. A. Peppley, “Biolubricants through renewable hydrocarbons: A perspective for new opportunities,” *Renew. Sustain. Energy Rev.*, vol. 113, p. 109261, Oct. 2019, doi: 10.1016/J.RSER.2019.109261.

[37] A. Srivastava and P. Sahai, “Vegetable oils as lube basestocks: A review,” *African J. Biotechnol.*, vol. 12, no. 9, pp. 880–891, Dec. 2015, doi: 10.4314/ajb.v12i9.

[38] H. Masood, R. Yunus, T. S. Y. Choong, U. Rashid, and Y. H. Taufiq Yap, “Synthesis and characterization of calcium methoxide as heterogeneous catalyst for trimethylolpropane esters conversion reaction,” *Appl. Catal. A Gen.*, vol. 425–426, pp. 184–190, May 2012, doi: 10.1016/J.APCATA.2012.03.019.

[39] J. Lindley and T. J. Mason, “Sonochemistry. Part2—Synthetic applications,” *Chem. Soc. Rev.*, vol. 16, no. 0, pp. 275–311, Jan. 1987, doi: 10.1039/CS9871600275.

[40] F. R. Young, “Cavitation,” Nov. 1999, doi: 10.1142/P172.

[41] R. Yunus, A. Fakhru’l-Razi, T. L. Ooi, D. R. A. Biak, and S. E. Iyuke, “Kinetics of transesterification of palm-based methyl esters with trimethylolpropane,” *J. Am. Oil Chem. Soc. 2004 815*, vol. 81, no. 5, pp. 497–503, 2004, doi: 10.1007/S11746-004-0930-7.

[42] M. Di Serio, R. Tesser, M. Dimiccoli, F. Cammarota, M. Nastasi, and E. Santacesaria, “Synthesis of biodiesel via homogeneous Lewis acid catalyst,” *J. Mol. Catal. A Chem.*, vol. 239, no. 1–2, pp. 111–115, Sep. 2005, doi: 10.1016/J.MOLCATA.2005.05.041.

[43] B. K. Sharma, A. Adhvaryu, and S. Z. Erhan, “Synthesis of hydroxy thio-ether derivatives of vegetable oil,” *J. Agric. Food Chem.*, vol. 54, no. 26, pp. 9866–9872, Dec. 2006, doi: 10.1021/JF061896F.

[44] B. Freedman, R. O. Butterfield, and E. H. Pryde, “Transesterification kinetics of soybean oil 1,” *J. Am. Oil Chem. Soc. 1986 6310*, vol. 63, no. 10, pp. 1375–1380, Oct. 1986, doi: 10.1007/BF02679606.

[45] B. Freedman, E. H. Pryde, and T. L. Mounts, “Variables affecting the yields of fatty esters from transesterified vegetable oils,” *J. Am. Oil Chem. Soc. 1984 6110*, vol. 61, no. 10, pp. 1638–1643, Oct. 1984, doi: 10.1007/BF02541649.

[46] G. Appiah, S. K. Tulashie, E. E. A. Akpari, E. R. Rene, and D. Dodoo, “Biolubricant production via esterification and transesterification processes: Current updates and perspectives,” *Int. J. Energy Res.*, vol. 46, no. 4, pp. 3860–3890, Mar. 2022, doi: 10.1002/ER.7453.

[47] A. L. De Lima, C. M. Ronconi, and C. J. A. Mota, “Heterogeneous basic catalysts for biodiesel production,” *Catal. Sci. Technol.*, vol. 6, no. 9, pp. 2877–2891, May 2016, doi: 10.1039/C5CY01989C.

[48] G. Kuo, J. Goodwin, and S. Pathak, “Acid catalyzed transesterification Synt hesis of Biodiesel via Acid Cat alysis Acid catalyzed transesterification,” *J. Chem. Pharm. Res.*, vol. 7, no. 3, pp. 1780–1786, 2015, Accessed: Apr. 29, 2022. [Online]. Available: www.jocpr.com.

[49] M. Hájek, A. Vávra, H. de P. Carmona, and J. Kocík, “The Catalysed Transformation of

Vegetable Oils or Animal Fats to Biofuels and Bio-Lubricants: A Review," *Catal. 2021, Vol. 11, Page 1118*, vol. 11, no. 9, p. 1118, Sep. 2021, doi: 10.3390/CATAL11091118.

[50] H. A. Hamid, R. Yunus, U. Rashid, T. S. Y. Choong, and A. H. Al-Muhtaseb, "Synthesis of palm oil-based trimethylolpropane ester as potential biolubricant: Chemical kinetics modeling," *Chem. Eng. J.*, vol. 200–202, pp. 532–540, Aug. 2012, doi: 10.1016/J.CEJ.2012.06.087.

[51] C. T. Ivan-Tan, A. Islam, R. Yunus, and Y. H. Taufiq-Yap, "Screening of solid base catalysts on palm oil based biolubricant synthesis," *J. Clean. Prod.*, vol. 148, pp. 441–451, Apr. 2017, doi: 10.1016/J.JCLEPRO.2017.02.027.

[52] T. Lin, S. Zhao, S. Niu, Z. Lyu, K. Han, and X. Hu, "Halloysite nanotube functionalized with La-Ca bimetallic oxides as novel transesterification catalyst for biodiesel production with molecular simulation," *Energy Convers. Manag.*, vol. 220, p. 113138, Sep. 2020, doi: 10.1016/J.ENCONMAN.2020.113138.

[53] M. Hájek *et al.*, "Transesterification of rapeseed oil by Mg-Al mixed oxides with various Mg/Al molar ratio," *Chem. Eng. J.*, vol. 263, pp. 160–167, Mar. 2015, doi: 10.1016/J.CEJ.2014.11.006.

[54] N. F. Sulaiman, S. L. Lee, S. Toemen, and W. A. W. A. Bakar, "Physicochemical characteristics of Cu/Zn/γ-Al2O3 catalyst and its mechanistic study in transesterification for biodiesel production," *Renew. Energy*, vol. 156, pp. 142–157, Aug. 2020, doi: 10.1016/J.RENENE.2020.04.021.

[55] T. Qu, S. Niu, Z. Gong, K. Han, Y. Wang, and C. Lu, "Wollastonite decorated with calcium oxide as heterogeneous transesterification catalyst for biodiesel production: Optimized by response surface methodology," *Renew. Energy*, vol. 159, pp. 873–884, Oct. 2020, doi: 10.1016/J.RENENE.2020.06.009.

[56] S. Yan, H. Lu, and B. Liang, "Supported CaO catalysts used in the transesterification of rapeseed oil for the purpose of biodiesel production," *Energy and Fuels*, vol. 22, no. 1, pp. 646–651, Jan. 2008, doi: 10.1021/EF070105O/ASSET/IMAGES/LARGE/EF-2007-00105O_0007.JPEG.

[57] M. Mohamad, N. Ngadi, S. L. Wong, M. Jusoh, and N. Y. Yahya, “Prediction of biodiesel yield during transesterification process using response surface methodology,” *Fuel*, vol. 190, pp. 104–112, Feb. 2017, doi: 10.1016/J.FUEL.2016.10.123.

[58] X. Liu, H. He, Y. Wang, S. Zhu, and X. Piao, “Transesterification of soybean oil to biodiesel using CaO as a solid base catalyst,” *Fuel*, vol. 87, no. 2, pp. 216–221, Feb. 2008, doi: 10.1016/J.FUEL.2007.04.013.

[59] N. Degirmenbasi, S. Coskun, N. Boz, and D. M. Kalyon, “Biodiesel synthesis from canola oil via heterogeneous catalysis using functionalized CaO nanoparticles,” *Fuel*, vol. 153, pp. 620–627, Aug. 2015, doi: 10.1016/J.FUEL.2015.03.018.

[60] M. B. Navas, I. D. Lick, P. A. Bolla, M. L. Casella, and J. F. Ruggera, “Transesterification of soybean and castor oil with methanol and butanol using heterogeneous basic catalysts to obtain biodiesel,” *Chem. Eng. Sci.*, vol. 187, pp. 444–454, Sep. 2018, doi: 10.1016/J.CES.2018.04.068.

[61] G. Moradi, M. Mohadesi, and Z. Hojabri, “Biodiesel production by CaO/SiO2 catalyst synthesized by the sol–gel process,” *React. Kinet. Mech. Catal.*, vol. 113, no. 1, pp. 169–186, Oct. 2014, doi: 10.1007/S11144-014-0728-9/FIGURES/7.

[62] M. Hájek, A. Tomášová, J. Kocík, and V. Podzemná, “Statistical evaluation of the mutual relations of properties of Mg/Fe hydrotalcites and mixed oxides as transesterification catalysts,” *Appl. Clay Sci.*, vol. 154, pp. 28–35, Mar. 2018, doi: 10.1016/J.CLAY.2017.12.039.

[63] S. Benjapornkulaphong, C. Ngamcharussrivichai, and K. Bunyakiat, “Al2O3-supported alkali and alkali earth metal oxides for transesterification of palm kernel oil and coconut oil,” *Chem. Eng. J.*, vol. 145, no. 3, pp. 468–474, Jan. 2009, doi: 10.1016/J.CEJ.2008.04.036.

[64] M. J. Borah, A. Das, V. Das, N. Bhuyan, and D. Deka, “Transesterification of waste cooking oil for biodiesel production catalyzed by Zn substituted waste egg shell derived CaO nanocatalyst,” *Fuel*, vol. 242, pp. 345–354, Apr. 2019, doi: 10.1016/J.FUEL.2019.01.060.

[65] “Preparation of CaO/γ-Al2O3 catalyst for biodiesel fuels. The catalytic activity in relation

to thermal treatment," *Phys. Chem. 2014 – 12th Int. Conf. Fundam. Appl. Asp. Phys. Chem.*, 2014.

[66] N. F. Sulaiman *et al.*, "Biodiesel production from refined used cooking oil using co-metal oxide catalyzed transesterification," *Renew. Energy*, vol. 153, pp. 1–11, Jun. 2020, doi: 10.1016/J.RENENE.2020.01.158.

[67] "Preparation of Biodiesel on Nano Ca-Mg-Al Solid Base Catalyst UnderUltrasonic Radiation in Microaqueous Media." http://www.shiyouhuagong.com.cn/EN/abstract/abstract1497.shtml (accessed May 01, 2022).

[68] A. C. Alba-Rubio *et al.*, "Heterogeneous transesterification processes by using CaO supported on zinc oxide as basic catalysts," *Catal. Today*, vol. 149, no. 3–4, pp. 281–287, Jan. 2010, doi: 10.1016/J.CATTOD.2009.06.024.

[69] M. Loudon and J. Parise, *Organic Chemistry*. W.H. Freeman & Company, 2021.

[70] J. D. Roberts, M. C. Caserio, and W. A. Benjamin, "BASIC PRINCIPLES OF ORGANIC CHEMISTRY SECOND EDITION," 1964.

[71] B. Mondal and A. K. Jana, "Techno-economic Feasibility of Reactive Distillation for Biodiesel Production from Algal Oil: Comparing with a Conventional Multiunit System," *Ind. Eng. Chem. Res.*, vol. 58, no. 27, pp. 12028–12040, Jul. 2019, doi: 10.1021/ACS.IECR.9B00347/SUPPL_FILE/IE9B00347_SI_001.PDF.

[72] K. Prasertsit, C. Mueanmas, and C. Tongurai, "Transesterification of palm oil with methanol in a reactive distillation column," *Chem. Eng. Process. Process Intensif.*, vol. 70, pp. 21–26, Aug. 2013, doi: 10.1016/J.CEP.2013.05.011.

[73] T. Poddar, A. Jagannath, and A. Almansoori, "Biodiesel Production using Reactive Distillation: A Comparative Simulation Study," *Energy Procedia*, vol. 75, pp. 17–22, Aug. 2015, doi: 10.1016/J.EGYPRO.2015.07.129.

[74] S. Hafeez, G. Manos, S. M. Al-Salem, E. Aristodemou, and A. Constantinou, "Liquid fuel synthesis in microreactors," *React. Chem. Eng.*, vol. 3, no. 4, pp. 414–432, Jul. 2018, doi: 10.1039/C8RE00040A.

[75] S. Kant Bhatia *et al.*, “An overview on advancements in biobased transesterification methods for biodiesel production: Oil resources, extraction, biocatalysts, and process intensification technologies,” *Fuel*, vol. 285, p. 119117, Feb. 2021, doi: 10.1016/J.FUEL.2020.119117.

[76] T. Xie, L. Zhang, and N. Xu, “Biodiesel synthesis in microreactors,” *Green Process. Synth.*, vol. 1, no. 1, pp. 61–70, Jan. 2012, doi: 10.1515/GREENPS-2011-0004/MACHINEREADABLECITATION/RIS.

[77] M. Tabatabaei *et al.*, “Reactor technologies for biodiesel production and processing: A review,” *Prog. Energy Combust. Sci.*, vol. 74, pp. 239–303, Sep. 2019, doi: 10.1016/J.PECS.2019.06.001.

[78] E. Fayyazi, B. Ghobadian, S. M. Mousavi, and G. Najafi, “Intensification of continues biodiesel production process using a simultaneous mixer- separator reactor,” *https://doi.org/10.1080/15567036.2018.1474293*, vol. 40, no. 9, pp. 1125–1136, May 2018, doi: 10.1080/15567036.2018.1474293.

[79] M. Y. Abduh *et al.*, “Synthesis and refining of sunflower biodiesel in a cascade of continuous centrifugal contactor separators,” *Eur. J. Lipid Sci. Technol.*, vol. 117, no. 2, pp. 242–254, Feb. 2015, doi: 10.1002/EJLT.201400206.

[80] G. Chen, R. Shan, J. Shi, and B. Yan, “Ultrasonic-assisted production of biodiesel from transesterification of palm oil over ostrich eggshell-derived CaO catalysts,” *Bioresour. Technol.*, vol. 171, pp. 428–432, Nov. 2014, doi: 10.1016/J.BIORTECH.2014.08.102.

[81] D. C. Boffito, S. Mansi, J. M. Leveque, C. Pirola, C. L. Bianchi, and G. S. Patience, “Ultrafast biodiesel production using ultrasound in batch and continuous reactors,” *ACS Sustain. Chem. Eng.*, vol. 1, no. 11, pp. 1432–1439, Nov. 2013, doi: 10.1021/sc400161s.

[82] K. G. Georgogianni, M. G. Kontominas, P. J. Pomonis, D. Avlonitis, and V. Gergis, “Conventional and in situ transesterification of sunflower seed oil for the production of biodiesel,” *Fuel Process. Technol.*, vol. 89, no. 5, pp. 503–509, May 2008, doi: 10.1016/J.FUPROC.2007.10.004.

[83] R. Selvaraj, I. G. Moorthy, R. V. Kumar, and V. Sivasubramanian, “Microwave mediated

production of FAME from waste cooking oil: Modelling and optimization of process parameters by RSM and ANN approach," *Fuel*, vol. 237, pp. 40–49, Feb. 2019, doi: 10.1016/J.FUEL.2018.09.147.

[84] I. Choedkiatsakul, K. Ngaosuwan, S. Assabumrungrat, S. Mantegna, and G. Cravotto, "Biodiesel production in a novel continuous flow microwave reactor," *Renew. Energy*, vol. 83, pp. 25–29, Nov. 2015, doi: 10.1016/J.RENENE.2015.04.012.

[85] Z. Qiu, L. Zhao, and L. Weatherley, "Process intensification technologies in continuous biodiesel production," *Chem. Eng. Process. Process Intensif.*, vol. 49, no. 4, pp. 323–330, Apr. 2010, doi: 10.1016/J.CEP.2010.03.005.

[86] J. McNutt and Q. S. He, "Development of biolubricants from vegetable oils via chemical modification," *J. Ind. Eng. Chem.*, vol. 36, pp. 1–12, Apr. 2016, doi: 10.1016/J.JIEC.2016.02.008.

[87] M. Y. Koh, T. I. Tinia, and A. Idris, "Synthesis of palm based biolubricant in an oscillatory flow reactor (OFR)," *Ind. Crops Prod.*, vol. 52, pp. 567–574, Jan. 2014, doi: 10.1016/J.INDCROP.2013.10.042.

[88] T. I. Tinia, M. F. M. Gunam Resul, and A. Idris, "Bioenergy II: Production of biodegradable lubricant from jatropha curcas and trimethylolpropane," *Int. J. Chem. React. Eng.*, vol. 7, 2009, doi: 10.2202/1542-6580.1957.

[89] E. Wang *et al.*, "Synthesis and oxidative stability of trimethylolpropane fatty acid triester as a biolubricant base oil from waste cooking oil," *Biomass and Bioenergy*, vol. 66, pp. 371–378, Jul. 2014, doi: 10.1016/J.BIOMBIOE.2014.03.022.

[90] P. S. Sreeprasanth, R. Srivastava, D. Srinivas, and P. Ratnasamy, "Hydrophobic, solid acid catalysts for production of biofuels and lubricants," *Appl. Catal. A Gen.*, vol. 314, no. 2, pp. 148–159, Nov. 2006, doi: 10.1016/J.APCATA.2006.08.012.

[91] S. Gryglewicz, M. Muszyński, and J. Nowicki, "Enzymatic synthesis of rapeseed oil-based lubricants," *Ind. Crops Prod.*, vol. 45, pp. 25–29, Feb. 2013, doi: 10.1016/J.INDCROP.2012.11.038.

[92] J. Ji, J. Wang, Y. Li, Y. Yu, and Z. Xu, "Preparation of biodiesel with the help of ultrasonic

and hydrodynamic cavitation," *Ultrasonics*, vol. 44, no. SUPPL., pp. e411–e414, Dec. 2006, doi: 10.1016/J.ULTRAS.2006.05.020.

[93] K. S. Suslick and D. J. Flannigan, "Inside a Collapsing Bubble: Sonoluminescence and the Conditions During Cavitation," *http://dx.doi.org/10.1146/annurev.physchem.59.032607.093739*, vol. 59, pp. 659–683, Apr. 2008, doi: 10.1146/ANNUREV.PHYSCHEM.59.032607.093739.

[94] D. J. Flannigan and K. S. Suslick, "Plasma formation and temperature measurement during single-bubble cavitation," *Nat. 2005 4347029*, vol. 434, no. 7029, pp. 52–55, Mar. 2005, doi: 10.1038/nature03361.

[95] D. J. Flannigan, S. D. Hopkins, C. G. Camara, S. J. Putterman, and K. S. Suslick, "Measurement of pressure and density inside a single sonoluminescing bubble," *Phys. Rev. Lett.*, vol. 96, no. 20, p. 204301, May 2006, doi: 10.1103/PHYSREVLETT.96.204301/FIGURES/3/MEDIUM.

[96] KS Suslick, "The chemical effects of ultrasound," *Sci. Am.*, vol. 260, no. 2, pp. 80–87, 1989, Accessed: Apr. 16, 2020. [Online]. Available: https://www.jstor.org/stable/24987145.

[97] Y. Gao, M. Wu, Y. Lin, and J. Xu, "Trapping and control of bubbles in various microfluidic applications," *Lab Chip*, vol. 20, no. 24, pp. 4512–4527, Dec. 2020, doi: 10.1039/D0LC00906G.

[98] M. H. Entezari and A. Keshavarzi, "Phase-transfer catalysis and ultrasonic waves II: saponification of vegetable oil," *Ultrason. Sonochem.*, vol. 8, no. 3, pp. 213–216, Jul. 2001, doi: 10.1016/S1350-4177(01)00079-7.

[99] P. R. Gogate, "Cavitational reactors for process intensification of chemical processing applications: A critical review," *Chem. Eng. Process. Process Intensif.*, vol. 47, no. 4, pp. 515–527, Apr. 2008, doi: 10.1016/J.CEP.2007.09.014.

[100] S. V. Sancheti and P. R. Gogate, "A review of engineering aspects of intensification of chemical synthesis using ultrasound," *Ultrasonics Sonochemistry*, vol. 36. Elsevier B.V., pp. 527–543, May 01, 2017, doi: 10.1016/j.ultsonch.2016.08.009.

[101] D. Meroni, R. Djellabi, M. Ashokkumar, C. L. Bianchi, and D. C. Boffito, "Sonoprocessing:

From Concepts to Large-Scale Reactors," *Chem. Rev.*, Nov. 2021, doi: 10.1021/ACS.CHEMREV.1C00438.

[102] "Ultrasound: its chemical, physical, and biological effects — University of Illinois Urbana-Champaign." https://experts.illinois.edu/en/publications/ultrasound-its-chemical-physical-and-biological-effects (accessed Apr. 22, 2022).

[103] J. Hartmann *et al.*, "Degradation of the drug diclofenac in water by sonolysis in presence of catalysts," *Chemosphere*, vol. 70, no. 3, pp. 453–461, Jan. 2008, doi: 10.1016/J.CHEMOSPHERE.2007.06.063.

[104] J. Madhavan, P. S. S. Kumar, S. Anandan, M. Zhou, F. Grieser, and M. Ashokkumar, "Ultrasound assisted photocatalytic degradation of diclofenac in an aqueous environment," *Chemosphere*, vol. 80, no. 7, pp. 747–752, Aug. 2010, doi: 10.1016/J.CHEMOSPHERE.2010.05.018.

[105] J. P. Lorimer and T. J. Mason, "Sonochemistry. Part 1—The physical aspects," *Chem. Soc. Rev.*, vol. 16, no. 0, pp. 239–274, Jan. 1987, doi: 10.1039/CS9871600239.

[106] K. Yasui, "Effect of volatile solutes on sonoluminescence," *J. Chem. Phys.*, vol. 116, no. 7, p. 2945, Feb. 2002, doi: 10.1063/1.1436122.

[107] C. PÉTRIER, N. GONDREXON, and P. BOLDO, "Ultrasons et sonochimie," *Chim. verte*, Jan. 2008, doi: 10.51257/A-V1-AF6310.

[108] P. Kanthale, M. Ashokkumar, and F. Grieser, "Sonoluminescence, sonochemistry (H2O2 yield) and bubble dynamics: Frequency and power effects," *Ultrason. Sonochem.*, vol. 15, no. 2, pp. 143–150, Feb. 2008, doi: 10.1016/J.ULTSONCH.2007.03.003.

[109] N. R. Khan, S. V. Jadhav, and V. K. Rathod, "Lipase catalysed synthesis of cetyl oleate using ultrasound: Optimisation and kinetic studies," *Ultrason. Sonochem.*, vol. 27, pp. 522–529, Nov. 2015, doi: 10.1016/J.ULTSONCH.2015.03.017.

[110] P. N. Dange, A. V. Kulkarni, and V. K. Rathod, "Ultrasound assisted synthesis of methyl butyrate using heterogeneous catalyst," *Ultrason. Sonochem.*, vol. 26, pp. 257–264, Sep. 2015, doi: 10.1016/J.ULTSONCH.2015.02.014.

[111] D. C. Boffito, S. Mansi, J. M. Leveque, C. Pirola, C. L. Bianchi, and G. S. Patience, "Ultrafast biodiesel production using ultrasound in batch and continuous reactors," *ACS Sustain. Chem. Eng.*, vol. 1, no. 11, pp. 1432–1439, Nov. 2013, doi: 10.1021/sc400161s.

[112] D. C. Boffito, F. Galli, P. R. Martinez, C. Pirola, C. L. Bianchi, and G. S. Patience, "Transesterification of triglycerides in a new ultrasonic-assisted mixing device," *Chem. Eng. Trans.*, vol. 43, pp. 427–432, 2015, doi: 10.3303/CET1543072.

[113] W. L. McLaughlin, A. Miller, A. Kovács, and K. K. Mehta, "Dosimetry Methods," in *Handbook of Nuclear Chemistry*, Springer US, 2011, pp. 2287–2318.

[114] F. J. Barba *et al.*, "Electron spin resonance as a tool to monitor the influence of novel processing technologies on food properties," *Trends Food Sci. Technol.*, vol. 100, pp. 77–87, Mar. 2020, doi: 10.1016/j.tifs.2020.03.032.

[115] G. Chatel and J. C. Colmenares, "Sonochemistry: from Basic Principles to Innovative Applications," *Topics in Current Chemistry*, vol. 375, no. 1. Springer Verlag, pp. 1–4, Feb. 01, 2017, doi: 10.1007/s41061-016-0096-1.

[116] R. D. Finch, "Sonoluminescence," *Ultrasonics*, vol. 1, no. 2, pp. 87–98, Apr. 1963, doi: 10.1016/0041-624X(63)90060-X.

[117] I. S. Akhatov, N. K. Vakhitova, and A. S. Topol'nikov, "Dynamics of a bubble in a liquid under laser pulse action," *J. Appl. Mech. Tech. Phys. 2002 431*, vol. 43, no. 1, pp. 43–49, 2002, doi: 10.1023/A:1013901909401.

[118] V. S. Sutkar and P. R. Gogate, "Design aspects of sonochemical reactors: Techniques for understanding cavitational activity distribution and effect of operating parameters," *Chem. Eng. J.*, vol. 155, no. 1–2, pp. 26–36, Dec. 2009, doi: 10.1016/J.CEJ.2009.07.021.

[119] Y. Son, Y. No, and J. Kim, "Geometric and operational optimization of 20-kHz probe-type sonoreactor for enhancing sonochemical activity," *Ultrason. Sonochem.*, vol. 65, p. 105065, Jul. 2020, doi: 10.1016/J.ULTSONCH.2020.105065.

[120] B. Avvaru and A. B. Pandit, "Experimental investigation of cavitational bubble dynamics under multi-frequency system," *Ultrason. Sonochem.*, vol. 15, no. 4, pp. 578–589, Apr. 2008, doi: 10.1016/J.ULTSONCH.2007.06.012.

[121] Z. Wei, J. A. Kosterman, R. Xiao, G. Y. Pee, M. Cai, and L. K. Weavers, “Designing and characterizing a multi-stepped ultrasonic horn for enhanced sonochemical performance,” *Ultrason. Sonochem.*, vol. 27, pp. 325–333, Nov. 2015, doi: 10.1016/J.ULTSONCH.2015.05.013.

[122] Q. A. Zhang, Y. Shen, X. H. Fan, J. F. G. Martín, X. Wang, and Y. Song, “Free radical generation induced by ultrasound in red wine and model wine: An EPR spin-trapping study,” *Ultrason. Sonochem.*, vol. 27, pp. 96–101, Nov. 2015, doi: 10.1016/j.ultsonch.2015.05.003.

[123] R. Lauricella and B. Tuccio, “Detection and characterisation of free radicals after spin trapping,” in *Electron Paramagnetic Resonance Spectroscopy: Applications*, Springer International Publishing, 2020, pp. 51–82.

[124] M. G. Bakker, B. Fowler, M. K. Bowman, and G. S. Patience, “Experimental methods in chemical engineering: Electron paramagnetic resonance spectroscopy-EPR/ESR,” *Can. J. Chem. Eng.*, vol. 98, no. 8, pp. 1668–1681, Aug. 2020, doi: 10.1002/cjce.23784.

[125] G. Chatel and J. C. Colmenares, “Sonochemistry: from Basic Principles to Innovative Applications,” *Topics in Current Chemistry*, vol. 375, no. 1. Springer Verlag, pp. 1–4, Feb. 01, 2017, doi: 10.1007/s41061-016-0096-1.

[126] T. J. Mason, J. P. Lorimer, D. M. Bates, and Y. Zhao, “Dosimetry in sonochemistry: the use of aqueous terephthalate ion as a fluorescence monitor,” *Ultrason. - Sonochemistry*, vol. 1, no. 2, pp. S91–S95, Jan. 1994, doi: 10.1016/1350-4177(94)90004-3.

[127] M. O’Leary *et al.*, “Observation of dose-rate dependence in a Fricke dosimeter irradiated at low dose rates with monoenergetic X-rays,” *Sci. Rep.*, vol. 8, no. 1, pp. 1–9, Dec. 2018, doi: 10.1038/s41598-018-21813-z.

[128] A. K. Jana and S. N. Chatterjee, “Estimation of hydroxyl free radicals produced by ultrasound in Fricke solution used as a chemical dosimeter,” *Ultrason. - Sonochemistry*, vol. 2, no. 2, pp. S87–S91, Jan. 1995, doi: 10.1016/1350-4177(95)00025-2.

[129] Y. Iida, K. Yasui, T. Tuziuti, and M. Sivakumar, “Sonochemistry and its dosimetry,” in *Microchemical Journal*, Jun. 2005, vol. 80, no. 2, pp. 159–164, doi: 10.1016/j.microc.2004.07.016.

[130] A. Ebrahiminia, M. Mokhtari-Dizaji, and T. Toliyat, “Dual frequency cavitation event sensor with iodide dosimeter,” *Ultrason. Sonochem.*, vol. 28, pp. 276–282, Aug. 2016, doi: 10.1016/j.ultsonch.2015.07.005.

[131] D. B. Rajamma, S. Anandan, N. S. M. Yusof, B. G. Pollet, and M. Ashokkumar, “Sonochemical dosimetry: A comparative study of Weissler, Fricke and terephthalic acid methods,” *Ultrason. Sonochem.*, vol. 72, p. 105413, Apr. 2021, doi: 10.1016/j.ultsonch.2020.105413.

[132] W. W. S. Ho, H. K. Ng, and S. Gan, “Advances in ultrasound-assisted transesterification for biodiesel production,” *Appl. Therm. Eng.*, vol. 100, pp. 553–563, May 2016, doi: 10.1016/J.APPLTHERMALENG.2016.02.058.

[133] I. Choedkiatsakul, K. Ngaosuwan, and S. Assabumrungrat, “Application of heterogeneous catalysts for transesterification of refined palm oil in ultrasound-assisted reactor,” *Fuel Process. Technol.*, vol. 111, pp. 22–28, Jul. 2013, doi: 10.1016/J.FUPROC.2013.01.015.

[134] D. C. Boffito *et al.*, “Ultrasonic enhancement of the acidity, surface area and free fatty acids esterification catalytic activity of sulphated ZrO2–TiO2 systems,” *J. Catal.*, vol. 297, pp. 17–26, Jan. 2013, doi: 10.1016/J.JCAT.2012.09.013.

[135] D. C. Boffito, F. Galli, C. Pirola, C. L. Bianchi, and G. S. Patience, “Ultrasonic free fatty acids esterification in tobacco and canola oil,” *Ultrason. Sonochem.*, vol. 21, no. 6, pp. 1969–1975, Nov. 2014, doi: 10.1016/J.ULTSONCH.2014.01.026.

[136] D. C. Boffito *et al.*, “Batch and Continuous Ultrasonic Reactors for the Production of Methyl Esters from Vegetable Oils,” pp. 87–114, 2015, doi: 10.1007/978-94-017-9624-8_3.

[137] B. Sajjadi, A. R. Abdul Aziz, and S. Ibrahim, “Mechanistic analysis of cavitation assisted transesterification on biodiesel characteristics,” *Ultrason. Sonochem.*, vol. 22, pp. 463–473, 2015, doi: 10.1016/J.ULTSONCH.2014.06.004.

[138] X. Deng, Z. Fang, and Y. H. Liu, “Ultrasonic transesterification of Jatropha curcas L. oil to biodiesel by a two-step process,” *Energy Convers. Manag.*, vol. 51, no. 12, pp. 2802–2807, Dec. 2010, doi: 10.1016/J.ENCONMAN.2010.06.017.

[139] K. G. Georgogianni, M. G. Kontominas, P. J. Pomonis, D. Avlonitis, and V. Gergis,

"Alkaline Conventional and in Situ Transesterification of Cottonseed Oil for the Production of Biodiesel," *Energy and Fuels*, vol. 22, no. 3, pp. 2110–2115, May 2008, doi: 10.1021/EF700784J.

[140] N. A. Patience, F. Galli, M. G. Rigamonti, D. Schieppati, and D. C. Boffito, "Ultrasonic Intensification To Produce Diester Biolubricants," *Ind. Eng. Chem. Res.*, vol. 58, no. 19, pp. 7957–7963, May 2019, doi: 10.1021/ACS.IECR.9B00717.

[141] S. Arumugam, P. Chengareddy, A. Tamilarasan, and V. Santhanam, "RSM and Crow Search Algorithm-Based Optimization of Ultrasonicated Transesterification Process Parameters on Synthesis of Polyol Ester-Based Biolubricant," *Arab. J. Sci. Eng.*, vol. 44, no. 6, pp. 5535–5548, Jun. 2019, doi: 10.1007/S13369-019-03847-1/FIGURES/9.

[142] S. Almasi, B. Ghobadian, G. Najafi, and M. Dehghani Soufi, "A novel approach for bio-lubricant production from rapeseed oil-based biodiesel using ultrasound irradiation: Multi-objective optimization," *Sustain. Energy Technol. Assessments*, vol. 43, p. 100960, Feb. 2021, doi: 10.1016/J.SETA.2020.100960.

[143] S. D. Gawas and V. K. Rathod, "Ultrasound Assisted Green Synthesis of 2-Ethylhexyl Stearate: A Cosmetic Bio-lubricant," *J. Oleo Sci.*, vol. 69, no. 9, pp. 1043–1049, 2020, doi: 10.5650/JOS.ESS19322.

[144] P. Chengareddy and A. Shanmugasundaram, "Vegetable Oil Based Compressor Oil-optimising of Tribological Characteristics," *https://doi.org/10.1080/14484846.2021.2022582*, 2022, doi: 10.1080/14484846.2021.2022582.

[145] D. C. Boffito, E. Martinez-Guerra, V. G. Gude, and G. S. Patience, "Conversion of refined and waste oils by ultrasound-assisted heterogeneous catalysis #30," in *Handbook of Ultrasonics and Sonochemistry*, Springer Singapore, 2016, pp. 931–963.

[146] T. S. Awad, H. A. Moharram, O. E. Shaltout, D. Asker, and M. M. Youssef, "Applications of ultrasound in analysis, processing and quality control of food: A review," *Food Research International*, vol. 48, no. 2. Elsevier, pp. 410–427, Oct. 01, 2012, doi: 10.1016/j.foodres.2012.05.004.

[147] N. Bhargava, R. S. Mor, K. Kumar, and V. S. Sharanagat, “Advances in application of ultrasound in food processing: A review,” *Ultrasonics Sonochemistry*, vol. 70. Elsevier B.V., p. 105293, Jan. 01, 2021, doi: 10.1016/j.ultsonch.2020.105293.

[148] S. Mitragotri and J. Kost, “Low-frequency sonophoresis: A review,” *Adv. Drug Deliv. Rev.*, vol. 56, no. 5, pp. 589–601, Mar. 2004, doi: 10.1016/j.addr.2003.10.024.

[149] A. Ahmadi *et al.*, “Recent advances in ultrasound-triggered drug delivery through lipid-based nanomaterials,” *Drug Discovery Today*, vol. 25, no. 12. Elsevier Ltd, pp. 2182–2200, Dec. 01, 2020, doi: 10.1016/j.drudis.2020.09.026.

[150] D. Schieppati, F. Galli, M. L. Peyot, V. Yargeau, C. L. Bianchi, and D. C. Boffito, “An ultrasound-assisted photocatalytic treatment to remove an herbicidal pollutant from wastewaters,” *Ultrason. Sonochem.*, vol. 54, pp. 302–310, Jun. 2019, doi: 10.1016/j.ultsonch.2019.01.027.

[151] X. Lu *et al.*, “A Review on Additives-assisted Ultrasound for Organic Pollutants Degradation,” *Journal of Hazardous Materials*, vol. 403. Elsevier B.V., p. 123915, Feb. 05, 2021, doi: 10.1016/j.jhazmat.2020.123915.

[152] Z. Khani, D. Schieppati, C. L. Bianchi, and D. C. Boffito, “The Sonophotocatalytic Degradation of Pharmaceuticals in Water by MnOx-TiO2 Systems with Tuned Band-Gaps,” *Catalysts*, vol. 9, no. 11, p. 949, Nov. 2019, doi: 10.3390/catal9110949.

[153] E. V. Rokhina, P. Lens, and J. Virkutyte, “Low-frequency ultrasound in biotechnology: state of the art,” *Trends in Biotechnology*, vol. 27, no. 5. Elsevier Current Trends, pp. 298–306, May 01, 2009, doi: 10.1016/j.tibtech.2009.02.001.

[154] B. A. Bhanvase and S. H. Sonawane, “Ultrasound assisted in situ emulsion polymerization for polymer nanocomposite: A review,” *Chemical Engineering and Processing: Process Intensification*, vol. 85. Elsevier, pp. 86–107, Nov. 01, 2014, doi: 10.1016/j.cep.2014.08.007.

[155] D. C. Boffito and D. Fernandez Rivas, “Process intensification connects scales and disciplines towards sustainability,” *Can. J. Chem. Eng.*, p. cjce.23871, Oct. 2020, doi: 10.1002/cjce.23871.

[156] M. Ashokkumar *et al.*, *Handbook of ultrasonics and sonochemistry*. Springer Singapore, 2016.

[157] S. Koda, T. Kimura, T. Kondo, and H. Mitome, "A standard method to calibrate sonochemical efficiency of an individual reaction system," *Ultrason. Sonochem.*, vol. 10, no. 3, pp. 149–156, May 2003, doi: 10.1016/S1350-4177(03)00084-1.

[158] A. H. Barati, M. Mokhtari -Dizaji, H. Mozdarani, S. Z. Bathaei, and Z. M. Hassan, "Free hydroxyl radical dosimetry by using 1 MHz low level ultrasound waves," International Journal of Radiation Research, 2006.

[159] D. C. Boffito, F. Galli, C. Pirola, C. L. Bianchi, and G. S. Patience, "Ultrasonic free fatty acids esterification in tobacco and canola oil," in *Ultrasonics Sonochemistry*, Nov. 2014, vol. 21, no. 6, pp. 1969–1975, doi: 10.1016/j.ultsonch.2014.01.026.

[160] A. Weissler, "Formation of Hydrogen Peroxide by Ultrasonic Waves: Free Radicals," *J. Am. Chem. Soc.*, vol. 81, no. 5, pp. 1077–1081, 1959, doi: 10.1021/ja01514a015.

[161] G. Mark *et al.*, "OH-radical formation by ultrasound in aqueous solution - Part II: Terephthalate and Fricke dosimetry and the influence of various conditions on the sonolytic yield," *Ultrason. Sonochem.*, vol. 5, no. 2, pp. 41–52, Jun. 1998, doi: 10.1016/S1350-4177(98)00012-1.

[162] A. Ebrahiminia, M. Mokhtari-Dizaji, and T. Toliyat, "Correlation between iodide dosimetry and terephthalic acid dosimetry to evaluate the reactive radical production due to the acoustic cavitation activity," *Ultrason. Sonochem.*, vol. 20, no. 1, pp. 366–372, Jan. 2013, doi: 10.1016/j.ultsonch.2012.05.016.

[163] M. P. Brenner, S. Hilgenfeldt, and D. Lohse, "Single-bubble sonoluminescence," *Reviews of Modern Physics*, vol. 74, no. 2. American Physical Society, pp. 425–484, May 13, 2002, doi: 10.1103/RevModPhys.74.425.

[164] H. Hasanzadeh, M. Mokhtari-Dizaji, S. Zahra Bathaie, Z. M. Hassan, V. Nilchiani, and H. Goudarzi, "Enhancement and control of acoustic cavitation yield by low-level dual frequency sonication: A subharmonic analysis," *Ultrason. Sonochem.*, vol. 18, no. 1, pp. 394–400, 2011, doi: 10.1016/j.ultsonch.2010.07.005.

[165] W. Lauterborn and W. Hentschel, “Cavitation bubble dynamics studied by high speed photography and holography: part one,” *Ultrasonics*, vol. 23, no. 6, pp. 260–268, Nov. 1985, doi: 10.1016/0041-624X(85)90048-4.

[166] V. Mišík and P. Riesz, “EPR study of free radicals induced by ultrasound in organic liquids II. Probing the temperatures of cavitation regions,” *Ultrason. Sonochem.*, vol. 3, no. 1, pp. 25–37, Feb. 1996, doi: 10.1016/1350-4177(95)00036-4.

[167] V. Migik and P. Riesz, “Recent applications of EPR and spin trapping to sonochemical studies of organic liquids and aqueous solutions,” ELSEVIER, 1996.

[168] G. R. Eaton, S. S. Eaton, D. P. Barr, and R. T. Weber, *Quantitative EPR*. Springer, 2010.

[169] R. L. Blakley, D. D. Henry, W. T. Morgan, W. L. Clapp, C. J. Smith, and D. Barr, “Quantitative electron paramagnetic resonance: The importance of matching the Q-factor of standards and samples,” *Appl. Spectrosc.*, vol. 55, no. 10, pp. 1375–1381, 2001, doi: 10.1366/0003702011953504.

[170] M. Brustolon and E. Giamello, *Electron Paramagnetic Resonance: A Practitioner’s Toolkit*. 2008.

[171] P. Bertrand and P. Bertrand, “The Electron Paramagnetic Resonance Phenomenon,” in *Electron Paramagnetic Resonance Spectroscopy*, Springer International Publishing, 2020, pp. 3–30.

[172] L. Xu *et al.*, “Mechanistic study on the combination of ultrasound and peroxymonosulfate for the decomposition of endocrine disrupting compounds,” *Ultrason. Sonochem.*, vol. 60, p. 104749, Jan. 2020, doi: 10.1016/j.ultsonch.2019.104749.

[173] Z. Wei, F. A. Villamena, and L. K. Weavers, “Kinetics and Mechanism of Ultrasonic Activation of Persulfate: An in Situ EPR Spin Trapping Study,” *Environ. Sci. Technol.*, vol. 51, no. 6, pp. 3410–3417, Mar. 2017, doi: 10.1021/acs.est.6b05392.

[174] M. M. Castellanos, D. Reyman, C. Sieiro, and P. Calle, “ESR-spin trapping study on the sonochemistry of liquids in the presence of oxygen. Evidence for the superoxide radical anion formation.,” *Ultrason. Sonochem.*, vol. 8, no. 1, pp. 17–22, Jan. 2001, doi: 10.1016/s1350-4177(99)00047-4.

[175] D. C. Boffito and T. Van Gerven, “Process Intensification and Catalysis,” in *Reference Module in Chemistry, Molecular Sciences and Chemical Engineering*, Elsevier, 2019.

[176] A. Barchouchi, S. Molina-Boisseau, N. Gondrexon, and S. Baup, “Sonochemical activity in ultrasonic reactors under heterogeneous conditions,” *Ultrason. Sonochem.*, vol. 72, p. 105407, Apr. 2021, doi: 10.1016/j.ultsonch.2020.105407.

[177] K. M. Schaich, “EPR Methods for Studying Free Radicals in Foods,” *ACS Symp. Ser.*, vol. 807, pp. 12–34, 2002, doi: 10.1021/bk-2002-0807.ch002.

[178] K. Abbas, N. Babić, and F. Peyrot, “Use of spin traps to detect superoxide production in living cells by electron paramagnetic resonance (EPR) spectroscopy,” *Methods*, vol. 109. Academic Press Inc., pp. 31–43, Oct. 15, 2016, doi: 10.1016/j.ymeth.2016.05.001.

[179] T. Kikuchi and T. Uchida, “Calorimetric method for measuring high ultrasonic power using water as a heating material,” *J. Phys. Conf. Ser.*, vol. 279, p. 012012, Feb. 2011, doi: 10.1088/1742-6596/279/1/012012.

[180] P. R. Gogate, V. S. Sutkar, and A. B. Pandit, “Sonochemical reactors: Important design and scale up considerations with a special emphasis on heterogeneous systems,” *Chem. Eng. J.*, vol. 166, no. 3, pp. 1066–1082, Feb. 2011, doi: 10.1016/j.cej.2010.11.069.

[181] Y. K. Zhang, D. H. Lu, and G. Z. Xu, “Synthesis and Plane Selective Spin Trapping of a Novel Trap 5, 5-Dimethy l-3-(2-ethoxycarbony lethyl)-1 -pyrroline N-oxide,” *Zeitschrift fur Naturforsch. - Sect. B J. Chem. Sci.*, vol. 45, no. 7, pp. 1075–1083, Jul. 1990, doi: 10.1515/znb-1990-0729.

[182] G. R. Buettner, “Spin Trapping: ESR parameters of spin adducts,” *Free Radical Biology and Medicine*, vol. 3, no. 4. Pergamon, pp. 259–303, Jan. 01, 1987, doi: 10.1016/S0891-5849(87)80033-3.

[183] P. Bilski, C. F. Chignell, J. Szychlinski, A. Borkowski, E. Oleksy, and K. Reszka, “Photooxidation of Organic and Inorganic Substrates during UV Photolysis of Nitrite Anion in Aqueous Solution,” *J. Am. Chem. Soc.*, vol. 114, no. 2, pp. 549–556, Jan. 1992, doi: 10.1021/ja00028a023.

[184] Y. KIRINO, T. OHKUMA, and T. KWAN, “Spin trapping with 5,5-dimethylpyrroline-N-

oxide in aqueous solution.," *Chem. Pharm. Bull. (Tokyo).*, vol. 29, no. 1, pp. 29–34, Jan. 1981, doi: 10.1248/cpb.29.29.

[185] H. Taniguchi and K. P. Madden, "DMPO-alkyl radical spin trapping: An in situ radiolysis steady-state ESR study," *Radiat. Res.*, vol. 153, no. 4, pp. 447–453, 2000, doi: 10.1667/0033-7587(2000)153[0447:DARSTA]2.0.CO;2.

[186] G. R. Buettner, "Spin Trapping: ESR parameters of spin adducts 1474 1528V," *Free Radical Biology and Medicine*, vol. 3, no. 4. Pergamon, pp. 259–303, Jan. 01, 1987, doi: 10.1016/S0891-5849(87)80033-3.

[187] R. Konaka, M. Kawai, H. Noda, M. Kohno, and R. Niwa, "Synthesis and evaluation of DMPO-type spin traps," *Free Radic. Res.*, vol. 23, no. 1, pp. 15–25, 1995, doi: 10.3109/10715769509064015.

[188] D. L. Haire, Y. Kotake, and E. G. Janzen, "An EPR/ENDOR study of aminoxyls (nitroxides) capable of intramolecular bonding: hydroxyalkyl radical spin adducts of nitrones," *Can. J. Chem.*, vol. 66, no. 8, pp. 1901–1911, Aug. 1988, doi: 10.1139/v88-307.

[189] R. Sato *et al.*, "Syntheses and spin trappings of 3-hydroxymethyl-5,5-dimethyl-1-pyrroline N-oxide and 3-(3-hydroxypropyl)-5,5-dimethyl-1-pyrroline N-oxide," *Chem. Lett.*, no. 10, pp. 1059–1060, Nov. 1997, doi: 10.1246/cl.1997.1059.

[190] M. Kubo, K. Sekiguchi, N. Shibasaki-Kitakawa, and T. Yonemoto, "Kinetic model for formation of DMPO-OH in water under ultrasonic irradiation using EPR spin trapping method," *Res. Chem. Intermed.*, 2012, doi: 10.1007/s11164-012-0536-7.

[191] A. Shanei and M. M. Shanei, "Effect of gold nanoparticle size on acoustic cavitation using chemical dosimetry method," *Ultrason. Sonochem.*, vol. 34, pp. 45–50, Jan. 2017, doi: 10.1016/j.ultsonch.2016.05.010.

[192] T. Tuziuti, K. Yasui, M. Sivakumar, Y. Iida, and N. Miyoshi, "Correlation between acoustic cavitation noise and yield enhancement of sonochemical reaction by particle addition," *J. Phys. Chem. A*, vol. 109, no. 21, pp. 4869–4872, Jun. 2005, doi: 10.1021/jp0503516.

[193] P. R. Gogate and A. B. Pandit, "Sonochemical reactors: Scale up aspects," in *Ultrasonics Sonochemistry*, May 2004, vol. 11, no. 3–4, pp. 105–117, doi:

10.1016/j.ultsonch.2004.01.005.

[194] V. S. Sutkar and P. R. Gogate, “Design aspects of sonochemical reactors: Techniques for understanding cavitational activity distribution and effect of operating parameters,” *Chemical Engineering Journal*, vol. 155, no. 1–2. Elsevier, pp. 26–36, Dec. 01, 2009, doi: 10.1016/j.cej.2009.07.021.

[195] A. V. Prabhu, P. R. Gogate, and A. B. Pandit, “Optimization of multiple-frequency sonochemical reactors,” in *Chemical Engineering Science*, Nov. 2004, vol. 59, no. 22–23, pp. 4991–4998, doi: 10.1016/j.ces.2004.09.033.

[196] G. J. Price and P. F. Smith, “Ultrasonic degradation of polymer solutions: 2. The effect of temperature, ultrasound intensity and dissolved gases on polystyrene in toluene,” *Polymer (Guildf).*, vol. 34, no. 19, pp. 4111–4117, Jan. 1993, doi: 10.1016/0032-3861(93)90675-Z.

[197] D. C. Boffito *et al.*, “Ultrasonic enhancement of the acidity, surface area and free fatty acids esterification catalytic activity of sulphated ZrO2-TiO2 systems,” *J. Catal.*, vol. 297, pp. 17–26, Jan. 2013, doi: 10.1016/j.jcat.2012.09.013.

[198] “Lubricants Market Size, Share | Industry Report, 2021-2028.” https://www.grandviewresearch.com/industry-analysis/lubricants-market (accessed Oct. 27, 2021).

[199] “Market Research Reports & Consulting | Grand View Research, Inc.” https://www.grandviewresearch.com/ (accessed Oct. 27, 2021).

[200] C. A, R. E, B. A, and B. MA, “Lubricants from chemically modified vegetable oils,” *Bioresour. Technol.*, vol. 101, no. 1, pp. 245–254, Jan. 2010, doi: 10.1016/J.BIORTECH.2009.08.035.

[201] S. Z. Erhan, B. K. Sharma, and J. M. Perez, “Oxidation and low temperature stability of vegetable oil-based lubricants,” *Ind. Crops Prod.*, vol. 24, no. 3, pp. 292–299, Nov. 2006, doi: 10.1016/J.INDCROP.2006.06.008.

[202] “Biolubricants Market Size | Global Industry Report, 2024.” https://www.grandviewresearch.com/industry-analysis/biolubricants-industry (accessed Oct. 27, 2021).

[203] S. Nogales-Delgado, J. M. Encinar, and Á. González Cortés, “High oleic safflower oil as a feedstock for stable biodiesel and biolubricant production,” *Ind. Crops Prod.*, vol. 170, p. 113701, Oct. 2021, doi: 10.1016/J.INDCROP.2021.113701.

[204] E. J. Parente *et al.*, “Production of biolubricants from soybean oil: Studies for an integrated process with the current biodiesel industry,” *Chem. Eng. Res. Des.*, vol. 165, pp. 456–466, Jan. 2021, doi: 10.1016/J.CHERD.2020.11.012.

[205] R. M. A. Saboya *et al.*, “Synthesis of biolubricants by the esterification of free fatty acids from castor oil with branched alcohols using cationic exchange resins as catalysts,” *Ind. Crops Prod.*, vol. 104, pp. 52–61, Oct. 2017, doi: 10.1016/J.INDCROP.2017.04.018.

[206] N. K. Attia, S. A. El-Mekkawi, O. A. Elardy, and E. A. Abdelkader, “Chemical and rheological assessment of produced biolubricants from different vegetable oils,” *Fuel*, vol. 271, p. 117578, Jul. 2020, doi: 10.1016/J.FUEL.2020.117578.

[207] V. V. Bokade and G. D. Yadav, “Synthesis of Bio-Diesel and Bio-Lubricant by Transesterification of Vegetable Oil with Lower and Higher Alcohols Over Heteropolyacids Supported by Clay (K-10),” *Process Saf. Environ. Prot.*, vol. 85, no. 5, pp. 372–377, Jan. 2007, doi: 10.1205/PSEP06073.

[208] F. J. Owuna *et al.*, “Chemical modification of vegetable oils for the production of biolubricants using trimethylolpropane: A review,” *Egypt. J. Pet.*, vol. 29, no. 1, pp. 75–82, Mar. 2020, doi: 10.1016/J.EJPE.2019.11.004.

[209] M. Gul *et al.*, “Effect of TMP-based-cottonseed oil-biolubricant blends on tribological behavior of cylinder liner-piston ring combinations,” *Fuel*, vol. 278, p. 118242, Oct. 2020, doi: 10.1016/J.FUEL.2020.118242.

[210] F. Zaccheria, M. Mariani, R. Psaro, P. Bondioli, and N. Ravasio, “Environmentally friendly lubricants through a zero waste process,” *Appl. Catal. B Environ.*, vol. 181, pp. 581–586, Feb. 2016, doi: 10.1016/J.APCATB.2015.08.032.

[211] M. F. M. Gunam Resul, T. I. Tinia, and A. Idris, “Kinetic study of jatropha biolubricant from transesterification of jatropha curcas oil with trimethylolpropane: Effects of temperature,” *Ind. Crops Prod.*, vol. 38, no. 1, pp. 87–92, Jul. 2012, doi:

10.1016/J.INDCROP.2012.01.012.

[212] M. Menkiti, H. Anaehobi, K. Oyoh, P. N.-J. of Chemical, and undefined 2015, "Process optimization and kinetics of biolubricant synthesis from fluted pumpkin seed," *core.ac.uk*, vol. 11, no. 27, 2015, Accessed: Jan. 23, 2022. [Online]. Available: https://core.ac.uk/download/pdf/236412798.pdf.

[213] T. S. Chang, H. Masood, R. Yunus, U. Rashid, T. S. Y. Choong, and D. R. A. Biak, "Activity of Calcium Methoxide Catalyst for Synthesis of High Oleic Palm Oil Based Trimethylolpropane Triesters as Lubricant Base Stock," *Ind. Eng. Chem. Res.*, vol. 51, no. 15, pp. 5438–5442, Apr. 2012, doi: 10.1021/IE2028365.

[214] M. Verziu, S. M. Coman, R. Richards, and V. I. Parvulescu, "Transesterification of vegetable oils over CaO catalysts," *Catal. Today*, vol. 167, no. 1, pp. 64–70, Jun. 2011, doi: 10.1016/J.CATTOD.2010.12.031.

[215] H. A. Choudhury, S. Chakma, and V. S. Moholkar, "Mechanistic insight into sonochemical biodiesel synthesis using heterogeneous base catalyst," *Ultrason. Sonochem.*, vol. 21, no. 1, pp. 169–181, Jan. 2014, doi: 10.1016/J.ULTSONCH.2013.04.010.

[216] V. G. Deshmane and Y. G. Adewuyi, "Synthesis and kinetics of biodiesel formation via calcium methoxide base catalyzed transesterification reaction in the absence and presence of ultrasound," *Fuel*, vol. 107, pp. 474–482, May 2013, doi: 10.1016/J.FUEL.2012.12.080.

[217] "ASTM D6584 - 17 Standard Test Method for Determination of Total Monoglycerides, Total Diglycerides, Total Triglycerides, and Free and Total Glycerin in B-100 Biodiesel Methyl Esters by Gas Chromatography." https://www.astm.org/Standards/D6584.htm (accessed Oct. 25, 2021).

[218] F. Gunstone, *Rapeseed and canola oil: production, processing, properties and uses*. 2004.

[219] A. D. Jorgensen, K. C. Picel, and V. C. Stamoudis, "Prediction of gas chromatography flame ionization detector response factors from molecular structures," *Anal. Chem.*, vol. 62, no. 7, pp. 683–689, Mar. 2002, doi: 10.1021/AC00206A007.

[220] F. W. Jones, "Estimation of Flame-Ionization Detector Relative Response Factors for Oligomers of Alkyl and Aryl Ether Polyethoxylates using the Effective Carbon Number

Concept," *J. Chromatogr. Sci.*, vol. 36, no. 5, pp. 223–226, May 1998, doi: 10.1093/CHROMSCI/36.5.223.

[221] T. Holm, "Aspects of the mechanism of the flame ionization detector," *J. Chromatogr. A*, vol. 842, no. 1–2, pp. 221–227, May 1999, doi: 10.1016/S0021-9673(98)00706-7.

[222] H. Laajimi, F. Galli, G. S. Patience, and D. Schieppati, "Experimental methods in chemical engineering: gas chromatography-GC," *Can. J. Chem. Eng.*, Mar. 2022, doi: 10.1002/CJCE.24395.

[223] M. Canakci and H. Sanli, "Biodiesel production from various feedstocks and their effects on the fuel properties," *J. Ind. Microbiol. Biotechnol.*, vol. 35, no. 5, pp. 431–441, May 2008, doi: 10.1007/S10295-008-0337-6.

[224] "Standard Specification for Biodiesel Fuel Blend Stock (B100) for Middle Distillate Fuels." https://www.astm.org/d6751-20a.html (accessed Jan. 17, 2022).

[225] G. Y. Chen, R. Shan, B. B. Yan, J. F. Shi, S. Y. Li, and C. Y. Liu, "Remarkably enhancing the biodiesel yield from palm oil upon abalone shell-derived CaO catalysts treated by ethanol," *Fuel Process. Technol.*, vol. 143, pp. 110–117, Mar. 2016, doi: 10.1016/J.FUPROC.2015.11.017.

[226] G. Y. Chen, R. Shan, J. F. Shi, and B. B. Yan, "Transesterification of palm oil to biodiesel using rice husk ash-based catalysts," *Fuel Process. Technol.*, vol. 133, pp. 8–13, May 2015, doi: 10.1016/J.FUPROC.2015.01.005.

[227] V. Vazquez Thyssen and E. Moreira Assaf, "Ni/CaO-SiO2 catalysts for assessment in steam reforming reaction of acetol," *Fuel*, vol. 254, p. 115592, Oct. 2019, doi: 10.1016/J.FUEL.2019.05.175.

[228] N. S. Lani, N. Ngadi, N. Y. Yahya, and R. A. Rahman, "Synthesis, characterization and performance of silica impregnated calcium oxide as heterogeneous catalyst in biodiesel production," *J. Clean. Prod.*, vol. 146, pp. 116–124, Mar. 2017, doi: 10.1016/J.JCLEPRO.2016.06.058.

[229] N. Girish, S. P. Niju, K. M. Meera Sheriffa Begum, and N. Anantharaman, "Utilization of a cost effective solid catalyst derived from natural white bivalve clam shell for

transesterification of waste frying oil," *Fuel*, vol. 111, pp. 653–658, Sep. 2013, doi: 10.1016/J.FUEL.2013.03.069.

[230] G. Chen, R. Shan, S. Li, and J. Shi, "A biomimetic silicification approach to synthesize CaO–SiO2 catalyst for the transesterification of palm oil into biodiesel," *Fuel*, vol. 153, pp. 48–55, Aug. 2015, doi: 10.1016/J.FUEL.2015.02.109.

[231] J. Boro, A. J. Thakur, and D. Deka, "Solid oxide derived from waste shells of Turbonilla striatula as a renewable catalyst for biodiesel production," *Fuel Process. Technol.*, vol. 92, no. 10, pp. 2061–2067, Oct. 2011, doi: 10.1016/J.FUPROC.2011.06.008.

[232] "Viscosity of ISO Viscosity Classification – viscosity table and viscosity chart :: Anton Paar Wiki." https://wiki.anton-paar.com/ca-fr/classification-de-la-viscosite-iso/ (accessed Oct. 28, 2021).

[233] DASÖL, "HYDRAULIC ISO 32/46/68." https://www.dasoel-lubricants.de/ (accessed Oct. 28, 2021).

[234] H. Laajimi, M. Mattia, R. S. Stein, C. L. Bianchi, and D. C. Boffito, "Electron paramagnetic resonance of sonicated powder suspensions in organic solvents," *Ultrason. Sonochem.*, vol. 73, p. 105544, May 2021, doi: 10.1016/J.ULTSONCH.2021.105544.

[235] M. M. van Iersel, N. E. Benes, and J. T. F. Keurentjes, "Importance of acoustic shielding in sonochemistry," *Ultrason. Sonochem.*, vol. 15, no. 4, pp. 294–300, Apr. 2008, doi: 10.1016/J.ULTSONCH.2007.09.015.

[236] S. M. Hingu, P. R. Gogate, and V. K. Rathod, "Synthesis of biodiesel from waste cooking oil using sonochemical reactors," *Ultrason. Sonochem.*, vol. 17, no. 5, pp. 827–832, Jun. 2010, doi: 10.1016/J.ULTSONCH.2010.02.010.

[237] S. S. Gandhi and P. R. Gogate, "Process intensification of fatty acid ester production using esterification followed by transesterification of high acid value mahua (lluppai ennai) oil: Comparison of the ultrasonic reactors," *Fuel*, vol. 294, p. 120560, Jun. 2021, doi: 10.1016/J.FUEL.2021.120560.

[238] A. A. Koutsouki, E. Tegou, A. Badeka, S. Kontakos, P. J. Pomonis, and M. G. Kontominas, "In situ and conventional transesterification of rapeseeds for biodiesel production: The effect

of direct sonication," *Ind. Crops Prod.*, vol. 84, pp. 399–407, Jun. 2016, doi: 10.1016/J.INDCROP.2016.02.031.

[239] D. Reay, "The role of process intensification in cutting greenhouse gas emissions," *Appl. Therm. Eng.*, vol. 28, no. 16, pp. 2011–2019, Nov. 2008, doi: 10.1016/J.APPLTHERMALENG.2008.01.004.

[240] D. Fernandez Rivas *et al.*, "Process intensification education contributes to sustainable development goals. Part 1," *Educ. Chem. Eng.*, vol. 32, pp. 1–14, Jul. 2020, doi: 10.1016/J.ECE.2020.04.003.

[241] D. Tharani and M. Ananthasubramanian, "Process intensification in separation and recovery of biogenic volatile fatty acid obtained through acidogenic fermentation of organics-rich substrates," *Chem. Eng. Process. - Process Intensif.*, vol. 169, p. 108592, Dec. 2021, doi: 10.1016/J.CEP.2021.108592.

[242] A. A. Kiss, J. J. Pragt, and C. J. G. van Strien, "REACTIVE DIVIDING-WALL COLUMNS—HOW TO GET MORE WITH LESS RESOURCES?," *http://dx.doi.org/10.1080/00986440902935507*, vol. 196, no. 11, pp. 1366–1374, 2009, doi: 10.1080/00986440902935507.

[243] S. Jegatheeswaran, F. Ein-Mozaffari, and J. Wu, "Process intensification in a chaotic SMX static mixer to achieve an energy-efficient mixing operation of non-newtonian fluids," *Chem. Eng. Process. - Process Intensif.*, vol. 124, pp. 1–10, Feb. 2018, doi: 10.1016/J.CEP.2017.11.018.

[244] M. Zhou, D. Bai, Y. Zong, L. Zhao, and J. N. Thornock, "Numerical investigation of turbulent reactive mixing in a novel coaxial jet static mixer," *Chem. Eng. Process. Process Intensif.*, vol. 122, pp. 190–203, Dec. 2017, doi: 10.1016/J.CEP.2017.09.017.

[245] M. Y. Zorainy *et al.*, "Microwave-Assisted Synthesis of the Flexible Iron-Based MIL-88B Metal-Organic Framework for Advanced Energetic Systems," 2021, doi: 10.21203/rs.3.rs-1182353/v1.

[246] N. M.S., A. K. J., S. K. P., and R. S., "Process intensified microwave absorption nanocomposite for stealth application," *Chem. Eng. Process. - Process Intensif.*, vol. 163, p.

108333, Jun. 2021, doi: 10.1016/J.CEP.2021.108333.

[247] C. R. Behloul, J. M. Commenge, and C. Castel, “Influence of the synergy between reaction, heat exchange and membrane separation on the process intensification of the dimethyl ether direct synthesis from carbon dioxide and hydrogen,” *Chem. Eng. Process. - Process Intensif.*, vol. 167, p. 108513, Oct. 2021, doi: 10.1016/J.CEP.2021.108513.

[248] P. Bernardo, E. Drioli, and G. Golemme, “Membrane Gas Separation: A Review/State of the Art,” *Ind. Eng. Chem. Res.*, vol. 48, no. 10, pp. 4638–4663, May 2009, doi: 10.1021/IE8019032.

[249] L. F. Chuah, S. Yusup, A. R. Abd Aziz, A. Bokhari, J. J. Klemeš, and M. Z. Abdullah, “Intensification of biodiesel synthesis from waste cooking oil (Palm Olein) in a Hydrodynamic Cavitation Reactor: Effect of operating parameters on methyl ester conversion,” *Chem. Eng. Process. Process Intensif.*, vol. 95, pp. 235–240, Sep. 2015, doi: 10.1016/J.CEP.2015.06.018.

[250] D. Dixit, P. Thanekar, and V. M. Bhandari, “Degradation of API pollutants using hydrodynamic cavitation and process intensification,” *Chem. Eng. Process. - Process Intensif.*, vol. 172, p. 108799, Feb. 2022, doi: 10.1016/J.CEP.2022.108799.

[251] H. Laajimi, M. Y. Zorainy, D. Schieppati, and D. C. Boffito, “CaO / SiO2 catalyzes the ultrasonic biodiesel transesterification to produce lubricant,” *Fuel Process. Technol.*

[252] Y. Son, M. Lim, M. Ashokkumar, and J. Khim, “Geometric optimization of sonoreactors for the enhancement of sonochemical activity,” *J. Phys. Chem. C*, vol. 115, no. 10, pp. 4096–4103, Mar. 2011, doi: 10.1021/JP110319Y/ASSET/IMAGES/JP110319Y.SOCIAL.JPEG_V03.

[253] J. L. Laborde, C. Bouyer, J. P. Caltagirone, and A. Gérard, “Acoustic cavitation field prediction at low and high frequency ultrasounds,” *Ultrasonics*, vol. 36, no. 1–5, pp. 581–587, Feb. 1998, doi: 10.1016/S0041-624X(97)00106-6.

[254] K. Thangavadivel, K. Okitsu, G. Owens, P. J. Lesniewski, and R. Nishimura, “Influence of sonochemical reactor diameter and liquid height on methyl orange degradation under 200 kHz indirect sonication,” *J. Environ. Chem. Eng.*, vol. 1, no. 3, pp. 275–280, Sep. 2013,

doi: 10.1016/J.JECE.2013.05.005.

[255] S. Fukunaga *et al.*, "Effect of geometrical configuration of reactor on a ZrP nano-dispersion process using ultrasonic irradiation," *Ultrason. Sonochem.*, vol. 52, pp. 157–163, Apr. 2019, doi: 10.1016/J.ULTSONCH.2018.11.008.

[256] A. V. Mohod and P. R. Gogate, "Ultrasonic degradation of polymers: Effect of operating parameters and intensification using additives for carboxymethyl cellulose (CMC) and polyvinyl alcohol (PVA)," *Ultrason. Sonochem.*, vol. 18, no. 3, pp. 727–734, May 2011, doi: 10.1016/J.ULTSONCH.2010.11.002.

[257] Y. No and Y. Son, "Effects of probe position of 20 kHz sonicator on sonochemical oxidation activity," *Jpn. J. Appl. Phys.*, vol. 58, no. SG, p. SGGD02, May 2019, doi: 10.7567/1347-4065/AB0ADB.

[258] J. Y. Hihn, M. L. Doche, A. Mandroyan, L. Hallez, and B. G. Pollet, "Respective contribution of cavitation and convective flow to local stirring in sonoreactors," *Ultrason. Sonochem.*, vol. 18, no. 4, pp. 881–887, Jul. 2011, doi: 10.1016/J.ULTSONCH.2011.02.006.

[259] J. Jordens, A. Honings, J. Degrève, L. Braeken, and T. Van Gerven, "Investigation of design parameters in ultrasound reactors with confined channels," *Ultrason. Sonochem.*, vol. 20, no. 6, pp. 1345–1352, Nov. 2013, doi: 10.1016/J.ULTSONCH.2013.03.012.

[260] H. min Peng, P. cheng Zhu, and P. hui Lu, "Acoustic streaming simulation and analyses in in vitro low frequency sonophoresis," *Sensors Actuators A Phys.*, vol. 263, pp. 744–753, Aug. 2017, doi: 10.1016/J.SNA.2017.05.046.

[261] S. Niazi, S. H. Hashemabadi, and M. M. Razi, "CFD simulation of acoustic cavitation in a crude oil upgrading sonoreactor and prediction of collapse temperature and pressure of a cavitation bubble," *Chem. Eng. Res. Des.*, vol. 92, no. 1, pp. 166–173, Jan. 2014, doi: 10.1016/J.CHERD.2013.07.002.

[262] B. Sajjadi, A. A. A. Raman, and S. Ibrahim, "A comparative fluid flow characterisation in a low frequency/high power sonoreactor and mechanical stirred vessel," *Ultrason. Sonochem.*, vol. 27, pp. 359–373, Nov. 2015, doi: 10.1016/J.ULTSONCH.2015.04.034.

[263] D. Rubinetti, D. A. Weiss, J. Müller, and A. Wahlen, "Numerical Modeling and Validation

Concept for Acoustic Streaming Induced by Ultrasonic Treatment," in *COMSOL CONFERENCE*, Oct. 2016.

[264] J. Klíma, A. Frias-Ferrer, J. González-García, J. Ludvík, V. Sáez, and J. Iniesta, "Optimisation of 20 kHz sonoreactor geometry on the basis of numerical simulation of local ultrasonic intensity and qualitative comparison with experimental results," *Ultrason. Sonochem.*, vol. 14, no. 1, pp. 19–28, Jan. 2007, doi: 10.1016/J.ULTSONCH.2006.01.001.

[265] M. Girard, D. Vidal, F. Bertrand, J. R. Tavares, and M. C. Heuzey, "Evidence-based guidelines for the ultrasonic dispersion of cellulose nanocrystals," *Ultrason. Sonochem.*, vol. 71, p. 105378, Mar. 2021, doi: 10.1016/J.ULTSONCH.2020.105378.

[266] L. Csoka, S. N. Katekhaye, and P. R. Gogate, "Comparison of cavitational activity in different configurations of sonochemical reactors using model reaction supported with theoretical simulations," *Chem. Eng. J.*, vol. 178, pp. 384–390, Dec. 2011, doi: 10.1016/J.CEJ.2011.10.037.

[267] I. Tudela, V. Sáez, M. D. Esclapez, M. I. Díez-García, P. Bonete, and J. González-García, "Simulation of the spatial distribution of the acoustic pressure in sonochemical reactors with numerical methods: A review," *Ultrason. Sonochem.*, vol. 21, no. 3, pp. 909–919, May 2014, doi: 10.1016/J.ULTSONCH.2013.11.012.

[268] S. S. Rashwan, I. Dincer, and A. Mohany, "Investigation of acoustic and geometric effects on the sonoreactor performance," *Ultrason. Sonochem.*, vol. 68, p. 105174, Nov. 2020, doi: 10.1016/J.ULTSONCH.2020.105174.

[269] Z. Wei and L. K. Weavers, "Combining COMSOL modeling with acoustic pressure maps to design sono-reactors," *Ultrason. Sonochem.*, vol. 31, pp. 490–498, Jul. 2016, doi: 10.1016/J.ULTSONCH.2016.01.036.

[270] M. N. Hussain, T. E. Samad, and I. Janajreh, "Physical and Chemical Analysis of Ultrasonic Transesterification through Numerical Simulation," *Jordan J. Mech. Ind. Eng.*, vol. 11, 2017.

[271] M. N. Hussain and I. Janajreh, "Acousto-chemical analysis in multi-transducer sonochemical reactors for biodiesel production," *Ultrason. Sonochem.*, vol. 40, pp. 184–

193, Jan. 2018, doi: 10.1016/J.ULTSONCH.2017.07.009.

[272] Sonics, “ACCESSORIES FOR 750 AND 500 WATT SYSTEMS,” Aug. 2021. https://www.sonics.com/site/assets/files/1160/vibra-cell-catalog-09-2021.pdf (accessed Apr. 08, 2022).

[273] Z. Xu, K. Yasuda, and S. Koda, “Numerical simulation of liquid velocity distribution in a sonochemical reactor,” *Ultrason. Sonochem.*, vol. 20, no. 1, pp. 452–459, 2013, doi: 10.1016/J.ULTSONCH.2012.04.011.

[274] S. V.D. Freitas, M. L. L. Paredes, J. L. Daridon, Á. S. Lima, and J. A. P. Coutinho, “Measurement and prediction of the speed of sound of biodiesel fuels,” *Fuel*, vol. 103, pp. 1018–1022, Jan. 2013, doi: 10.1016/J.FUEL.2012.09.082.

[275] A. Kumar, T. Kumaresan, A. B. Pandit, and J. B. Joshi, “Characterization of flow phenomena induced by ultrasonic horn,” *Chem. Eng. Sci.*, vol. 61, no. 22, pp. 7410–7420, Nov. 2006, doi: 10.1016/J.CES.2006.08.038.

[276] Q. Tang and J. Hu, “Diversity of acoustic streaming in a rectangular acoustofluidic field,” *Ultrasonics*, vol. 58, pp. 27–34, Apr. 2015, doi: 10.1016/J.ULTRAS.2014.11.015.

[277] L. Spicci, “Design and Optimization of a Multi-Purpose, High-Power Ultrasonic Reactor,” 2019.

[278] J. Jordens, B. Gielen, L. Braeken, and T. Van Gerven, “Determination of the effect of the ultrasonic frequency on the cooling crystallization of paracetamol,” *Chem. Eng. Process. Process Intensif.*, vol. 84, pp. 38–44, Oct. 2014, doi: 10.1016/J.CEP.2014.01.006.

[279] R. F. Contamine, A. M. Wilhelm, J. Berlan, and H. Delmas, “Power measurement in sonochemistry,” *Ultrason. Sonochem.*, vol. 2, no. 1, pp. S43–S47, Jan. 1995, doi: 10.1016/1350-4177(94)00010-P.

[280] M. C. Menkiti, H. C. Anaehobi, and O. D. Onukwuli, “Kinetics and parametric study of transesterification synthesis of biolubricant from melon-based methyl esters,” *http://dx.doi.org/10.1080/17597269.2016.1163212*, vol. 7, no. 5, pp. 489–500, Sep. 2016, doi: 10.1080/17597269.2016.1163212.

[281] S. Kitanović, D. Milenović, and V. B. Veljković, “Empirical kinetic models for the resinoid extraction from aerial parts of St. John’s wort (Hypericum perforatum L.),” *Biochem. Eng. J.*, vol. 41, no. 1, pp. 1–11, Aug. 2008, doi: 10.1016/J.BEJ.2008.02.010.

[282] N. A. Tsochatzidis, P. Guiraud, A. M. Wilhelm, and H. Delmas, “Determination of velocity, size and concentration of ultrasonic cavitation bubbles by the phase-Doppler technique,” *Chem. Eng. Sci.*, vol. 56, no. 5, pp. 1831–1840, Mar. 2001, doi: 10.1016/S0009-2509(00)00460-7.

[283] J. M. Costa and A. F. de Almeida Neto, “Ultrasound-assisted electrodeposition and synthesis of alloys and composite materials: A review,” *Ultrason. Sonochem.*, vol. 68, p. 105193, Nov. 2020, doi: 10.1016/J.ULTSONCH.2020.105193.

[284] J. Hofmann, U. Freier, and M. Wecks, “Ultrasound promoted C-alkylation of benzyl cyanide—effect of reactor and ultrasound parameters,” *Ultrason. Sonochem.*, vol. 10, no. 4–5, pp. 271–275, Jul. 2003, doi: 10.1016/S1350-4177(03)00083-X.

[285] E. Abedi, K. Pourmohammadi, M. Jahromi, M. Niakousari, and L. Torri, “The Effect of Ultrasonic Probe Size for Effective Ultrasound-Assisted Pregelatinized Starch,” *Food Bioprocess Technol.*, vol. 12, no. 11, pp. 1852–1862, Nov. 2019, doi: 10.1007/S11947-019-02347-2/TABLES/2.